Structure and excitations of liquid helium

A D B WOODS

Atomic Energy of Canada Limited, Chalk River, Ontario, Canada

R A COWLEY

Department of Physics, University of Edinburgh, Mayfield Road,
Edinburgh EH9 3JZ, Scotland

Abstract

During the past decade there has been considerable progress in the study of the structure and elementary excitations of liquid helium. This has largely arisen from the development and refinement of neutron, x ray and light scattering techniques and also from more detailed ultrasonic measurements. A large part of this review is concerned with describing the results of these experiments and their implications for theories of liquid helium. During the last few years there has also been considerable progress made in the theory of the excitations in liquid helium. These developments are briefly reviewed and the most promising lines of development indicated.

This review was completed in August, 1972.

Rep. Prog. Phys. 1973 **36** 1135–1231

Contents

	Page
1. Introduction	1137
2. Neutron and x ray scattering techniques	1139
2.1. Scattering theory	1139
2.2. Neutron scattering techniques	1143
2.3. x ray scattering techniques	1147
3. Neutron and x ray experimental results	1148
3.1. The static structure factor	1148
3.2. The dynamic structure factor and its moments	1150
3.3. One-phonon excitations at $T = 1{\cdot}1$ K and $P \simeq 0$	1153
3.4. Pressure and temperature dependence of the one-phonon scattering	1156
3.5. Multiphonon scattering	1160
3.6. The independent particle region	1162
4. Ultrasonic measurements	1166
4.1. Experimental techniques	1166
4.2. Experimental results	1168
4.3. Theoretical analysis	1174
5. Light scattering measurements	1183
5.1. Experimental techniques	1183
5.2. Experimental results	1185
5.3. Theoretical analysis	1189
6. Theories of liquid helium	1200
6.1. Microscopic theory	1200
6.2. Calculations of $S(Q)$	1210
6.3. Direct calculations of the density fluctuations	1215
7. Conclusions	1225
Acknowledgments	1227
References	1227

1. Introduction

Liquid helium has been a source of fascination for physicists ever since helium gas was first liquefied by Kammerlingh Onnes in 1908. Its boiling point at atmospheric pressure is 4·2 K and it remains a liquid at absolute zero unless a pressure of about 25 atm is applied. At a temperature of 2·17 K it has a phase transition above which it is usually referred to as He I and below, He II. This phase transition is marked by an anomaly in the specific heat, C_p, and because of the similarity between the C_p against T curve and the Greek letter λ, the temperature at which the anomaly occurs is known as the λ point. Above the transition temperature liquid helium, in spite of its obvious quantum properties, shows many of the thermodynamic and hydrodynamic properties characteristic of a classical liquid. Below 2·17 K it exhibits many unusual properties, the most outstanding of which is that of superfluidity—the apparent vanishing of flow resistance for passage of the liquid through narrow channels. These properties are characteristic of natural helium which is nearly 100% ^{4}He. The lighter isotope ^{3}He is present in natural helium in such small quantities (about one part in 10^6) that its effects are not noticeable in most experiments.

The normal boiling point of pure ^{3}He is 3·2 K and it, also, does not solidify at $T = 0$ except under pressure. It does not, however, have a λ transition, at least above a few millikelvins, nor does it exhibit any superfluid properties. The differences in the properties of these two isotopes of helium are believed to arise from the differences in their nuclear spins: ^{4}He has zero spin and should therefore obey Bose–Einstein statistics and ^{3}He, with a spin of $\frac{1}{2}$, should obey Fermi–Dirac statistics and therefore be analogous in some respects to nuclear matter. In spite of the great interest in ^{3}He and ^{3}He–^{4}He mixtures this article will not discuss their properties. Many excellent reviews on the thermodynamic and hydrodynamic properties of both isotopes of helium and their mixtures exist and are valuable sources of further background information. This article will chiefly be concerned more with those properties of ^{4}He which may be probed by the scattering of various forms of radiation–electromagnetic, particle and acoustic.

The anomalous thermodynamic and flow properties of superfluid helium have given rise to an overwhelming amount of experimental and theoretical activity over the past half century. On the one hand experimentalists have been concerned to elucidate these properties in as much detail as possible, while on the other hand theoreticians have been fascinated by the problem of understanding these properties in terms of the known interactions between helium atoms.

Attempts to understand the macroscopic properties of superfluid helium led to the phenomenological two-fluid model of London based on the concept of a Bose–Einstein condensation. In this model, which has been described in detail in many excellent reviews and monographs, superfluid helium is assumed to consist of two interpenetrating fluids, a 'superfluid' component and a 'normal' component. A theoretical basis for this model was provided when Landau (1941, 1947) suggested that the properties of liquid helium could be explained by considering the system as a background fluid plus a spectrum of weakly interacting elementary excitations above the ground state. These excitations were given the names 'phonons' and

'rotons' and were associated with the normal fluid while the background fluid was identified with the superfluid.

Landau pictured the phonon excitations as long wavelength density fluctuations with energy, E, directly proportional to their momentum, p, and travelling with the velocity of sound c. Thus

$$E = cp \tag{1.1}$$

in the long wavelength limit. In calculations of hydrodynamic properties such as the viscosity (Landau and Khalatnikov 1949) these excitations were assumed to exhibit dispersion such that

$$E = cp(1-\gamma p^2) \tag{1.2}$$

where $\gamma \sim 10^{37}\ \mathrm{g^{-2}\,cm^{-2}\,s^2}$. At shorter wavelengths (larger p) the E against p dispersion curve for the energies of the excitations passed through a minimum such that

$$E = \Delta + \frac{(p-p_0)^2}{2\mu} \tag{1.3}$$

where $\Delta \simeq 9$ K, $p_0/\hbar \simeq 2\ \mathrm{Å}^{-1}$ and $\mu \simeq 0{\cdot}5$ helium masses. The excitations in the region of this parabolic minimum were given the name 'rotons'.

At the time of Landau's classic work the main interest was to explain the anomalous thermodynamic and hydrodynamic properties below the λ point. At these temperatures ($<2{\cdot}17$ K) only those excitations near $p = 0$ and $p = p_0$ had sufficiently high thermal populations to have a significant effect on the low temperature macroscopic properties. Accordingly, Landau did not concern himself with the details of the dispersion curve far from these values of p. The parameters in the expressions for the excitation energies were deduced from macroscopic properties such as the velocities of first and second sound and specific heat.

This development which is described in detail in the monograph by Khalatnikov (1965) is a more microscopic and more powerful theory than the two-fluid model, but it is still a phenomenological theory because the concepts and parameters are obtained from experiment rather than from the microscopic interactions between the atoms. Feynman (1954), and Feynman and Cohen (1956), attempted to obtain a more microscopic model and put Landau's ideas on a firmer theoretical basis. Cohen and Feynman (1957) also suggested that the excitation spectrum could be directly determined by neutron inelastic scattering experiments.

The first observation of the excitations in liquid helium was made by Palevsky *et al* (1957) using neutron inelastic scattering. Since then measurements of the detailed shape of the energy against momentum (or wave vector) dispersion curve for the excitations have been made in several laboratories. These experiments confirmed Landau's essential ideas and hence have provided both a basis for more detailed microscopic theories, and a framework for the interpretation of many recent experiments. In particular since the dispersion relation in liquid helium is far simpler than the phonon dispersion relation in a solid, experiments on the excitations in liquid helium are now frequently used as a testing ground for theories of the effects of the interactions between excitations. In recent years refinements in neutron, x ray, light scattering and ultrasonic techniques have provided a wealth of experimental results of sufficient precision to permit stringent tests of theoretical developments. It is the purpose of this article to review the present status of these experimental results on the static and dynamic structure of liquid helium and briefly to indicate their relevance to current theoretical concepts. In most of the

article we shall restrict attention to the low temperature properties, and although we shall describe the temperature dependence of many properties we shall not attempt a detailed description of the properties near the λ point transition. This has recently been studied extensively as a test of modern theories of second-order phase transitions and we omit discussion of it because many of its features are characteristic of phase transitions rather than of liquid helium. The techniques and results of x ray and neutron scattering are, in many respects, complementary to each other and are discussed in §§2 and 3. The wavelengths of both x rays and thermal neutrons are $\sim 10^{-8}$ cm and are thus of the correct magnitude to be diffracted by solids and liquids through reasonably large angles. For reasons of intensity, however, it is usually possible to obtain greater precision with x rays. On the other hand the energies of thermal neutrons are $\sim 10^{-2}$ eV and hence energy changes caused by interaction with elementary excitations are readily measured; the corresponding x ray energy is $\sim 10^{4}$ eV and thus energy changes $\sim 10^{-3}$ eV or so are practically impossible to measure directly. In addition to the x ray and neutron scattering experiments, which are able to probe the system over a wide range of wave vector transfer Q ($Q = p/\hbar$), there are other techniques which give extremely valuable information. Of these techniques we shall discuss ultrasonic measurements in §4 and light scattering in §5. Because of the long wavelengths of these forms of radiation the measurements are restricted to very small ($\sim 2 \times 10^{-3}$ Å^{-1}) values of Q but the energy resolution obtainable with these techniques leads to information about the interactions between the excitations which cannot readily be obtained in other ways.

Some of the theoretical ideas which are directly related to the experiments are described in §§2–5. More microscopic theories which are less directly relevant but nevertheless important contributions to our understanding of liquid helium are briefly discussed in §6.

2. Neutron and x ray scattering techniques

2.1. *Scattering theory*

2.1.1. *Dynamic and static structure factor.* A function of central importance in the description of liquid helium, and indeed of any fluid, is the dynamic structure factor $S(\boldsymbol{Q}, \omega)$, first discussed by Van Hove (1954). The Fourier transform of $S(\boldsymbol{Q}, \omega)$ over the momentum and energy variables $\boldsymbol{Q}$ and ω yields the time dependent pair correlation function, $G(\boldsymbol{r}, t)$, which, for a classical system, is the probability that, given an atom at position $\boldsymbol{r} = 0$ and time $t = 0$, there is an atom at position $\boldsymbol{r}$ and time t. $S(\boldsymbol{Q}, \omega)$ is thus related to a detailed record of the spatial and temporal behaviour of atoms in the fluid. Van Hove showed that the partial differential coherent neutron scattering cross section per atom for a monatomic system is given by

$$\frac{\mathrm{d}^2\sigma}{\mathrm{d}\Omega\,\mathrm{d}E} = \frac{\sigma}{4\pi\hbar}\frac{k'}{k_0}S(\boldsymbol{Q}, \omega). \tag{2.1}$$

In this expression $\mathrm{d}\Omega$ is the solid angle acceptance of the scattered beam and $\mathrm{d}E$ the corresponding energy interval. The wavenumbers k_0 and k' ($k = 2\pi/\lambda$) refer, respectively, to the incident and scattered neutron beams, σ is the bound atom scattering cross section, $\boldsymbol{Q}$ the momentum transfer, and $\hbar\omega$ the energy transfer which takes place in the scattering process. This result was derived on the basis

of the first Born approximation. In view of the isotropy of a liquid the vector nature of $\boldsymbol{Q}$ is not important and we shall, instead, be concerned with the quantity $Q = |\boldsymbol{Q}|$.

Direct information about $S(Q, \omega)$ may be obtained in certain scattering experiments where it is possible to observe both the momentum transfers ($\hbar Q$) and the energy transfers ($\hbar\omega$) in the distribution of the scattered radiation. As mentioned in § 1, both parameters can readily be measured in a neutron scattering experiment. The wavelengths of typical x rays are of the correct magnitude to probe a large range of Q space but since $\mathrm{d}E$ in (2.1) in any practical x ray experiment is very much larger than typical excitation energies, x ray scattering experiments essentially integrate over all energy transfers. Thus the scattered x ray intensity depends on

$$S(Q) = \int_{-\infty}^{\infty} S(Q, \omega)\, \mathrm{d}\omega. \tag{2.2}$$

While x ray scattering is therefore inappropriate for investigations of the motions of atoms it is capable of yielding precise information about the time independent spatial distribution of atoms. The function $S(Q)$ is the familiar static structure factor which is related to the pair correlation function $g(\boldsymbol{r})$ through the expression

$$S(\boldsymbol{Q}) = 1 + \rho \int \exp(\mathrm{i}\boldsymbol{Q}.\boldsymbol{r})(g(\boldsymbol{r}) - 1)\, \mathrm{d}\boldsymbol{r} \tag{2.3}$$

where $g(\boldsymbol{r})$ is the probability that, if there is an atom at the origin, then, at the same time, there is an atom a distance $\boldsymbol{r}$ away. In a nonvibrating crystal $S(\boldsymbol{Q})$ is simply a diffraction pattern which mainly consists of elastic (Bragg) peaks at reciprocal lattice points, the positions and intensities of which allow the spatial structure to be determined. In a vibrating crystal it is also possible to observe the thermal diffuse scattering which is caused by the lattice vibrations. The intensities of the neutron or x ray peaks arising from the Bragg scattering are reduced from the values they would have in an ideal rigid lattice by the Debye–Waller factor. This is a function of the total momentum transfer and the amplitudes of the atomic vibrations and is similar to the recoil-free fraction which arises in the Mössbauer effect. Knowledge of $S(\boldsymbol{Q})$ obtained from integrating the scattering over all energy transfers thus gives direct information about the instantaneous positions of the atoms. Measurements of the Debye–Waller factors give indirect information on the atomic motions.

In a typical liquid $S(Q)$ does not consist of sharp peaks but rather is a continuous distribution which, at nonzero temperature, has a temperature dependent value at $Q = 0$, a broad maximum usually near $Q = 2\ \text{Å}^{-1}$ ($Q = (4\pi/\lambda)\sin(\phi/2)$ for elastic scattering where λ is the wavelength of the radiation and ϕ the angle of scattering) and subsidiary maxima at larger values of Q. This structure reflects the short range order in the liquid. As Q becomes large $S(Q)$ approaches unity and the effects of correlations between atoms disappear. Experiments to determine $S(Q)$ have been carried out for a large number of liquids, including liquid helium, using both x ray and neutron scattering techniques.

Many of the properties of $S(Q, \omega)$ have been measured by neutron scattering for a number of classical liquids as well as for liquid helium. The scattering function at small Q and ω, corresponding to large distances and long times, consists of a 'quasi-elastic' peak centred on zero energy transfer, the width of which is related to the diffusion coefficient. In the large Q and large ω regime the interatomic interactions are of little importance and the scattering is similar to that expected from a

gas of free particles. It consists of a Doppler broadened distribution with an energy width which rises linearly with Q, and a mean energy, given by the peak position, which rises quadratically with Q.

2.1.2. *Conservation equations.* The conservation equations in a scattering experiment may be expressed as

$$\boldsymbol{k}_0 - \boldsymbol{k}' = \boldsymbol{Q} = \boldsymbol{q} \tag{2.4}$$

and

$$E_0 - E' = \hbar\omega \tag{2.5}$$

where $\boldsymbol{k}_0$ and $\boldsymbol{k}'$ are wave vectors of the incident and scattered radiation, respectively, and E_0 and E' the corresponding energies. $\boldsymbol{Q}$ is the wave vector transfer in the experiment and $\boldsymbol{q}$ the intrinsic wave vector of the excitation. In liquid helium these are identical and so we shall use $\boldsymbol{Q}$ and $\boldsymbol{q}$ interchangeably in such a way as to conform to normal usage.

In many systems the excitations above the ground state may be described by a well defined dispersion relation, connecting their energy and momentum, so that

$$\hbar\omega = \hbar\omega(\boldsymbol{q}). \tag{2.6}$$

In such cases the constraints imposed on the scattering by (2.4), (2.5) and (2.6) ensure that the scattered neutron energy distributions contain sharp peaks corresponding to scattering by single excitations. Conversely the observation of sharp peaks, broadened only by the experimental resolution, is evidence that a dispersion relation does exist and knowledge of the quantities in (2.4) and (2.5) allows this dispersion relation to be determined. Such experiments are readily done with neutron scattering but, for the reasons mentioned above, other forms of radiation are not as universal because of the inability to determine ω (x rays) or the inability to make measurements over a large range of Q (optics and acoustics).

2.1.3. *Moments of* $S(Q, \omega)$. In discussions of scattering from liquids it is often convenient, particularly in the case of neutron scattering, to consider the moments of $S(Q, \omega)$ defined as

$$\langle\omega\rangle_n = \int_{-\infty}^{\infty} \omega^n S(Q, \omega)\, \mathrm{d}\omega. \tag{2.7}$$

The moment for which $n = 0$ is just the static structure factor, $S(Q)$, and is the function obtained by simply integrating the observed energy distribution over all energy transfers. It is directly obtainable from the x ray scattering and may be obtained from the neutron scattering either by integrating the observed energy distribution for various momentum transfers or by carrying out the experiment so that there is no energy analysis of the scattered beam and scattered neutrons of all energies are observed. The problems associated with the latter are discussed in § 2.2.2.

The moment $n = 1$ is given by

$$\int_{-\infty}^{\infty} \omega S(Q, \omega)\, \mathrm{d}\omega = \frac{\hbar Q^2}{2M} \tag{2.8}$$

where M is the mass of the helium atom in this case. The expression (2.8) is variously known as the first moment theorem or the f-sum rule. For a monatomic system such as liquid helium it is quite general in its validity provided that there are no

velocity dependent forces between the atoms. As there is no reason to believe that it is invalid, it is customary to use (2.8) and the $S(Q)$ obtained from the integrated energy distribution to provide critical checks on the accuracy of the observed energy distributions. This is particularly useful when considering possible high energy tails on the distributions. If the observed energy distribution were a single symmetrical peak, such as a gaussian, then the centre of this peak would be at the position expected for scattering from a gas of free particles.

The static susceptibility of the liquid is directly related to the $n = -1$ moment. The function $G(Q)$ is defined as

$$G(Q) = \int_{-\infty}^{\infty} \frac{1}{\omega} S(Q, \omega)\, \mathrm{d}\omega \tag{2.9}$$

and

$$\lim_{Q \to 0} G(Q) = \frac{1}{2Mc^2}$$

where c is the isothermal velocity of sound (Pines 1966a,b).

The higher order moments ($n = 2, 3, \ldots$) are of limited interest partly because it is difficult to obtain useful theoretical expressions for them (they often depend on the details of the interatomic interactions) and partly because it is extremely difficult to determine them experimentally with sufficient precision for them to serve as significant tests of any theory. A second-moment relation which is valid at high temperatures is applicable to classical liquids but not to liquid helium. An expression for the third moment of the scattering from liquid helium has been worked out by Puff (1965) but its relationship to available experimental results has not been established.

2.1.4. *Feynman theory and structure of* $S(Q, \omega)$. The first detailed calculation of the dispersion curve for the elementary excitations in liquid ^{4}He was carried out by Feynman (1954). He obtained the result

$$E(Q) = \frac{\hbar^2 Q^2}{2MS(Q)}. \tag{2.10}$$

This result follows from the moment relations of § 2.1.3 if it is assumed that all of the scattering occurs in a sharp δ function peak whose energy corresponds to the phonon excitation energy. If

$$S(Q, \omega) = Z(Q)\, \delta(\omega - \omega(Q))$$

then

$$\int_{-\infty}^{\infty} \omega S(Q, \omega)\, \mathrm{d}\omega = Z(Q)\, \omega(Q)$$

$$= \frac{\hbar Q^2}{2M}$$

and

$$S(Q) = Z(Q)$$

leading directly to (2.10).

It is well known, however, that (2.10) is correct only as $Q \to 0$ and that $E(Q)$, from (2.10), for $Q \sim 2$ Å^{-1} is about a factor of two higher than is observed. Thus, as pointed out by Cohen and Feynman (1957) and emphasized by Miller *et al* (1962),

$S(Q,\omega)$ must contain scattering which does not arise solely from the excitation of a single phonon. More generally

$$S(Q,\omega) = Z(Q)\,\delta(\omega-\omega(Q)) + S_{\mathrm{II}}(Q,\omega). \tag{2.11}$$

In the case of scattering by phonons in a harmonic crystal $S_{\mathrm{II}}(Q,\omega)$, in addition to Bragg peaks, has contributions from scattering with the excitation of more than one phonon. This extra scattering is usually referred to as multiphonon scattering and, by analogy, in this article we will refer to $S_{\mathrm{II}}(Q,\omega)$ as the multiphonon part of the scattering.

It was shown by Feynman that, at $T = 0$,

$$\lim_{Q\to 0} S(Q) = \frac{\hbar Q}{2Mc} \tag{2.12}$$

which, in conjunction with (2.10), leads directly to (1.1). Since $S_{\mathrm{II}}(Q)$ is proportional to Q^4 (Miller *et al* 1962) it follows that

$$\lim_{Q\to 0} Z(Q) = \frac{\hbar Q}{2Mc} \tag{2.13}$$

also.

In the high Q limit where interatomic interactions are not important (and, incidentally, for all Q for an ideal gas) $S(Q) = 1$ and (2.10) reduces to the energy of a free particle and the corresponding scattering is as described in § 2.1.1.

2.1.5. *Qualitative description of the one-phonon scattering.* The apparently valid description of the excitations in liquid helium in terms of well-defined phonons encourages the use of the analogy with the phonons in a harmonic crystal, in spite of the lack of long range spatial order in the liquid. This analogy can be used, with limited success, to discuss the neutron scattering from liquid helium. As in liquid helium the energies of long wavelength phonon excitations in a crystal depend linearly on their momenta and at low temperature, the constant-Q (§ 2.2.2), energy loss, one-phonon neutron cross section is proportional to

$$\frac{Q^2}{\omega}\exp(-Q^2u^2)$$

where $\exp(-Q^2u^2)$ is the Debye–Waller factor and u is the mean amplitude of vibration of the atoms. In a harmonic crystal u may be calculated, on the Debye model, from the temperature and the Debye temperature, θ_{D}. Assuming that θ_{D} for the liquid is similar to that for the solid near the same density its value is ~ 25 K. In the low Q limit $\exp(-Q^2u^2)$ is unity and ω is proportional to Q. Thus the one-phonon intensity in the harmonic solid has the same Q dependence as in liquid helium. The effect of the Debye–Waller factor with $\theta_{\mathrm{D}} = 25$ K is to make the cross section a maximum near the position of the roton minimum (~ 2 Å^{-1}) and then for it to fall rapidly at larger Q. As discussed in § 3.3.1 this behaviour is in qualitative agreement with observed intensities although there are significant discrepancies.

2.2. *Neutron scattering techniques*

2.2.1. *Neutron sources.* The principal sources of thermal neutrons are nuclear reactors. Neutrons of high energy (~ 1 Mev) are produced in the fission process and are slowed down in a moderator which is usually composed of atoms of low

atomic weight and low neutron absorption cross section. In equilibrium the neutron energy distribution is maxwellian with parameters determined by the temperature of the moderator. In most reactors the moderator is usually at room temperature (300 K) although in some reactors the moderator temperature is significantly higher than this. It is also possible to install special moderators, at the end of specific beam tubes in the reactor, which are at either very low or very high temperatures. Liquid hydrogen is often used as a cold moderator while beryllium, beryllium oxide and graphite are suitable for hot moderators at temperatures in excess of 1000°C. Although the room temperature moderator is the most useful for neutron scattering studies of liquid helium, and incidentally most other systems, the cold moderator, with its increase in neutron flux at low energies, has some advantages for the low-energy-transfer, high resolution experiments which characterize the one-phonon part of the scattering. The increase in neutron flux at high energies available with a hot moderator is useful in studies of the high-energy-transfer, high-momentum-transfer region.

It is also possible to produce beams of thermal neutrons from particle accelerators. The energetic charged particles interact with matter to produce high energy neutrons which are then moderated to thermal energies. Such sources exist but none of these give neutron fluxes as high as can be obtained in the better nuclear reactors, although in principle this process can yield higher fluxes than can readily be obtained from a reactor.

In order for them to be used in a scattering experiment beams of thermal neutrons are taken out through holes in the reactor shield. From the maxwellian spectrum a narrow energy slice is selected and allowed to fall on the specimen. The energy and direction of a scattered beam are measured and the corresponding energy and momentum transfers determined from (2.4) and (2.5). The techniques for carrying out these measurements are discussed in the next subsection. Figure 1 shows a schematic diagram of the NRU reactor at Chalk River, which was the source of neutrons for the authors' measurements discussed in this review.

2.2.2. *Neutron spectrometers.* In order to carry out neutron inelastic scattering experiments it is necessary to be able to define the wavelength (or energy) and direction of the neutron beams incident on and scattered by the specimen. (In studies of crystals it is also necessary to define the orientation of the crystal with respect to these beams but this is not necessary for liquids.) There are two principal techniques for determining these parameters—the pulsed beam time-of-flight and the crystal spectrometer. Many instruments combining both principles have also been built and have uses in special applications.

In the standard pulsed beam technique the incident beam is chopped by a mechanical rotor (or series of rotors) into pulses of monoenergetic neutrons with typical pulse lengths of about 10 μs. The energies of the scattered neutrons are determined by their electronically measured time-of-flight over a known path length. Although the duty cycle is usually less than 1% much of the intensity loss can be recovered through the use of a large array of detectors. Such techniques are particularly suited for use in conjunction with a pulsed neutron source such as might be obtained from an accelerator or a pulsed reactor and have been described in detail by Brugger (1965).

A variation of the time-of-flight spectrometer known as the rotating crystal spectrometer (RCS) (Brockhouse 1961) is of some interst because of its extensive use

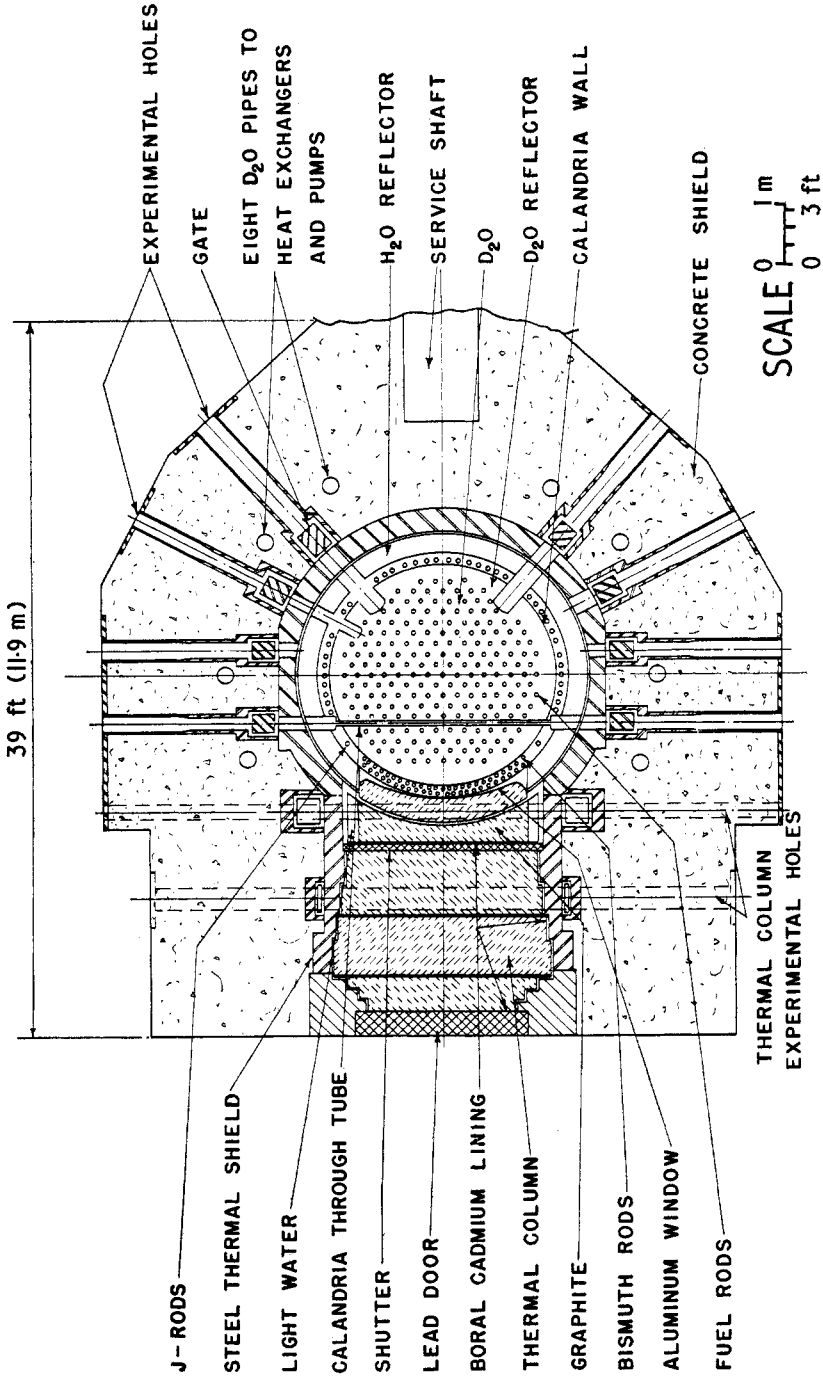

Figure 1. Plan view of NRU reactor showing arrangement of beam holes. From Brockhouse *et al* (1960).

in liquid helium experiments (Cowley and Woods 1971, Harling 1971). In this method the mechanical rotors for velocity selection are replaced by a single crystal spinning about a vertical axis. Whenever the crystal planes come into the Bragg position a burst of monoenergetic neutrons is reflected from the crystal and impinges on the specimen. Other features of the spectrometer are similar to those of the ordinary time-of-flight devices. A schematic diagram of this type of spectrometer is shown in figure 2.

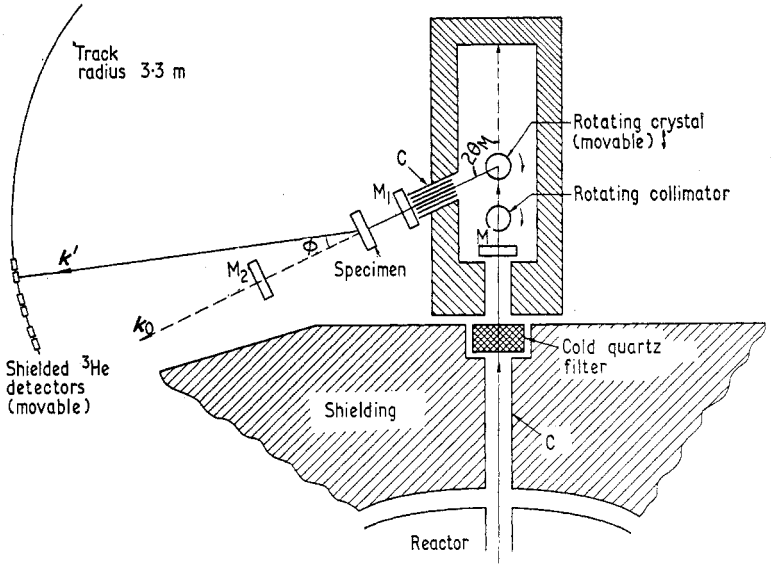

Figure 2. Schematic diagram of rotating crystal spectrometer (RCS). The collimators are denoted by C and monitor counters by M, M_1 and M_2. From Cowley and Woods (1971).

In the triple-axis crystal spectrometer (TACS), shown schematically in figure 3 and discussed in detail by Iyengar (1965), the neutron wavelength (and hence energy) is determined by means of Bragg reflection from the monochromator and the analyser single crystals. The neutron directions are defined by collimators. The detector is usually a gas filled proportional counter containing either ^{10}B or ^{3}He. Although the crystal spectrometer does not, usually, have more than one detector it does have a significant advantage over time-of-flight devices. By programmed control over the spectrometer angles it is possible to determine neutron energy distributions at fixed and preselected values of the wave vector transfer $\boldsymbol{Q}$ (Brockhouse 1961). In experiments with fixed scattering angle ϕ and fixed incident neutron wave vector $\boldsymbol{k}_0$, the neutron wave vector transfer, $\boldsymbol{Q}$, is a function of $\boldsymbol{k}'$ and, hence, of the energy transfer $\hbar\omega$. The observed energy distributions, therefore, extend over a range of $\boldsymbol{Q}$ and are not suitable for a direct comparison with theory. The ability to carry out constant-$\boldsymbol{Q}$ experiments is a great boon and is particularly useful in regard to many of the liquid helium experiments where it is often necessary to cover a large range of energy transfers for a given wave vector transfer.

One of the most serious difficulties with both of these instruments arises from the reflection by the monochromating and analysing crystals of neutrons of energies which differ from those desired. In particular, a crystal set to reflect a beam of wave vector $\boldsymbol{k}_0$ and energy E_0 will usually also reflect neutrons of wave vector $2\boldsymbol{k}_0$

and energy $4E_0$. It is common to suppress the effect of this order contamination through the use of (111) reflecting planes of Ge crystals (for which the (222) reflections are absent) or by the use of a beryllium, quartz or pyrolytic graphite filter.

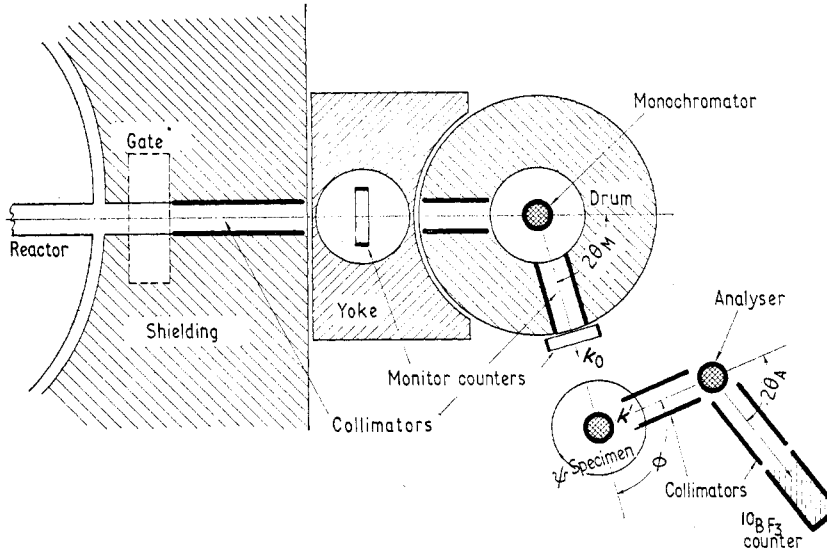

Figure 3. Schematic diagram of triple-axis crystal spectrometer (TACS). From Cowley and Woods (1971)

2.3. *x ray scattering techniques*

2.3.1. *Instruments.* A comprehensive review of x ray scattering from liquids has been given in this series by Furukawa (1962). The most recent such experiments on liquid helium have been carried out by Achter and Meyer (1969) and by Hallock (1972). The spectrometer used by Achter and Meyer is described in detail by Narahara (1968) who used it for measurements of ^{3}He. A schematic diagram of the Hallock spectrometer is shown in figure 4. The x ray beam is produced initially from commercially available x ray tubes which, in these experiments, makes use of the Cu Kα radiation ($\lambda = 1{\cdot}54$ Å). The monochromatic character of the beam is improved through the use of either a crystal monochromator or a suitable filter. (As a point of interest typical x ray beams are about 1 mm in width while neutron beams are typically about 5 cm.) Electronic techniques are used in the detection system in order to eliminate events which do not arise from the detection of Cu Kα x rays. Because of the low temperatures required for the experiment, specially designed specimen containers must be built which will be reasonably transparent to the x ray beam. Beryllium is generally used as window material because of its small atomic number, and hence its relatively low x ray scattering power. Mylar is also used for window material in some applications. This problem is not so serious in neutron scattering and reasonably thick aluminium windows, which scatter only a very small fraction of the beam, are convenient to use.

2.3.2. *x ray measurements.* The intensity of x rays scattered from a fluid is

$$I(\phi, Q) = \sigma_T\, T(\phi)\, N(\phi)\, (\sigma_e\, S(Q) + \sigma_i) \tag{2.14}$$

where σ_T is the Thompson cross section for scattering by a free electron, $T(\phi)$ is a geometry dependent transmission factor, $N(\phi)$ is the number of atoms in the sample which contribute to the scattering and is also angle dependent, σ_e is the elastic or coherent x ray scattering cross section, and σ_i is the inelastic or incoherent x ray scattering cross section arising from Compton scattering. $T(\phi)$ takes into account depletion of the beam arising from multiple scattering and absorption processes.

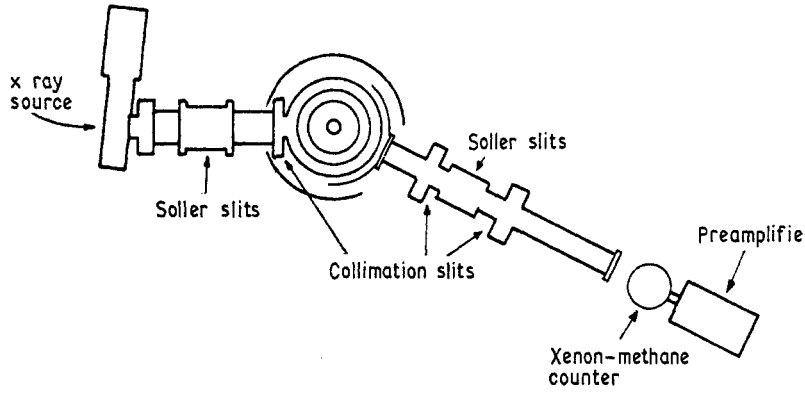

Figure 4. Schematic diagram of Hallock's x ray spectrometer. From Hallock (1972).

Since only a few per cent of the incident beam is removed by the presence of the helium, this factor may be readily evaluated. $N(\phi)$ is usually allowed for by measuring the scattering from an ideal gas for which $S(Q) = 1$. Neon gas at 77 K is very suitable for this purpose and is the gas usually used. The cross sections σ_e and σ_i have been calculated by Kim and Inokuti (1968) for helium and by Tavard *et al* (1967) for neon and include the form factor.

With the aid of the factors which can be calculated, $S(Q)$ is derived from measurements of the intensity, I, of x rays scattered, as a function of scattering angle ϕ, from the liquid helium sample, the neon gas sample, and the empty cassette.

3. Neutron and x ray experimental results

3.1. *The static structure factor*

3.1.1. *Measurements of* $S(Q)$. Experiments to determine $S(Q)$ of liquid helium by means of x ray scattering have gone through three phases. The earliest attempts were made by Keesom and Taconis (1938) and Reekie (1940) from the scattering of Cu Kα x rays. The second phase, which gave a more detailed description of $S(Q)$, involved a number of investigations in the 1950s (Tweet 1954, Beaumont and Reekie 1955, Gordon *et al* 1958) and included some measurements as a function of temperature, while the third phase consisted of the very precise and pretty work of Achter and Meyer (1969) and Hallock (1972). In parallel with the x ray experiments, studies of neutron scattering were begun at Chalk River by Hurst and Henshaw (1955). Subsequent measurements by Henshaw (1960a,b) investigated the temperature and pressure dependence of the neutron scattering.

Figure 5 shows $S(Q)$ as determined from both x ray and neutron scattering. The general features of the results from the three sets of measurements shown are in

reasonably good agreement with one another although discrepancies do exist. The neutron scattering measurements of Henshaw (1960a) indicate that the height of the first diffraction peak near $Q = 2{\cdot}0$ Å^{-1} is closer to 1·5 than to the 1·33 quoted by Achter and Meyer and which is consistent with the earlier neutron measurement of Hurst and Henshaw. Henshaw did not comment on the discrepancy and the reasons for it are unknown.

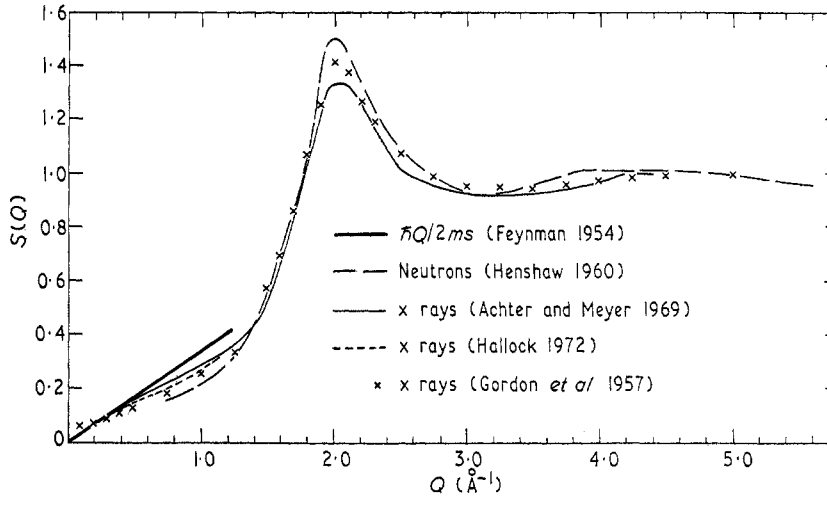

Figure 5. The static structure factor, $S(Q)$, determined by various measurements.

In regions of significant discrepancy between the results of Henshaw and the most recent x ray results, the values of $S(Q)$ as determined from integrating over all energy transfers in the inelastic neutron scattering experiments (Cowley and Woods 1971) agree more nearly with the x ray results. We believe the results of the x ray measurements are to be preferred over the neutron scattering results.

3.1.2. *The low temperature static structure factor.* All measurements of $S(Q)$ show quite distinctly the first diffraction maximum near $Q = 2{\cdot}0$ Å^{-1} but the details of a second maximum near $Q = 4{\cdot}5$ Å^{-1} are less well established. There is an indication of a second peak in the neutron measurements but the recent x ray measurements do not extend to large enough values of Q to be able to confirm this.

The more recent low temperature results (temperature dependence will be discussed in § 3.1.4) at small, but finite, Q are consistent with the Feynman expression (2.12)

$$\lim_{Q\to 0} S(Q) = \frac{\hbar Q}{2Mc}$$

although deviations are evident at values of Q as low as 0·4 Å^{-1}. Miller *et al* (1962) from considerations of their knowledge at that time of $S(Q)$, $\omega(Q)$ and $Z(Q)$, predicted that $S(Q)$ would exhibit a maximum, or at least a shoulder, for $Q \simeq 0{\cdot}6$ Å^{-1}. Hallock's measurements do not show a maximum but they do indicate an inflection point in agreement with the spirit of this prediction.

The first maximum in $S(Q)$ is lower than in most other liquids and subsidiary maxima are less distinct. This implies that the short range order is less well defined presumably on account of the large zero-point motion.

Through the use of the inverse of equation (2.3) it is possible to transform the measurements of $S(Q)$ to obtain information about the spatial distribution of atoms. Hurst and Henshaw (1955) analysed their results in this way and deduced that, at low temperatures, the average atom in liquid helium has eight nearest neighbours at a mean distance of 3·7 Å and a second shell of perhaps eleven neighbours at 5·25 Å. These results are compared with calculations in § 6.2 and reasonable, although by no means complete, agreement is found.

3.1.3. *Pressure dependence of* $S(Q)$. The only measurements of the pressure dependence of $S(Q)$ are the neutron scattering measurements of Henshaw (1960b). As the pressure is raised the height of the first maximum increases and the position moves to larger values of Q. For values of Q less than that of the maximum (2·0 Å^{-1}) $S(Q)$ decreases with increasing pressure. Accurate determinations of the very small Q behaviour ($Q \sim 0{\cdot}3$ Å^{-1}) were not made. For $Q > 3{\cdot}0$ Å^{-1} $S(Q)$ was independent of pressure within the accuracy of the experiment.

3.1.4. *Temperature dependence of* $S(Q)$. Although the early measurements of $S(Q)$ were carried out at a variety of different temperatures, systematic studies of the temperature dependence of $S(Q)$ were made in only two cases: (i) the neutron scattering measurements of Henshaw (1960a), and (ii) the low Q x ray measurements of Hallock.

Henshaw compared $S(Q)$ at 2·29 K (just above the λ point) with $S(Q)$ at 1·06 K under normal vapour pressure in both cases. Additional measurements at $T = 2{\cdot}46$ K were, within error, identical with those at 2·29 K. The only discernible difference between the curves at 2·29 K and 1·06 K is in the region of the first maximum where it is higher (by about 5%) and narrower at the higher temperature.

Hallock's measurements covered the ranges $0{\cdot}133$ Å$^{-1} \leqslant Q \leqslant 1{\cdot}125$ Å^{-1} and $0{\cdot}38$ K $\leqslant T \leqslant 4{\cdot}60$ K. In general $S(Q)$ was greater at the higher temperatures and the effects of temperature were most pronounced at small Q. At the three highest temperatures, 3·30 K, 4·00 K and 4·60 K, $S(Q)$ showed a distinct minimum, the position of which shifted to larger Q as the temperature increased. The low temperature low Q results are in accord with the expression (Feynman and Cohen 1956)

$$S(Q) = \frac{\hbar Q}{2Mc} \coth\left(\frac{\hbar Q c}{2k_{\mathrm{B}} T}\right), \tag{3.1}$$

the finite temperature extension of equation (2.12) where k_{B} is Boltzmann's constant.

3.2. *The dynamic structure factor and its moments*

3.2.1. *Measurements of* $S(Q, \omega)$. As discussed in § 2.1.1, neutron inelastic scattering may be used to determine the dynamic structure factor, $S(Q, \omega)$. Some typical scattered neutron energy distributions, which are directly proportional to $S(Q, \omega)$ at fixed values of Q, are shown in figure 6 (Cowley and Woods 1971, Woods *et al* 1972). Other measurements which concentrate on certain specific aspects of $S(Q, \omega)$ are discussed in §§ 3.4, 3.5 and 3.7.

In accord with the discussion (§ 2.1.4) of equation (2.11) the observed distributions exhibit a well defined sharp peak, which is broadened only by the instrumental resolution, and, at somewhat higher energies, a broader distribution. Both the

energy width and the intensity of the broad distribution are strong functions of Q. At values of $Q > 3{\cdot}5$ Å^{-1} the intensity of the sharp peak is practically zero.

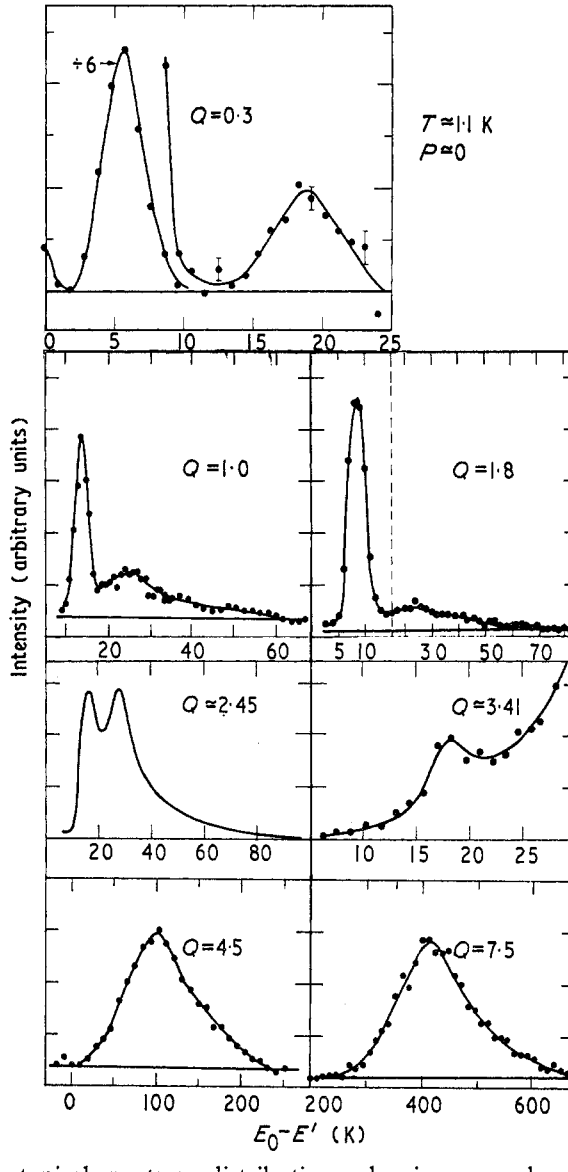

Figure 6. Some typical neutron distributions showing one-phonon and multiphonon contributions. The missing part of the $Q \simeq 3{\cdot}41$ distribution is similar to the $Q = 4{\cdot}5$ distribution with the peak at ~ 70 K. The points have been omitted for $Q \simeq 2{\cdot}45$ because they would be indistinguishable in the figure. From Cowley and Woods (1971) and Woods *et al* (1972).

3.2.2. *The $n = 0$ moment.* The static structure factor, $S(Q)$, is just the $n = 0$ moment of $S(Q, \omega)$ and is given by (2.2), that is

$$S(Q) = \int_{-\infty}^{\infty} S(Q, \omega)\, \mathrm{d}\omega.$$

The measurements of $S(Q, \omega)$ by Cowley and Woods (1971) when integrated over all energy transfers gave reasonable agreement with the results of the x ray scattering measurements (Achter and Meyer 1969, Hallock 1972). The precision of the neutron experiments was not sufficiently high to determine whether or not there are any significant discrepancies between the x ray and neutron measurements.

3.2.3. *The $n = 1$ moment.* The $n = 1$ moment is given by equation (2.8) and may be determined directly from appropriate integration of the distributions shown in figure 6, each point in a distribution being weighted by the corresponding energy transfer. The resulting first moment, divided by $\hbar Q^2/2M$, is shown in figure 7. The

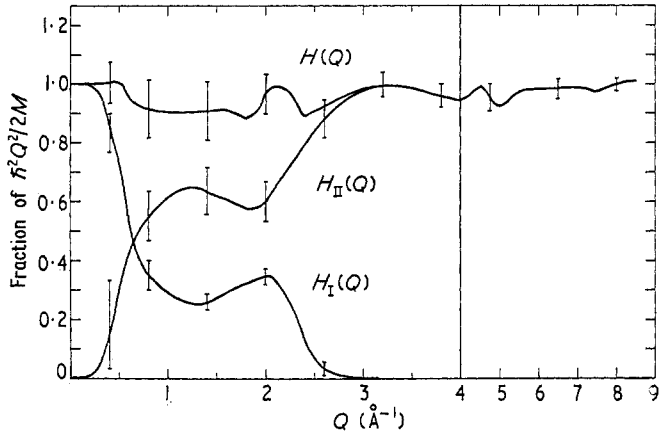

Figure 7. The first moment of $S(Q, \omega)$ in liquid helium at 1·1 K showing the contributions of one-phonon and multiphonon components. From Cowley and Woods (1971).

closeness of this ratio, $H(Q)$, to unity is satisfying and suggests that the major contributions to the scattering, particularly at high energy transfers, have been accounted for.

The division of $H(Q)$ into contributions from the sharp one-phonon peak, $H_I(Q)$, and the broad multiphonon distribution, $H_{II}(Q)$, is also shown in figure 7. At those values of Q where there is no distinct separation between the two components (generally $0{\cdot}7 < Q < 3{\cdot}5$ Å^{-1}) the one-phonon peak was estimated by insisting that its high energy side be symmetrical with its low energy side. This is not necessarily strictly correct particularly if phonon interactions are important enough to cause any broadening of the lines which might be masked by the multiphonon distributions. Nevertheless the division assumed likely gives a reasonable estimate of $H_I(Q)$ which may be interpreted as an effective Debye–Waller factor (Ambegaokar *et al* 1965).

3.2.4. *The $n = -1$ moment.* The $n = -1$ moment, defined by equation (2.9), was also determined from the results of Cowley and Woods and is shown in figure 8. Its determination is considerably more precise than that of any positive moment because the principal contribution comes from the low energy part of the distributions which is dominated by the one-phonon scattering. $G_{II}(Q)$ (the contribution to $G(Q)$ from the multiphonon scattering) exceeds $G_I(Q)$ only for $Q > 2{\cdot}3$ Å^{-1} while $H_{II}(Q)$ is greater than $H_I(Q)$ for $Q > 0{\cdot}6$ Å^{-1}.

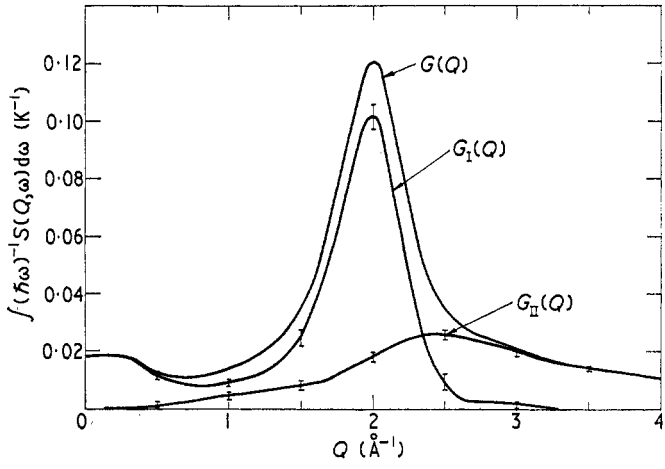

Figure 8. The inverse first moment showing the contributions of one-phonon and multi-phonon components. From Cowley and Woods (1971).

3.3. *One-phonon excitations at* $T = 1{\cdot}1$ K *and* $P \simeq 0$

3.3.1. *The phonon dispersion curve.* The position, in energy, of the sharp peaks in the scattered neutron distributions define the dispersion curve for the excitations in superfluid helium. Following the work of Palevsky *et al* (1957, 1958), who first demonstrated the existence of well defined excitations in helium, most of the essential features of the dispersion curve were measured by Yarnell *et al* (1959) and Henshaw and Woods (1961a). Both of these latter measurements were carried out at about 1·1 K and should be reasonably representative of the situation at $T = 0$, particularly since measurements to date have not shown any significant temperature dependence in the widths, positions or intensities of the corresponding neutron groups for $T \leqslant 1{\cdot}5$ K. The more recent results of Cowley and Woods (1971) have extended the results to higher and lower values of Q. These results are shown in figure 9 and agree very well with the previous measurements of Yarnell *et al* and Henshaw and Woods. The region $1{\cdot}5 < Q < 2{\cdot}3$ Å^{-1} has recently been studied by Dietrich *et al* (1972).

The form of the dispersion is very similar to that calculated by Feynman and Cohen (1956). There is an initial linear rise with a slope corresponding to the velocity of sound (equation (1.1)) followed by a maximum and the well known 'roton' minimum (equation (1.3)). However, the results demonstrate that the shape of the dispersion curve in the region of the minimum is not symmetric about p_0 and attempts to fit a parabola to the curve over any finite range of Q is unsatisfactory; as the fitted range of Q is increased the values of the derived parameters vary. The value of Δ at the minimum is $8{\cdot}67 \pm 0{\cdot}04$ K. On the other hand, Dietrich *et al* found that their results were reasonably well represented by a parabola within 0·25 Å^{-1} of the minimum. Beyond the roton minimum the curve attains a slope approximately equal to its initial slope and then levels off at an energy of about 2Δ.

Bendt *et al* (1959) and Singh (1968) have calculated various thermodynamic properties of liquid helium, such as the entropy, specific heat, normal fluid density and velocity of sound, from the parameters of the dispersion curve obtained by Yarnell *et al.* Agreement between these calculations and experiment was generally

within a few per cent. More extensive comparisons over wide ranges of temperature and pressure are possible with more recent model parameters such as those deduced by Donnelly (1972).

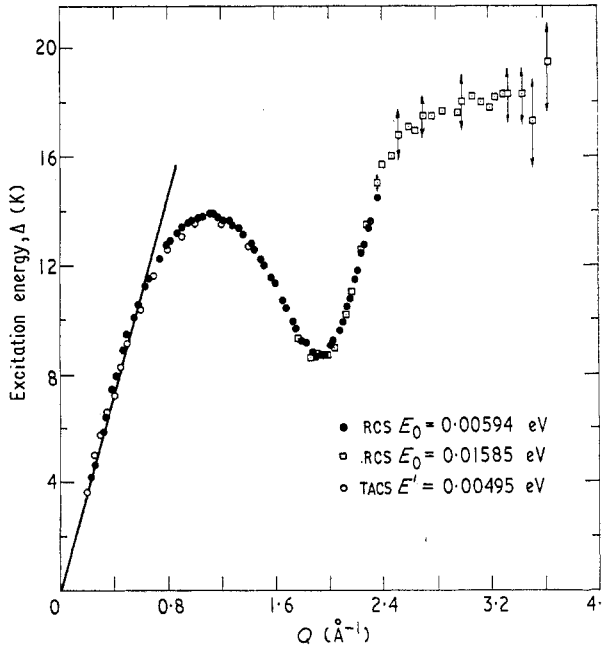

Figure 9. The dispersion curve for He II for the elementary excitations at $T = 1{\cdot}1$ K and $P \simeq 0$. Data obtained by rotating crystal spectrometer (RCS) and triple axis crystal spectrometer (TACS) as indicated. From Cowley and Woods (1971).

The intensities of the neutron groups arising from the scattering by single phonons are shown in figure 10. For $Q < 0{\cdot}3$ Å^{-1} the results are consistent with a linear increase in intensity with Q in agreement with (2.13), which also describes the low Q behaviour for a harmonic solid, and with the x ray measurements of $S(Q)$. For $0{\cdot}3 < Q < 1{\cdot}0$ the one-phonon intensity is roughly constant and increases rapidly to a maximum at about 2·0 Å^{-1}, beyond which it exhibits a very rapid fall-off. For $Q \simeq 3{\cdot}5$ Å^{-1} the intensity is about 1% of that at 2·0 Å^{-1}. An effective Debye–Waller factor for the one-phonon intensity is given by $H_{\mathrm{I}}(Q)$, shown in figure 7, and is very similar to the Debye–Waller factor for a harmonic solid with $\theta_{\mathrm{D}} \simeq 25$ K except for the pronounced depression near $Q = 1{\cdot}0$ Å^{-1}. This depression has also been observed for phonons in BCC solid helium (Osgood *et al* 1972) as has been emphasized by Werthamer (1972). The explanation that the depression in $H_{\mathrm{I}}(Q)$ for solid helium arises from interactions between one- and two-phonon scattering (Sears and Khanna 1972, Horner 1972, McMahon and Guyer 1973) may also be valid in the liquid. Such a view is strengthened by the results of measurements at higher pressures described in § 3.4.1.

3.3.2. *Phonon dispersion at low Q.* From equations (2.10) and (2.12) we see that, in the limit of low Q,

$$E(Q) = \hbar\omega(Q) = \hbar Q c. \tag{3.2}$$

The most commonly assumed form for a series expansion in powers of Q is

$$\omega(Q) = cQ(1-\gamma\hbar^2 Q^2 - \delta\hbar^4 Q^4) \tag{3.3}$$

which is also applicable to phonons in a harmonic solid. The applicability of (3.3) to the description of the phonon dispersion in liquid helium near $T = 0$ has been questioned by several authors. Feenberg (1971) showed that a $1/r^6$ interatomic potential has a Fourier transform, $v(Q)$, containing terms in $|Q|^3$. In the Bogoliubov theory, § 6.1.2, the expansion of $\omega(Q)$ then contains a term proportional to Q^4.

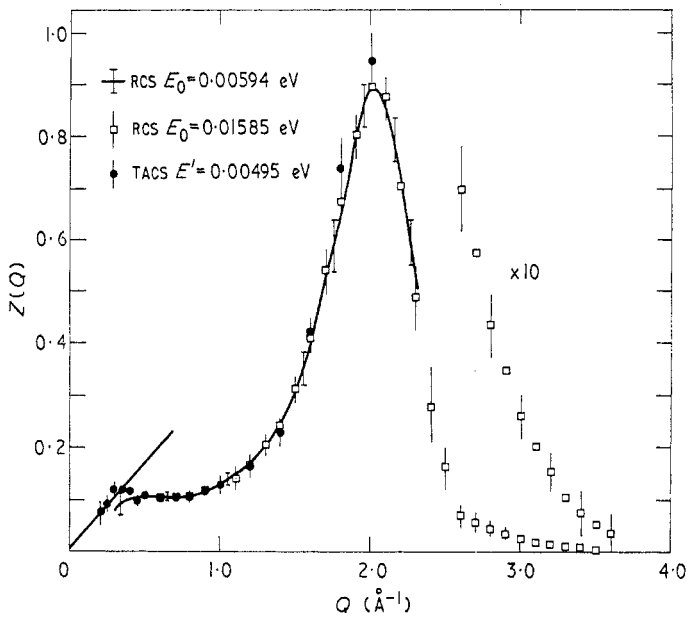

Figure 10. Intensities of the one-phonon neutron groups at 1·1 K. Data from RCS and TACS as indicated. From Cowley and Woods (1971).

Gould and Wong (1971), as described in § 6.1.4, have shown that for the dilute Bose gas there are terms in the expansion of $\omega(Q)$ of the form $Q^4 \ln(1/Q)$. We must therefore treat equation (3.3) with care, but from the analysis of the neutron scattering results alone, it is not possible to determine that equation (3.3) is invalid. On the assumption that (3.3) is valid it is possible to deduce values for γ and δ from the neutron results. At the saturated vapour pressure the results (Woods and Cowley 1970) are $\gamma = (0 \pm 2) \times 10^{36}\ \mathrm{g^{-2}\,cm^{-2}\,s^2}$ and $\delta = (2{\cdot}4 \pm 0{\cdot}3) \times 10^{75}\ \mathrm{g^{-4}\,cm^{-4}\,s^4}$. Specific heat measurements, however (Phillips *et al* 1970), suggest that γ is large ($\sim 10^{37}\ \mathrm{g^{-2}\,cm^{-2}\,s^2}$) and negative while, as discussed in § 4.3.1, the analysis of ultrasonic measurements indicates the presence of a region of anomalous dispersion for $Q \lesssim 0{\cdot}1\ \mathrm{Å^{-1}}$. The pressure dependence of the phonon dispersion for $Q < 0{\cdot}2\ \mathrm{Å^{-1}}$ at $P = 24$ atm is discussed in §§ 3.4.1 and 4.3.1.

In the spirit of the expansions given by Pines and Woo (1970) the intensities of the one-phonon neutron groups may be expressed as

$$Z(Q) = \frac{\hbar Q}{2Mc}(1 - Z_2 Q^2 - Z_4 Q^4 \ldots). \tag{3.4}$$

The experimental one-phonon intensities of Cowley and Woods are reasonably well fitted for $Q \lesssim 1{\cdot}0$ Å^{-1}, if $Z_2 = 1{\cdot}5 \pm 0{\cdot}2$ Å^2 and $Z_4 = -0{\cdot}9 \pm 0{\cdot}2$ Å^4. For $Q > 0{\cdot}3$ Å^{-1} the one-phonon intensities diverge from the measurements of $S(Q)$ (Hallock 1972) indicating that neutron scattering by more than one phonon occurs with significant probability even at these low wave vectors. This scattering will be discussed in more detail in § 3.5.1.

3.3.3. *Phonon dispersion at high Q.* The dispersion curve shown in figure 9 exhibits a plateau for $Q > 2{\cdot}5$ Å^{-1} at an energy $\sim 2\Delta$. In this region the one-phonon intensities decrease rapidly with Q (figure 10), thus making accurate determination of the energies and intensities difficult.

The behaviour of the large wave vector phonons was first discussed by Pitaevskii (1959) who showed that their decay into pairs of phonons may occur if either the phonon group velocity exceeds the velocity of sound or if the phonon energy exceeds 2Δ. Phonon stability has also been discussed by Jackson and Feenberg (1962).

In the former case the dispersion relation is continuous through a critical wave vector, Q_c, and the attentuation increases beyond Q_c. In the latter case the energy approaches 2Δ exponentially, but the dispersion curve then ends abruptly at Q_c. Figure 9 shows that the velocity reaches a maximum at $Q = 2{\cdot}27$ Å^{-1}, which is almost exactly equal to the velocity of sound and hence very nearly satisfies the condition for the first case. At larger wave vectors the velocity reduces and the energy approaches 2Δ. There is some indication that the observed energy is slightly greater than 2Δ for $Q > 2{\cdot}8$ Å^{-1} although the accuracy in this region is not high enough to be certain of this. Results at higher pressure, however (§ 3.4.1), suggest that this effect is more pronounced at $P = 25{\cdot}3$ atm. Pitaevskii's theory, which also predicts the rapid decrease in the one-phonon intensity, appears to be qualitatively correct although it is most probably inadequate in detail.

More recently Ruvalds and Zawadowski (1970) have proposed that phonons near the roton minimum interact to form a two-roton bound state with a Q-independent dispersion relation and that the 'one-phonon' peaks observed in the neutron scattering for $Q > 2{\cdot}8$ Å^{-1} arise from scattering from this bound state. This intriguing concept will be discussed in more detail in §§ 3.5.3, 5.3.3 and 6.3.2.

3.4. *Pressure and temperature dependence of the one-phonon scattering*

3.4.1. *Pressure dependence.* Measurements of the phonon dispersion at $P = 25{\cdot}3$ atm were made by Henshaw and Woods (1961b) and the results are shown in figure 11. In addition Dietrich *et al* (1972) studied the roton minimum region as a function of pressure and Svensson *et al* (1972) the dispersion of long wavelength phonons at $P = 24$ atm.

At these higher pressures the low temperature sound velocity is about 50% higher than at the vapour pressure (Abraham *et al* 1970) and this is reflected in the higher initial slope. At the maximum, near $Q = 1{\cdot}1$ Å^{-1}, the phonon energy is about 10% higher, while at the roton minimum the energy is 7·0 K compared with 8·67 K at $P \simeq 0$. Beyond the minimum the curve has approximately the same slope at the two pressures and at 25 atm shows signs of levelling off at an energy which is greater than 2Δ. The corresponding intensities of the one-phonon neutron groups reflect these energy changes: as expected from equation (2.8) the neutron

groups have lower intensities when the phonon energy is higher and vice versa (Svensson *et al* 1972, Woods *et al* 1973), although the detailed pressure dependence shows unexpected features. At $P = 24$ atm and $Q = 1{\cdot}13$ Å^{-1} the phonon energy exceeds 2Δ, giving rise to the possibility of phonon decay into two rotons. There is,

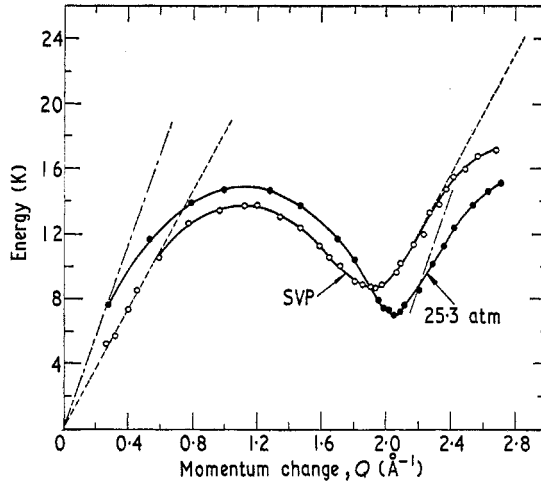

Figure 11. The dispersion curve at $T = 1{\cdot}1$ K and $P = 25{\cdot}3$ atm.

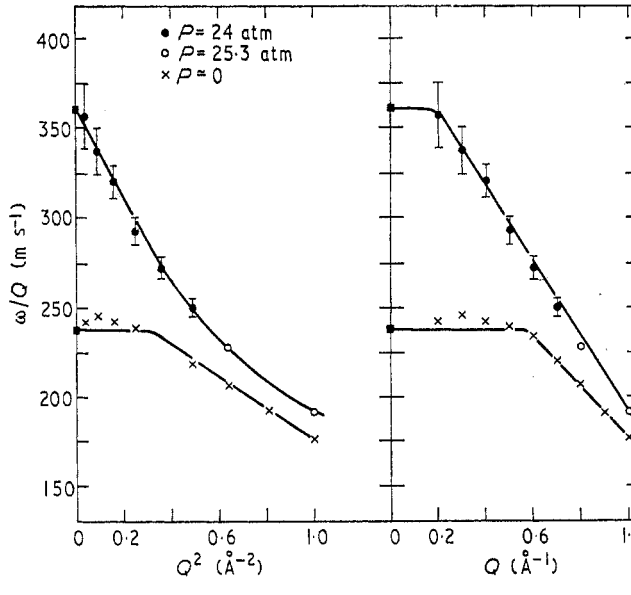

Figure 12. Phonon velocities at $P = 0$, 24 and 25·3 atm. From Svensson *et al* (1973).

however, no indication in the neutron scattering that this threshold triggers a new decay mechanism. It is possible that the reason for this apparent stability is a pressure dependent effect which is also operative in the Pitaevskii regime (Brockhouse *et al* 1964).

The measurements of Svensson *et al* (1972), shown in figure 12, indicate that at 24 atm the phonon energies for $0{\cdot}2$ Å$^{-1} \leqslant Q \leqslant 0{\cdot}7$ Å^{-1} may be fitted to the first two

terms of (3.3) with $\gamma = (6{\cdot}2 \pm 0{\cdot}6) \times 10^{37}\ \mathrm{g^{-2}\,cm^{-2}\,s^2}$, in contrast with the very small value of γ at $P \simeq 0$ but in better agreement with that derived from analysis of specific heat measurements (Phillips *et al* 1970). Ultrasonic measurements also suggest that γ is positive at high pressure as discussed in § 4.3.1.

Dietrich *et al* (1972) have studied the pressure dependence of the neutron scattering in the vicinity of the roton minimum. The value of Δ at $T \simeq 1{\cdot}3$ K derived from their experiments decreases approximately linearly with pressure for $P > 5$ atm and varies somewhat more rapidly, by a factor about 2 below this. Their value for $(\rho/\Delta)\,\partial\Delta/\partial\rho$, where ρ is the density, is $-0{\cdot}94 \pm 0{\cdot}05$ at the saturated vapour pressure. At 1 atm and 10 atm their results beyond the roton minimum show that the slope of the dispersion curve attains that of the velocity of sound at that pressure. It is then possible for the phonons to decay as discussed in § 3.3.3.

3.4.2. *Temperature dependence*

Most of the experiments to study the temperature dependence of the one-phonon excitations were confined to the roton region of the dispersion curve (Larsson and Otnes 1959, Yarnell *et al* 1959, Henshaw and Woods 1961a, Dietrich

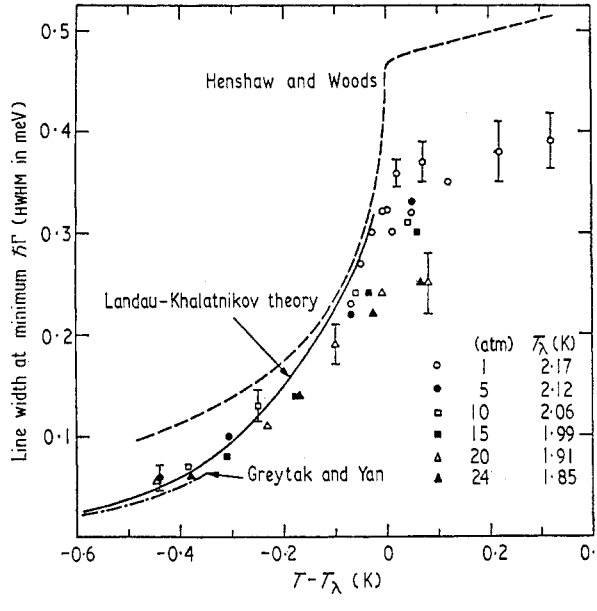

Figure 13. Temperature dependence of roton line widths (1 meV = 11·6 K). From Dietrich *et al* (1972).

et al 1972). In addition to the neutron scattering results, light (Raman) scattering measurements have also been used to determine the temperature dependence of rotons (Greytak and Yan 1971). Because of their direct relevance to the neutron measurements, the results of these light scattering measurements will be included here rather than in § 5.2.2.

The temperature dependence of the width of the neutron groups in the roton region is shown in figure 13. The width increases slowly at low temperature, very rapidly just below T_λ, and slowly above T_λ. There is possibly a discontinuity in the

slope at T_λ. In this region the full width at half maximum is about twice the mean energy transfer corresponding to the centre of the neutron group. The concept of well defined excitations is, therefore, not really valid in this region of Q and T.

The various experimental determinations of the temperature dependence of the roton line width are reasonably consistent with one another, particularly when differences in analysis are taken into account. For example the resolution function, which had an energy width of about 2 K, was not removed from the results of Henshaw and Woods while Dietrich *et al* did allow for instrument resolution and also separated the annihilation and creation contributions to their observed line shapes near the λ point. These differences account for most of the apparent discrepancies between the two sets of results.

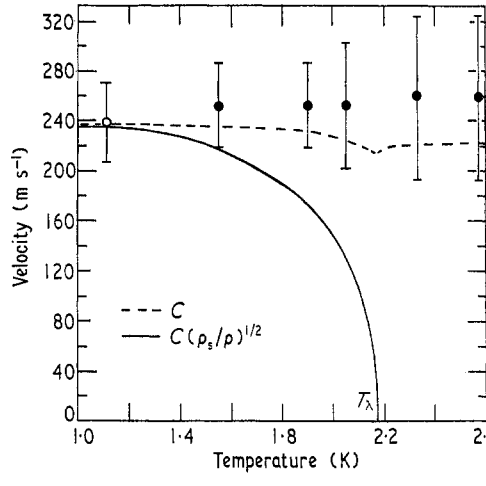

Figure 14. Phonon velocity as a function of temperature for $Q \simeq 0{\cdot}38$ Å^{-1}. The vertical bars correspond to peak widths and do not represent errors. From Woods (1965a).

Dietrich *et al* show their results (figure 13) as a function of $T - T_\lambda(P)$ and suggest that they lie on a universal curve independent of pressure, although there is possibly some trend towards smaller widths near T_λ at higher pressure.

These results, and those of the light scattering measurements, are reasonably consistent with the Landau and Khalatnikov (1949) expression which reduces to

$$\delta E = \frac{\hbar^2 Q^2}{15\eta_R}\left(\frac{k_B T}{(2\pi)^3 \mu}\right)^{1/2} \exp(-\Delta/k_B T) \tag{3.5}$$

where η_R is the contribution of roton–roton scattering to the viscosity. This expression agrees very well with the experimental results and supports the Landau–Khalatnikov model of strong hard core repulsive interactions between rotons as discussed in § 5.3.4.

In addition to these studies near the roton minimum there are measurements of the temperature dependence of long wavelength phonons (Woods 1965a, Cowley and Woods 1971) and of the dispersion curve over a wide range of Q at 2·1 K, just below T_λ (Cowley and Woods 1971). The results in the long wavelength region disagree with the prediction by Hohenberg and Martin (1964) that the phonon velocity would be proportional to the superfluid density and, hence, be zero at the λ point. The measured phonon velocity (figure 14) shows only slight temperature

dependence up to about $T = 3{\cdot}0$ K. At $Q = 0{\cdot}2$ Å^{-1} the widths of the neutron groups increase slowly with temperature but show no sign of a discontinuity at T_λ while at $Q = 0{\cdot}6$ Å^{-1} there is a strong temperature dependence in the vicinity of T_λ and the results are very similar to those at the roton minimum. Pines (1966a,b), by analogy with the theory of zero sound in Fermi liquids or of plasmons in an electron gas, suggested that the existence of phonons above T_λ results from the short range correlations in the liquid (see § 6.1.4).

At $T = 2{\cdot}1$ K Cowley and Woods made measurements over a large range of Q. At large Q ($\gtrsim 2{\cdot}4$ Å^{-1}) the broadened one-phonon peak merged with the multiphonon scattering so that the distinction between them was unobservable. The peak positions shown in figure 20 of Cowley and Woods are therefore strongly influenced by a Q-dependent and unknown contribution from the multiphonon scattering. It is thus not reasonable to treat these results as determinations of the energies of well defined excitations. Near $Q = 1{\cdot}0$ Å^{-1} it was also not possible to observe a distinct one-phonon peak. Under optimum conditions the one-phonon intensities in this region are low (figure 10). As the temperature is raised the peaks broaden, thus reducing the peak height, and phonon–phonon interactions, which become more important as the temperature is raised, perhaps increase the interference between the one-phonon and multiphonon components, thus reducing the peak height still more. On the other hand these results, which were obtained with a rotating crystal spectrometer, could be significantly improved. There is no reason to suppose that a peak could not be observed in this region of Q and T under better experimental conditions.

3.5. *Multiphonon scattering*

3.5.1. *Description.* In addition to the sharp peaks in figure 6, which are attributed to one-phonon scattering, there is, on the high energy side of these peaks, intensity which rises to a broad maximum at about 25 K and extends to relatively large (~ 80 K) energy transfers. For $Q > 2{\cdot}5$ Å^{-1} the scattering is dominated by this broad intensity, the mean position (in energy) of which rises rapidly with Q. This region is discussed in more detail in § 3.6.1.

Figure 15 summarizes the results for $0{\cdot}3$ Å$^{-1} < Q < 4{\cdot}0$ Å^{-1}. The shaded region corresponds to the energy transfer range between the upper and lower half-height positions on these broad distributions. These distributions are not symmetrical, often exhibit structure and have long tails. There is no justification for assuming that they correspond to a second branch of well defined excitations. The width of the distribution varies with wave vector mainly through the Q dependence of the energy corresponding to the upper half-height position. This position extrapolates to a value which is almost equal to that of the lower half-height, rises to a maximum near $Q = 1{\cdot}5$ Å^{-1} and exhibits a minimum near $2{\cdot}2$ Å^{-1}.

The intensity of the broad distribution at $Q = 0{\cdot}3$ Å^{-1} is $< 1\%$ of that for one-phonon excitations near the roton minimum (Woods *et al* 1972a). It rises slowly and smoothly with Q and dominates the scattering at large Q. It is approximately equal to the one-phonon contribution near $Q = 1{\cdot}2$ Å^{-1}, falls below it in the range $1{\cdot}2$ Å$^{-1} < Q < 2{\cdot}2$ Å^{-1} and exceeds it for $Q > 2{\cdot}2$ Å^{-1}.

At small wave vector transfers this scattering may be expressed as

$$S_{\mathrm{II}}(Q,\omega) = (G_4 Q^4 + G_6 Q^6 + \ldots)\, f(Q,\omega)$$

where $f(Q,\omega)$ is normalized so that $\int_{-\infty}^{\infty} f(Q,\omega)\,\mathrm{d}\omega = 1$ and the first moment is

given by $\bar{\omega}+Q^2\bar{\omega}_2$. Analysis of the experimental results gives $G_4 = 0{\cdot}55 \pm 0{\cdot}1$ Å^4, $G_6 = -0{\cdot}4 \pm 0{\cdot}5$ Å^6, $\bar{\omega} = 18 \pm 2$ K and $\bar{\omega}_2 = 8 \pm 2$ K Å^2 (Cowley and Woods 1971).

If the scattering satisfies the first moment sum rule, equation (2.8), then these coefficients are related to those of equations (3.3) and (3.4) by (Pines and Woo 1970)

$$\frac{\hbar}{2M}(Z_2+\gamma\hbar^2) = G_4\bar{\omega}.$$

The results given above clearly satisfy this result well within the experimental errors.

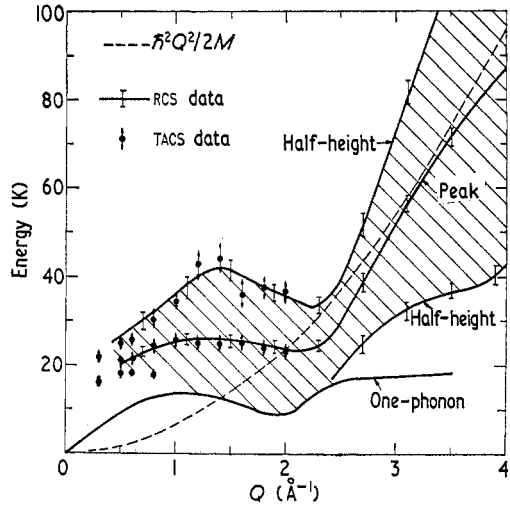

Figure 15. The energy against wave vector dependence of the scattering at intermediate Q at 1·1 K. From Cowley and Woods (1971).

3.5.2. *Pressure dependence of the multiphonon scattering.* The multiphonon scattering has been studied at 24 atm by Woods *et al* (1973) at several wave vector transfers in the range $0{\cdot}5$ Å$^{-1} < Q < 2{\cdot}05$ Å^{-1}. The results are similar to those at 0·7 atm, the major differences being more intensity in the multiphonon component relative to the one-phonon scattering at the lower values of Q, and evidence of intensity at energies below the one-phonon peak position.

The appearance of scattering intensity at energies below the one-phonon peak is particularly puzzling. As discussed in the following section, the 'multiphonon' scattering most likely arises from processes in which more than one phonon is excited in addition to interference between these and the one-phonon processes involving phonon decay. There is no obvious way in which a phonon can decay so as to give rise to scattering at lower energies unless, perhaps, second sound excitations are involved (see §6.1.4). Such an effect may well be enhanced at high pressure (§5.3.2) where the ratio of specific heats, C_p/C_v, departs more from unity and there is thus more coupling between first and second sound (Vinen 1971).

3.5.3. *Interpretation.* The simplest, and hence most attractive, explanation of the broad component is in terms of scattering by more than one phonon. Such processes are well known in neutron scattering by harmonic crystals and were discussed

by Cohen and Feynman (1957) and by Miller *et al* (1962) for liquid helium. At small Q two-phonon processes dominate while at larger Q scattering by many phonons becomes important, as evidenced by the fact that the distributions extend to energy transfers (figure 6) which are much larger than the maximum energy of two phonons on the dispersion curve (~ 35 K).

The intensity of the two-phonon process is expected to be proportional to the joint density of states, that is, the number of pairs of phonons which add up to $\omega = \omega_1 + \omega_2$ at wave vector Q, to $\omega_1^{-1}\omega_2^{-1}$ in analogy with the corresponding term for harmonic crystals, and perhaps to other terms depending on the properties of the two excitations (the subscripts denote separate phonons involved in the process). In calculations of the Raman scattering (§ 5.3.3) the intensity of the scattering near 2Δ is peaked and very strong while that near $2\Delta_1$ (Δ_1 is the maximum energy near $Q = 1{\cdot}1$ Å^{-1}) is much weaker and does not give rise to a maximum. It is therefore surprising that the neutron distributions show a peak at 19 K for $Q \simeq 0{\cdot}3$, close to 2Δ, but at larger Q the peak is closer to $2\Delta_1$. The rise in the minimum in the upper half-height position beyond $Q = 2{\cdot}2$ Å^{-1} may partly arise from the fact that scattering by two Δ_1 phonons is not possible for $Q > 2{\cdot}2$ Å^{-1}.

The shape of the multiphonon distributions may also be influenced by interference with the one-phonon processes. This interference has been invoked to explain the anomalously low intensity of the one-phonon peak near $1{\cdot}1$ Å^{-1} (§ 3.3.1) and there will be an associated increase in the intensity of the multiphonon scattering.

Iwamoto (1970), Iwamoto *et al* (1971), Pitaevskii (1970) and Zawadowski *et al* (1972) have considered the effect of roton–roton interactions on the shape of the scattering cross section. They all conclude that the interaction may have a significant effect on the shape. Zawadowski *et al* (1972) performed some detailed calculations in which the multiphonon scattering is observed entirely through the one-phonon part of the cross section. Their results which are discussed in detail in § 6.3.3 are in qualitative agreement with the observed neutron scattering.

Soda *et al* (1970) have used the two moment theorems (2.2) and (2.8) to discuss the scattering. They approximate $S_{\mathrm{II}}(Q, \omega)$ by $S_{\mathrm{II}}(Q)\,\delta(\omega - \omega_2(Q))$ and then deduce $Z(Q)$ and $S_{\mathrm{II}}(Q)$ from the moment theorems and the observed one-phonon and multiphonon peak frequency. The results are similar to the experimental results for these quantities but differ in detail because of the oversimplified form assumed for $S_{\mathrm{II}}(Q, \omega)$.

3.6. *The independent particle region*

3.6.1. *Experimental results.* For $Q \geqslant 2{\cdot}5$ Å^{-1} the one-phonon intensity drops rapidly to near zero, $S(Q) \simeq 1$, and the width and mean energy of the 'multiphonon' component are similar to that expected for scattering by a gas of free particles. This region is therefore better described by an independent particle model than by a phonon model. It also exists, of course, for solids but is rarely considered.

Scattering in this region was observed by Woods (1965b) for Q up to $4{\cdot}0$ Å^{-1} and more extensive measurements by Cowley and Woods (1968, 1971) up to $9{\cdot}0$ Å^{-1}. Harling (1971) studied the scattering up to $20{\cdot}3$ Å^{-1} and Martel, Svensson and Woods (unpublished) up to $12{\cdot}0$ Å^{-1}. No measurements were made at elevated pressures but some of the experiments studied the temperature dependence of the scattering.

The observations at large Q are qualitatively described in terms of the impulse approximation in which

$$S(Q) = \frac{1}{N}\sum_{\boldsymbol{p}} n(\boldsymbol{p})\,\delta\left(\omega - \frac{\hbar Q^2}{2M} - \frac{\hbar \boldsymbol{Q}.\boldsymbol{p}}{M}\right) \tag{3.6}$$

where $n(\boldsymbol{p})$ is the number of particle having wave vector $\boldsymbol{p}$ and the delta function expresses conservation of energy and momentum. According to this expression the mean energy transfer is $\hbar^2 Q^2/2M$. The term in $\boldsymbol{Q}.\boldsymbol{p}$ averages to zero and thus gives no contribution to the peak position but is responsible for a width of about $\boldsymbol{Q}.\bar{\boldsymbol{p}}/M$ which increases linearly with Q.

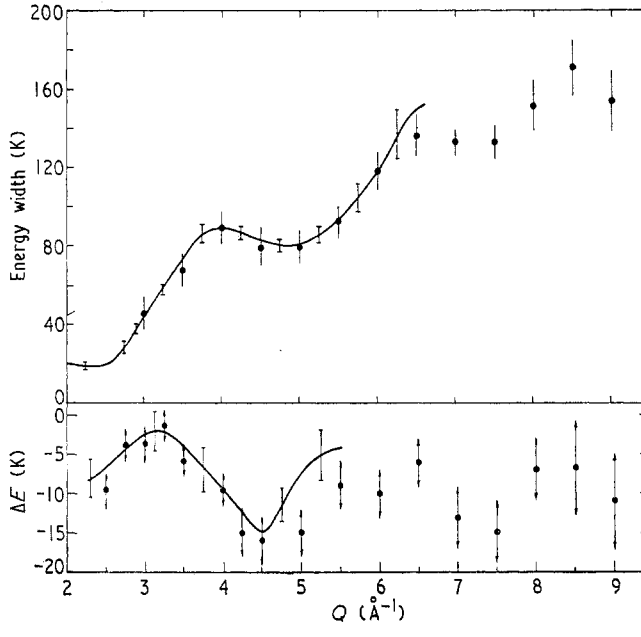

Figure 16. (*a*) Widths and (*b*) energies $-\hbar^2 Q^2/2M$ of the peak of the scattering at 1·1 K.

There are, however, very definite departures from the free particle or impulse approximation. In particular, the departures of the widths and energies of the peaks from their mean values exhibit oscillations as a function of Q as shown in figure 16. These oscillations were observed also at $T = 4{\cdot}2$ K and hence are not characteristic of the superfluid only. (The positions in energy of the peaks are taken to be the mean of the energies corresponding to half the maximum intensity on each side of the peak.) The oscillations in the width, at least, persist to 12·0 Å^{-1} but were not observed by Harling in experiments extending to 20·3 Å^{-1}. Except at the largest scattering angles the width of Harling's distributions were dominated by instrumental resolution and there is, therefore, no reason to suppose that there is any disagreement between the two experiments.

The widths of the distributions were measured as a function of temperature for fixed angles of scattering corresponding to 5·1 Å^{-1} (Cowley and Woods) and 14·3 Å^{-1} (Harling). Both results (figure 17) show little temperature dependence above the λ point and a much stronger dependence below. The results indicate that, at 5·1 Å^{-1}, the most rapid variation occurs between 2·0 K and the λ point.

All of the measured distributions are smooth and are not readily decomposed into two distinct peaks. The statistical errors are such that it is difficult to tell if there is any asymmetry in the peaks at the higher values of Q although it is apparent for distributions at lower Q. The deviations of the mean energy from the free-particle value coupled with the necessity to satisfy the first moment theorem, (2.8), suggest, however, that some asymmetry must exist at least out to 9·0 Å^{-1}.

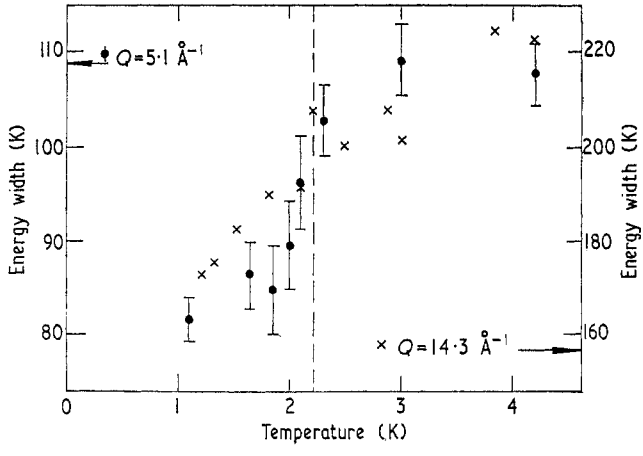

Figure 17. Temperature dependence of the width of the peak at 5·1 Å^{-1} (Cowley and Woods) and at 14·3 Å^{-1} (Harling).

3.6.2. *Occupation of zero momentum state.* One of the fundamental ideas underlying the modern theory of liquid helium is that of macroscopic occupation of the zero momentum state. All of the superfluid helium cannot be in this state, however, because of the interaction between helium particles. This interaction leads to a depletion of the zero momentum state which is believed to be about 90%. Inspection of (3.6) shows that if $p = 0$ the resultant neutron scattering distribution is still centred at $\hbar^2 Q^2/2M$ but has zero width. Thus, a measure of the intensity of a component of the scattering, which is narrow relative to that of the Doppler broadened distribution on which it is superimposed, gives a measure of the ratio $n(0)/N$, the fractional number of particles in the zero momentum state. Miller *et al* (1962) recognized that, in principle, neutron scattering measurements at large Q could determine this ratio, but the specific proposal to determine $n(0)/N$ by means of a neutron scattering experiment was first made by Hohenberg and Platzman (1966).

This theory is in practice considerably oversimplified because it neglects the scattering of the helium atoms with one another, and also neglects any coherent scattering effects. The absence, in the experimental results, of a sharp peak from scattering by the particles in the zero momentum state has stimulated the development of several theories largely based on the moments.

Sears (1969, 1970) expressed the scattering function as a Gram–Charlier expansion in Hermite polynomials. For incoherent scattering the coefficients of this expansion may be obtained from the moments of the velocity distribution of the helium atoms in the ground state. Sears (1969) then showed that at large Q the leading term in the moments can be summed to give exactly the result of the impulse approximation (3.6). Secondly, he considered coherent effects and showed

that at large Q the leading terms are identical with those of the incoherent scattering function.

The impulse approximation is therefore valid at sufficiently large Q, but we have less knowledge about how large is sufficiently large. Hohenberg and Platzman (1966) estimated $Q > 25$ Å^{-1} for which it would be necessary to use neutrons with an energy of 1 eV. Sears (1971) suggested that 80 Å^{-1} might be required, which since it would necessitate an incident energy for the neutrons of 8 eV makes the experiment very formidable. It seems likely therefore that the direct observation of a sharp peak well resolved from the Doppler broadened peak may not be feasible. Several attempts have therefore been made to deduce $n(0)/N$ from the experimental results with the aid of plausible assumptions.

Puff and Tenn (1970) developed a model in which the scattering is divided into a part from the condensate and another part from the atoms with $\boldsymbol{p} \neq 0$. Both contributions were assumed to be of a gaussian form with the former having a width determined by the He–He scattering cross section. Harling (1971) fitted this model to his results and obtained $n(0)/N = 0{\cdot}088 \pm 0{\cdot}013$ where the error, which results entirely from counting statistics, is a lower limit. More recently Gibbs and Harling (1973) have included coherent scattering effects in the model and by so doing eliminated the small 1% frequency shift used in Harling's original analysis.

Kerr *et al* (1970) developed a model similar to the shielded potential model described in §6.1.4. Their model introduced two arbitrary functions which they obtained from the zero-, first- and third-moment theorems, and further made use of the distribution of particles $n(\boldsymbol{p})$ calculated by McMillan (1965), §6.2. They conclude that $n(0)/N \simeq 0{\cdot}06$.

Finally Gersch and Smith (1971) have used equation (3.6) directly with $n(\boldsymbol{p})$ as determined by McMillan (1965) and as modified by Reatto and Chester (1967), see §6.2. The peak from the condensate was assumed to be broadened by the He–He scattering for which the cross section was taken to be twice as large as by Puff and Tenn (1970). They emphasize that the shape of $S(Q, \omega)$ differs considerably from a gaussian due to the nongaussian shape of $n(\boldsymbol{p})$. They find that Harling's data is best described by $n(0)/N = 0{\cdot}06$.

In the absence of a distinct peak, the best evidence for the existence of the condensate is probably contained in the temperature dependence of the widths of the distributions as a function of temperature (figure 17). The variation above the λ point is very slight, as expected, since the dominant contribution to the widths comes from the zero point motion. Below the λ point the width decreases much more rapidly and, at 5·1 Å^{-1} at least, shows little variation below 2·0 K. This is precisely the behaviour one would expect if the component reflecting the condensate had a finite energy width but was significantly narrower than the Doppler broadened component and if the value of $n(0)/N$ varied rapidly just below the λ point. As pointed out by Puff and Tenn (1970) the temperature variation of the widths reflect changes in the average kinetic energy. This is undoubtedly correct and expresses the inter-relationship between various macroscopic phenomena near the λ point. It does not, however, lead to a microscopic description of the observation and is irrelevant to any explanation in terms of the condensate.

Cowley and Woods (1971) deduced that $n(0)/N = 0{\cdot}17 \pm 0{\cdot}10$ on the assumptions that the distribution of particles with nonzero momentum, both below and above the λ point, was that given by McMillan (1965) and that the distribution of scattering from the particles in the condensate was of lorentzian form. The

neutron distributions were calculated for various values of $n(0)/N$ and for different widths of the lorentzian, and comparison of these curves with the observed ones suggested that $n(0)/N$ was in the range 0·07 to 0·27.

It is important to realize that all of these estimates for $n(0)/N$ depend strongly on the model used to describe the scattering and on the assumed shapes for the various distributions. All estimates are therefore tentative and the quoted errors have little significance.

3.6.3. *Analysis of high Q results.* Figure 16 illustrates that the high Q results consist of single peaks which are very nearly characteristic of scattering by a gas of free particles but, in addition, there are oscillations in shifts and widths. Sears (1970) extended his theory to account for these oscillations. He proposed approximate expressions for the first four moments of the coherent scattering function at large Q by considering the moments of the incoherent function and the high temperature limits of the coherent function. He then used his results and McMillan's (1965) calculation of $n(\boldsymbol{p})$ to calculate $S(Q, \omega)$ from the first five terms of the Gram–Charlier series. The results show oscillations in the width and position similar to those observed experimentally but both the magnitude and phase of the calculated oscillations are in error.

Fernandez and Gersch (1969) attributed this oscillatory behaviour to the effect of the hard core repulsion between helium atoms. In their model the interaction was cut off abruptly at the edge of the hard core giving rise to spurious oscillations at large Q. The real potential has no such singularity and hence their explanation of the oscillations is probably spurious.

Kerr *et al* (1970) also obtained oscillations from their model but the discrepancy with experiment is rather larger than in the calculations of Sears (1970). It is interesting that the oscillations arise from coherent interference phenomena and are exhibited at large Q in these dynamical properties but not in the static structure factor. Calculations of $S(Q, \omega)$ at large Q on microscopic models by Sunakawa *et al* (1970) and by Jackson (1969) are described in § 6.3.3.

The shift of the peak position from the free particle value suggests that if the first-moment theorem is correct, and there is no reason to doubt this, the peak must be asymmetrical with extra intensity on the high energy side and cannot, therefore, be exactly described by a gaussian or any other symmetrical function. This is reasonable in view of the result (quoted in Sears 1969) that the odd moments of the scattering about the recoil energy position, which will vanish for a symmetrical distribution, depend on interatomic forces which are not zero except for a perfect gas.

Harling (1971), Gibbs and Harling (1973) and Sears (1970) have made calculations of the temperature variation of the average kinetic energy per atom from the neutron scattering results and conclude that they are consistent with values derived from thermodynamic data.

4. Ultrasonic measurements

4.1. *Experimental techniques*

The propagation of ultrasonic waves in liquid helium has been studied by many workers ever since the pioneering work of Findlay *et al* (1938) and of Pellam and Squire (1947). The basic principle behind most of the measurements is that an

ultrasonic wave is generated and then detected after it has traversed a known distance in the liquid helium. The transit time and the decay then give the velocity and attenuation of the wave in the helium. Despite the similarity in principle between the different experiments, a variety of different techniques have been devised to overcome the considerable difficulties which arise if the results are to be of the high precision needed to test current theoretical predictions. Of the recent measurements those of Barmatz and Rudnick (1968) near the λ point and those of Abraham *et al* (1969) and Roach *et al* (1972b) at low temperatures are particularly detailed and extensive.

Barmatz and Rudnick (1968) used two transducers in a cylindrical cavity containing liquid helium under carefully controlled conditions of temperature and pressure. Ultrasonic waves were generated by the drive transducer, and the signal from the pick-up transducer fed through an amplifier and phase shifter into a generator which produced the initial ultrasonic signal. By adjustment of the amplifier and phase shifter the system was made to resonate with a resonant mode of the cavity, which may then be followed as the temperature of the helium is varied. With this technique velocity changes could be measured with an accuracy of 1 part in 10^5, and by measuring the Q factor of the resonance the attenuation could be obtained with an absolute accuracy of about 15%. All of the measurements were obtained using an ultrasonic frequency of 22 kHz and a temperature stability of 2×10^{-6} K.

In the low temperature measurements of the group at the Argonne National Laboratory the helium was cooled either by adiabatic demagnetization (Abraham *et al* 1969), or more recently with a ^{3}He–^{4}He dilution refrigerator (Roach *et al* 1970). In many of their measurements two quartz transducers are placed in the liquid helium to generate and detect the ultrasonic waves. A continuously running oscillator may feed power either into the helium bath or into a line consisting of an attenuator and delay. The switching is under the control of two RF switches. In one technique the power is fed alternately into the two lines and the resulting pulses compared. Adjustment of the delay and attenuator to give the same signal from both lines then enabled the velocity and attenuation of the ultrasonic wave in the helium to be obtained. In the other technique the two switches were activated nearly in phase with one another, and the attenuator and delay adjusted to give destructive interference between the two signals. Using these techniques the attenuation has been measured from 17 mK to 2·0 K with pressures between 0 and 25 atm and with frequencies between 12 and 256 MHz.

Recently this group has employed a modified technique to measure accurately the change in velocity with frequency at low temperatures. The helium cell used is shown in figure 18 and the electrical system was modified to generate synchronized 30 MHz and 90 MHz waves. The ultrasonic waves are generated in the helium by the quartz transducer and then detected after reflection from the reflecting surface. The reflecting surface is carried on a quartz block which slides accurately under the influence of the helium in the pressurizing chamber. By moving the reflecting surface the path length of the ultrasonic waves may be varied, and hence any difference in the velocity between 30 MHz and 90 MHz observed with a fractional accuracy of 2×10^{-6}.

Two other techniques have also been used to measure properties at higher frequencies. Woolf *et al* (1966) set up ultrasonic waves in liquid helium with frequencies of 556 and 723 MHz. The resulting density fluctuations of the liquid

were used as a diffraction grating for an incident laser beam. The angle of deflection of the laser beam, and its width, provided a measure of the wavelength and attenuation of the ultrasonics.

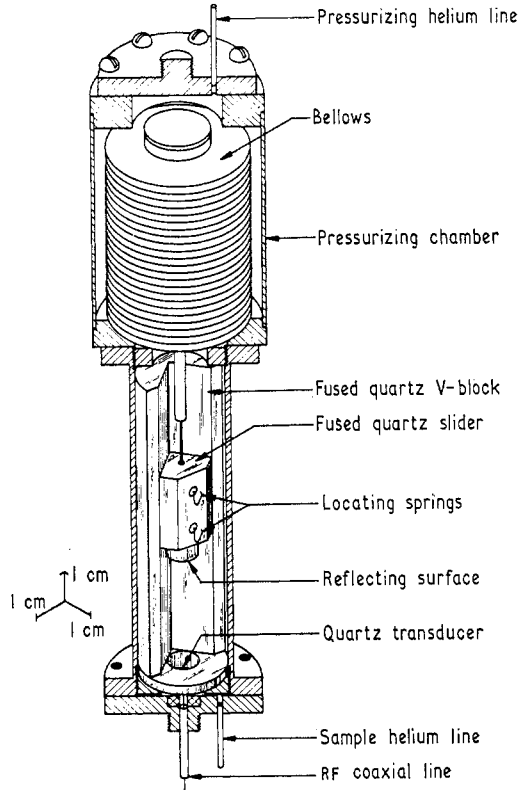

Figure 18. The cavity containing the liquid helium in the experiments of Roach *et al* (1972a).

Anderson and Sabisky (1972) have used a thin film technique to measure the frequency at 20–60 GHz. The ultrasonic waves were generated in SrF_2, doped with paramagnetic Tm, which had a helium film absorbed on a cleaved surface. Interferometric techniques were used to determine the phase shift introduced by the helium film. The phase shift was assumed to arise partly from the transit time of the ultrasonics in the film, and partly from a phase shift at the SrF_2 helium interface. Analysis of the results for different frequencies and film thicknesses enabled them to determine the velocity as a function of frequency at 1·38 K.

4.2. *Experimental results*

The temperature dependence of the velocity of sound and the attenuation in liquid helium is shown schematically in figure 19. The attenuation has two maxima; one at the λ point and the other at about 0·8 K. The velocity also has a slight maximum at 0·8 K, but a minimum at the λ point before increasing to a maximum at about 2·5 K.

A detailed study of the behaviour of both the attenuation and velocity near the λ point was reported by Barmatz and Rudnick (1968). In figures 20 and 21 are

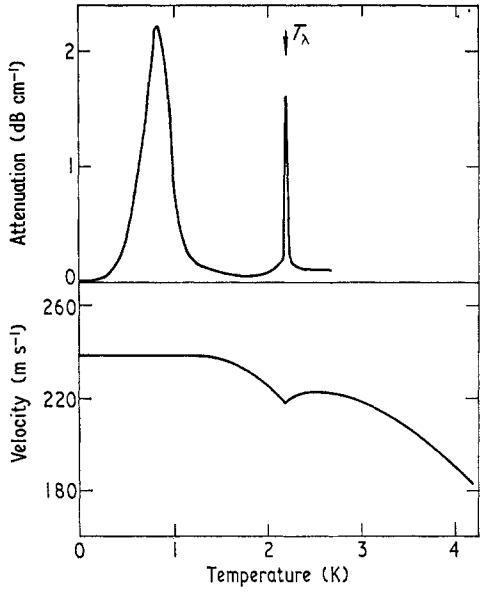

Figure 19. The temperature dependence of the ultrasonic attenuation and velocity at 2 MHz in liquid helium.

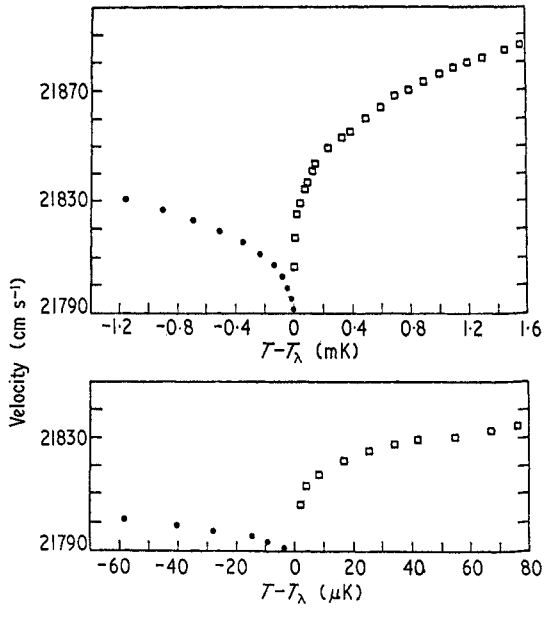

Figure 20. The ultrasonic velocity at 22 kHz in two temperature regions close to T_λ. From Barmatz and Rudnick (1968).

shown some of their results. Both the change in the velocity and the peak in the attenuation are assumed to arise from the fluctuations occurring near the λ point. Pippard (1951) suggested that the attenuation above the λ point arises because there are small inclusions of He II in the He I. These inclusions become larger and more numerous as the λ point is approached, and consequently more effective at scattering the sound waves. Landau and Khalatinikov (1954) developed the theory by use of the mean field or Landau (1937) theory of phase transitions. The experimental results are only qualitatively described by this theory since it fails to include

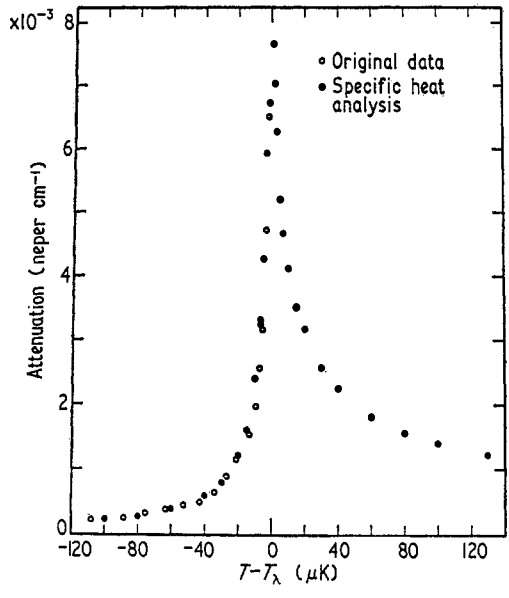

Figure 21. Temperature dependence of the attenuation at 22 kHz with the background attenuation corrected. (1 neper = 8·686 dB.) The temperature in the specific heat analysis was determined using a constant heat input and calculating the temperature from the known specific heat. From Barmatz and Rudnick (1968).

the effects of the short range correlations. More recently the dynamical scaling theory of phase transitions has been applied to this problem by Ferrell *et al* (1967) and by Swift and Kadanoff (1968). This theory gives better agreement with the measurements, but is still not entirely satisfactory. Since it is beyond the scope of this review to discuss critical phenomena in detail, we refer the interested reader to the original papers for a fuller description of both the experimental and theoretical results.

The peak in the velocity and attenuation at about 0·8 K has been studied by Chase (1953), Chase and Herlin (1955), Whitney (1956), Newell and Wilks (1956), Dransfeld *et al* (1958), Jeffers and Whitney (1965) and Waters *et al* (1967), but the most complete measurements have been reported by Abraham *et al* (1969) and by Roach *et al* (1972b). These latter two papers give their results both in pictorial and tabular form. Measurements have been made of both the frequency and temperature dependence of the attenuation at the saturated vapour pressure. The temperature dependence of the attenuation is shown in figure 22. At low temperatures the results show that the attenuation is nearly proportional to T^4. The

frequency dependence of the attenuation is shown in figure 23 for various temperatures. At low temperatures the attenuation increases approximately linearly with frequency; at intermediate temperatures ($\sim 1{\cdot}0$ K) the behaviour is complex, while at higher temperatures the attenuation varies as the square of the frequency.

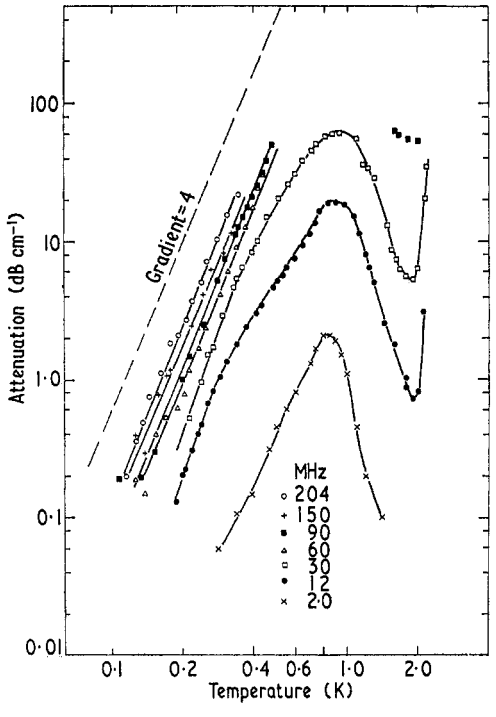

Figure 22. The temperature dependence of the attenuation for various frequencies at saturated vapour pressure. The data were taken from Abraham *et al* (1969) except that at 2 MHz which are from Jeffers and Whitney (1965) and Chase and Herlin (1955).

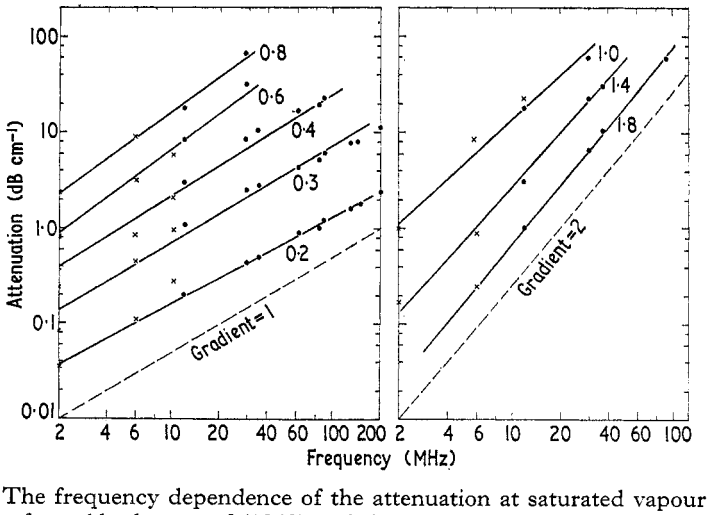

Figure 23. The frequency dependence of the attenuation at saturated vapour pressure. The circles are from Abraham *et al* (1969) and the crosses from Jeffers and Whitney (1965).

The pressure dependence of the attenuation is shown in figure 24. At low pressures the attenuation varies as T^4, at higher pressures it has a similar behaviour at very low temperature but there is also a shoulder where the attenuation is almost linear in temperature, after which the attenuation rises more steeply again. As the pressure is increased the temperature at which the shoulder appears decreases, until at the highest pressures the attenuation is very small below 0·6 K.

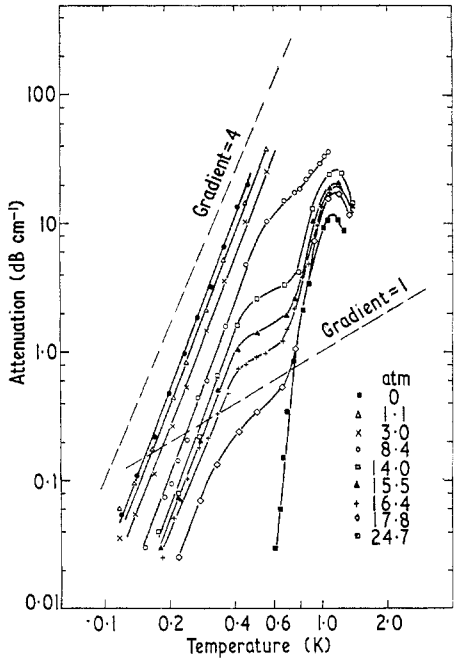

Figure 24. The temperature dependence of the attenuation for various pressures at 45 MHz from Roach *et al* (1972*b*).

The behaviour of the temperature dependence of the velocity at low temperatures is shown in figure 25. Initially the velocity increases with increasing temperature, in a manner which is not very dependent upon frequency, and then decreases. The pressure dependence of the velocity, Gruneisen constant and density at 0·45 K was obtained by Abraham *et al* (1970), and the results are shown in figure 26. The velocity and density increase with increasing pressure, but the Gruneisen constant decreases.

More recently Roach *et al* (1972a) have measured the frequency dependence of the velocity in liquid helium below 60 mK, with improved accuracy. If the dispersion relation at that temperature is written as

$$\omega(q) = cq(1+\alpha_1 q)$$

then they find

$$\alpha_1 = 0 \pm 0{\cdot}01 \text{ Å}.$$

In contrast the measurement of Anderson and Sabisky (1972) at higher frequencies, 30 GHz instead of 30 MHz, and at higher temperatures, 1·38 K, gave $\alpha_1 = 0{\cdot}275 \pm 0{\cdot}030$ Å. It is at present unknown whether this difference results from

the very different conditions of temperature and frequency in the two experiments, or whether Anderson and Sabisky's technique using thin films does not give results which are representative of the properties of the bulk material. Certainly the results of Roach *et al* (1972a) are more in accord with theoretical expectations.

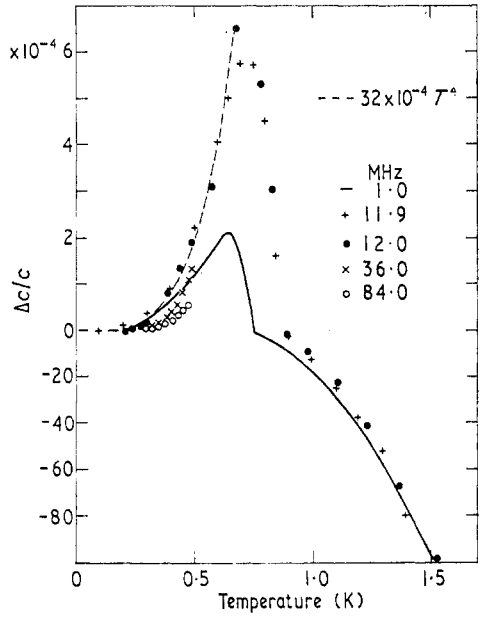

Figure 25. The temperature dependence of the velocity of sound at various frequencies at saturated vapour pressure. The results at 1 and 11·9 MHz are from Whitney and Chase (1967) and the others from Abraham *et al* (1969).

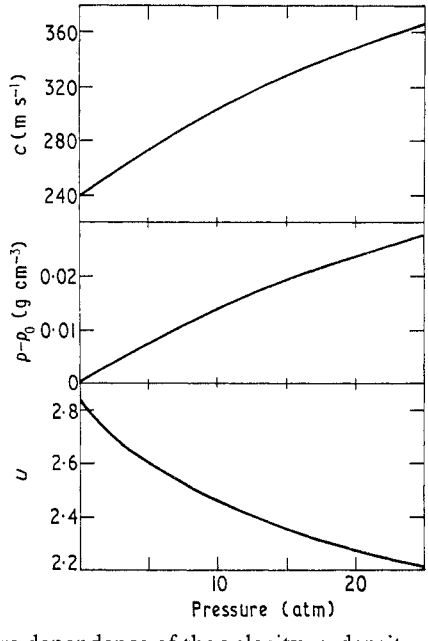

Figure 26. The pressure dependence of the velocity, c, density, $\rho - \rho_0$, and Gruneisen constant, $u = (\rho/c)\,(dc/d\rho)$, at 0·45 K. From Abraham *et al* (1970).

4.3. *Theoretical analysis*

In this section we discuss the origin and theory of the peak in the ultrasonic attenuation at about 0·8 K. At very low temperatures the excitations in liquid helium have a lifetime, τ, which is very long, in fact sufficiently long that the frequency of an ultrasonic wave, ω, is such that $\omega\tau \gg 1$. Under these conditions the ultrasonic wave propagates in an almost collisionless manner, only occasionally scattering off a thermal excitation. At higher temperatures the lifetimes of the excitations become much shorter so that $\omega\tau \ll 1$ for ultrasonic frequencies. The ultrasonic wave then propagates thermodynamically with many collisions of the excitations within each period of the ultrasonic wave. The peak in the attenuation arises when $\omega\tau = 1$, and the ultrasonic wave is then strongly scattered by the thermally excited excitations. This transition from collisionless to thermodynamic behaviour is a testing ground for theories about the establishment of thermodynamic equilibrium and thus, in liquid helium, has attracted a great deal of experimental and theoretical work. Initially it was hoped that the theory would be much simpler than for solids; there is one isotropic branch of the dispersion relation instead of three anisotropic branches, but, as we shall see later, liquid helium has proved to have its own peculiar difficulties. In the first part of this section we shall describe the theories developed for $T < 0{\cdot}6$ K, where the rotons do not play a role. In the second part we describe the theory needed to include the effects of rotons.

4.3.1. *Attenuation below* 0·6 K. Below 0·6 K the ultrasonic attenuation arises entirely from the collisions between the ultrasonic wave and thermally excited phonons, which are then scattered with conservation of energy and momentum. The simplest process is that discussed by Pethick and ter Haar (1966) in which an ultrasonic wave with frequency ω and wave vector $\boldsymbol{q}$ collides with a thermally excited phonon of wave vector $\boldsymbol{q}_1$ and frequency ω_1, to give a phonon of wave vector $\boldsymbol{q}_2$ and frequency ω_2. Conservation of energy and momentum then gives:

$$\left.\begin{aligned} \boldsymbol{q}+\boldsymbol{q}_1 &= \boldsymbol{q}_2 \\ \omega+\omega_1 &= \omega_2. \end{aligned}\right\} \tag{4.1}$$

In the case of ultrasonic waves, ω is at most about 100 MHz, whereas thermally excited phonons at 0·5 K have a frequency of 10 GHz. The wave vector $\boldsymbol{q}$ and frequency ω are therefore for the most part much less than $\boldsymbol{q}_1$ and ω_1.

In this temperature region we expect that $\omega\tau > 1$, where τ is the lifetime of the thermal phonons but it is reasonable to expect that the lifetime of the thermal phonons will play an important role. This lifetime relaxes the conservation of energy condition (4.1) by an extent determined by this lifetime. The imaginary part of the self-energy of the ultrasonic phonon may now be calculated by second-order perturbation theory to give

$$\Gamma(\boldsymbol{q},\omega) = \frac{36}{\hbar^2}\sum_{\boldsymbol{q}_1} |V(\boldsymbol{q},\boldsymbol{q}_1,-\boldsymbol{q}_2)|^2 \frac{(\Gamma_1+\Gamma_2)(n_1-n_2)}{(\omega+\omega_1-\omega_2)^2+(\Gamma_1+\Gamma_2)^2} \tag{4.2}$$

where Γ_1 and Γ_2 are the imaginary parts of the self-energy $\Gamma(\boldsymbol{q}_1,\omega_1)$ and $\Gamma(\boldsymbol{q}_2,\omega_2)$ for the modes 1 and 2 respectively, or equivalently the inverse of their lifetimes, while the coupling coefficient is $V(\boldsymbol{q},\boldsymbol{q}_1,-\boldsymbol{q}_2)$, and n_1 and n_2 are the Bose occupation numbers.

Since $\boldsymbol{q}_1$ and $\boldsymbol{q}_2$ are much larger than the ultrasonic wave vector, $\boldsymbol{q}$, we may put $\Gamma_1 = \Gamma_2$ and $\omega_1 - \omega_2 = -c_1 q \cos\theta$, where θ is the angle between $\boldsymbol{q}_1$ and $\boldsymbol{q}$, and c_1 is the group velocity of the excitations with wave vector $\boldsymbol{q}_1$; $c_1 = (\partial\omega/\partial q)|_{q=q_1}$. Furthermore since $\omega\tau > 1$ and $\tau = 1/\Gamma_1$, while the velocity c_1 is almost independent of wave vector, the largest contribution to equation (4.2) occurs, for $\omega = cq$ when $\cos\theta = 1$. $\boldsymbol{q}$, $\boldsymbol{q}_1$ and $\boldsymbol{q}_2$ are all nearly parallel to one another. The coefficients are then identical whether we use the hydrodynamic approach of Khalatnikov (1965) or the phonon approach of Wehner and Klein (1969a), and are given by

$$V(\boldsymbol{q}, \boldsymbol{q}_1, -\boldsymbol{q}_2) = \left(\frac{\hbar^3 q q_1 q_2 c}{72 v \rho}\right)^{1/2} (u+1)$$

where v is the volume of the liquid of density, ρ, and u is the Gruneisen constant, $(\rho/c)(\mathrm{d}c/\mathrm{d}\rho)$. The imaginary part of the self-energy, equation (2.2), may be rewritten as

$$\Gamma(\boldsymbol{q}, \omega) = \left(\frac{\hbar}{2\pi}\right)^2 \frac{qc(u+1)^2}{2\rho k_\mathrm{B} T} \int_0^\infty n_1(n_1+1)\, q_1^4 \int_0^\pi \frac{2\Gamma_1 \sin\theta\, \mathrm{d}\theta}{(\omega - c_1 q \cos\theta)^2 + 4\Gamma_1^2}\, \mathrm{d}q_1$$

where we have used the fact that $\boldsymbol{q}_1$ and $\boldsymbol{q}_2$ are much larger than $\boldsymbol{q}$ and expanded $n_1 - n_2$ in terms of $\boldsymbol{q}$.

The integration over θ may be performed explicitly to give

$$\Gamma(\boldsymbol{q}, \omega) = \left(\frac{\hbar}{2\pi}\right)^2 \frac{(u+1)^2 qc}{2\rho k_\mathrm{B} T} \int_0^\infty n_1(n_1+1)\, q_1^4 \times \left\{\tan^{-1}\left(\frac{\omega}{\Gamma_1}\right) - \tan^{-1}\left(\frac{q(c_0 - c_1)}{2\Gamma_1}\right)\right\} \mathrm{d}q_1. \tag{4.3}$$

In the usual development of the analysis further approximations are made. The maximum of $n_1(n_1+1)\, q_1^4$ occurs when $q_1 = 3k_\mathrm{B} T/\hbar c_1$ and the term in curly brackets is replaced by its value for this particular q_1 namely

$$\bar{\Gamma} = \Gamma_1 \quad \text{and} \quad \bar{c} = c_1 \quad \text{with } q_1 = 3k_\mathrm{B} T/\hbar c_1.$$

The integral over $\mathrm{d}q_1$ may then be performed if n_1 is replaced by its exponential approximation to give the attenuation, $\alpha = \Gamma(\omega/c_0, \omega)/c$, as

$$\alpha = A\omega T^4 \frac{2}{\pi}\left\{\tan^{-1}\left(\frac{\omega}{\bar{\Gamma}}\right) - \tan^{-1}\left(\frac{\omega(c_0 - \bar{c})}{2c_0 \bar{\Gamma}}\right)\right\} \tag{4.4}$$

where

$$A = \frac{3k_\mathrm{B}^4 (u+1)^2}{2\pi\hbar^3 c^6 \rho}. \tag{4.5}$$

Wehner and Klein (1969b) and Abraham *et al* (1969) obtain a numerical factor of $\pi^3/60$ (ie 0·51) which is slightly different from our $3/2\pi$ (ie 0·48). This difference is not of great importance, but we are unable to reproduce their result.

This result is expected to be most satisfactory when $\omega \gg \bar{\Gamma}$. The first term in the curly brackets of equation (4.4) then gives $\pi/2$ but the second term depends upon the sign of $c_0 - \bar{c}$. If the velocity decreases with increasing q, $\bar{c} < c_0$; then at large ω this term cancels the first term. If there is no dispersion $c = c_0$ the second term is

zero, while if there is anomalous dispersion, the term contributes $\pi/2$. In short we expect

$$\alpha = A\omega T^4 \times \begin{cases} 0 & \text{when } \bar{c} < c_0 \\ 1 & \text{when } \bar{c} = c_0 \\ 2 & \text{when } \bar{c} > c_0. \end{cases}$$

In figure 22 we showed the temperature dependence of the attenuation at the saturated vapour pressure; the results at low temperatures clearly vary approximately as T^4. In figure 23 we showed the frequency dependence of the attenuation at low temperatures; again the frequency dependence is in approximate agreement

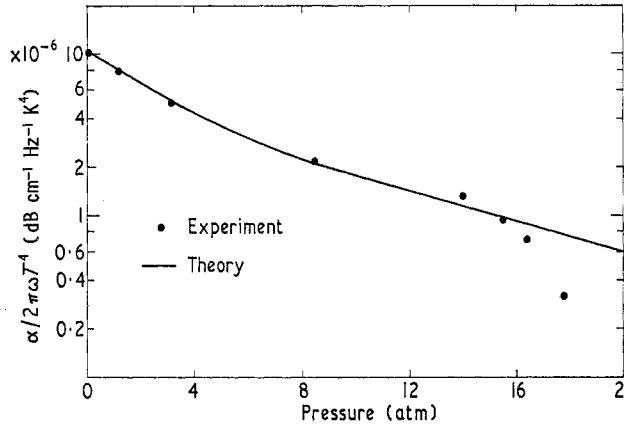

Figure 27. Attenuation $\alpha/2\pi\omega T^4$ as determined from the results of Roach *et al* (1972b) and figure 24 and compared with the calculated value of $2A$ from the data of Abraham *et al* (1970) and figure 26.

with the theory. In figure 27 we show the pressure dependence of the coefficient $2A$ as determined by the experimental results, and as determined by equation (4.5) using the pressure dependent ρ, c and u measurements given in figure 26. The results are in excellent accord with theory up to 16 atm provided that we assume anomalous dispersion (Maris and Massey 1970), namely that $\bar{c} > c_0$.

Specific heat measurements of Phillips *et al* (1970) also suggest that the dispersion is anomalous at low pressures and becomes normal at high pressures, as described in §§ 3.3.2 and 3.4.1.

In the pressure dependent measurements shown in figure 24, the T^4 region occurred only at the lowest temperature, and there was a region in which the behaviour was almost linear in temperature. An explanation of these results was put forward by Jackle and Kehr (1971a). Their suggestion is that as q_1 varies in equation (4.3) the velocity c_1 varies in such a way that at small q_1 it is larger than c_0, but when q_1 is greater than some wave vector q_c, c_1 becomes smaller than c_0. Since the attenuation for large ω is zero when $c_1 < c_0$, the integral in equation (4.3) should be cut off at q_c and not at infinity. They suggest that when $\omega > \bar{\Gamma}$ the attenuation is given by

$$\alpha = 2A\omega T^4 F(q_c)/F(\infty) \tag{4.6}$$

where

$$F(q_c) = \int_0^{q_0} \mathrm{d}q_1\, q_1^4\, n_1(n_1+1).$$

In the limit when $k_B T > cq_c$ the attenuation becomes

$$\alpha = \frac{A}{36} \frac{\hbar c q_c^3}{k_B} \omega T.$$

A linear temperature dependence is shown in figure 24 for the shoulder at various frequencies. By fitting equation (4.6) to the experimental results Jackle and Kehr deduce that q_c decreases as the pressure increases from 14 atm to 19 atm, as shown in figure 28. Below 14 atm no plateau occurs because q_c is sufficiently large that the phonons with $q_1 > q_c$ are not thermally excited, while at the highest pressure the

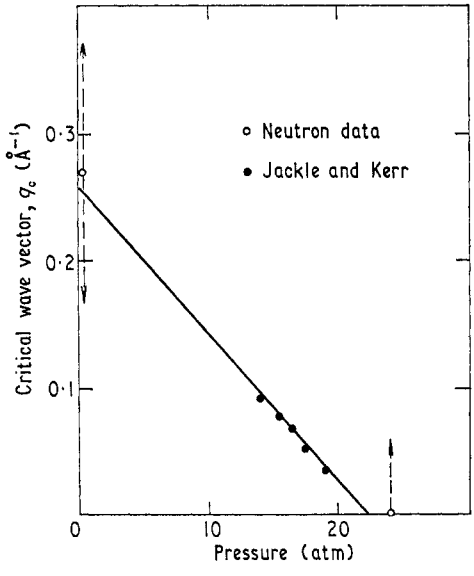

Figure 28. The pressure dependence of q_c from Jackle and Kehr (1971a) and from the neutron data of Svensson *et al* (1972).

attenuation below 0·6 K is negligible, suggesting that c_1 is less than c_0 for all thermally excited phonons. These conclusions are in excellent accord with the neutron scattering results of Svensson *et al* (1972) as described in §3.4.1 and figure 12. Clearly the wave vector at which the slope of the dispersion curve becomes equal to c_0 decreases with increasing pressure and in figure 28 we show the values for q_c obtained from neutron scattering results at 0 and 24 atm. These results were obtained from figure 12 by assuming that q_c was one half the wave vector for which the phase velocity $\omega(q)/q$ was equal to c_0. Despite this very crude approximation, the large errors on the neutron scattering measurements, and the uncertainties of the theory, the agreement between these values of q_c is very good. We may conclude therefore that the three-phonon scattering process is indeed responsible for the ultrasonic attenuation below 0·6 K, and that the dispersion curve initially shows anomalous dispersion, but that at small wave vectors, which decrease with increasing pressure, the phonon phase velocity decreases to a value below that for the ultrasonic waves.

Although this agreement is very satisfactory it is of a largely qualitative nature. When a quantitative comparison is attempted two further difficulties arise. These

are illustrated in figure 29 where we show the ultrasonic attenuation divided by $2A\omega T^4$ for 36 MHz. It is seen that equation (4.4), curve A, necessarily predicts that $\alpha/2A\omega T^4$ is always less than unity whereas experiment shows that initially at least it increases above unity as T increases.

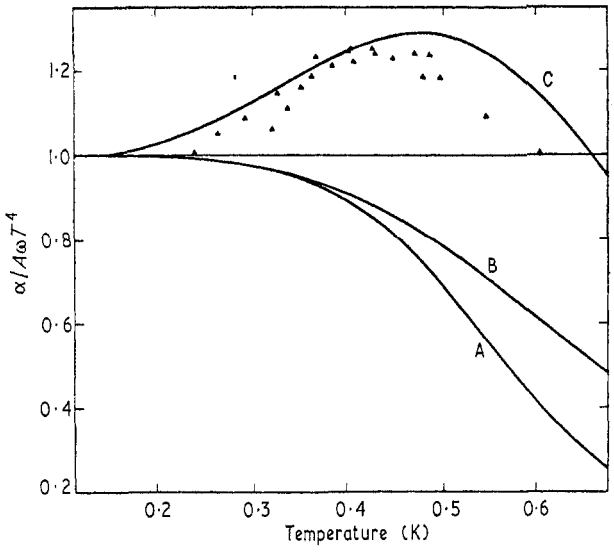

Figure 29. Theoretical and experimental results for the attenuation at 36 MHz. The experimental data are from Abraham *et al* (1969) and $A = 1{\cdot}7 \times 10^{-7}$ CGS units and the curves are three theoretical predictions: curve A, bubble diagram with $\bar{\Gamma}$; curve B, bubble diagram with Γ_1; curve C, lowest order vertex correction. From Wehner and Klein (1969b).

There are two approximations made in the derivation of equation (4.4) which might be responsible for this discrepancy. Firstly, it was derived from equation (4.3) by replacing Γ_1 by $\bar{\Gamma}$. In principle Γ_1 may be calculated from equation (4.2) in the same manner as we obtained the ultrasonic attenuation but without assuming q is small compared with q_1. The second approximation is more difficult to treat because it questions the validity of equation (4.2). The ultrasonic phonon is scattered by a thermal phonon, but as shown by equation (4.1), energy and momentum conservation imply that the energy is in most cases still flowing in the same direction. It may, therefore, be scattered back into the ultrasonic wave. In contrast equation (4.3) assumes this energy is entirely dissipated after the first collision. Because of this Khalatnikov and Chernikova (1966a) have suggested that Γ_1 in equation (4.3) should not be the width from the three-phonon process, equation (4.2), but only that part of the width which arises from wide angle scattering processes. Disatnik (1967) suggested a phenomenological form for Γ_1 to take account of conservation of energy and momentum, and more recently Saslow (1972) has given a form for Γ_1 with which the theory at low frequency becomes identical with that obtained from hydrodynamics.

The perturbation theory which was used to derive equation (4.2) is invalid because the energy denominators are of order Γ_1, which is $O(V^2)$, so that for ultrasonic frequencies the contribution of the whole term is $O(V^2/V^2)$ namely $O(1)$, and the perturbation theory is not convergent. Sham (1967) discussed this problem in

detail for crystals and showed that the correct behaviour could be obtained only if the infinite set of ladder diagrams shown in figure 30 were included in the self-energy. The sum of this series is known as a vertex correction to the self-energy, and its inclusion is accomplished only by solving a complicated integral equation.

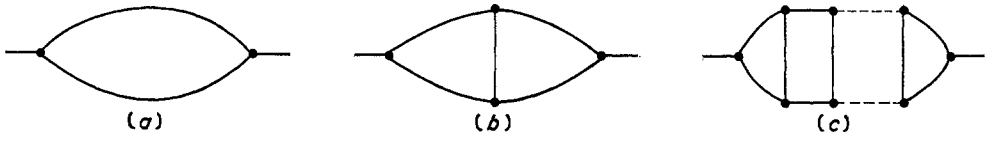

Figure 30. Schematic diagrams of the self-energy calculated with (*a*) the simple three-phonon scattering, (*b*) the first vertex correction and (*c*) the infinite series of terms.

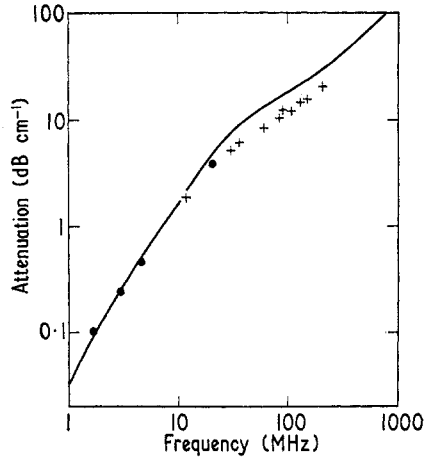

Figure 31. The frequency dependence of the ultrasonic attenuation at 0·35 K. The solid line is the calculation of Maris (1972) and the experimental data are taken from: ● Waters *et al* (1967); + Abraham *et al* (1969). From Maris (1972).

This problem was approached by Wehner and Klein (1969b) who assumed that the dispersion relation was linear

$$\omega(q) = c_0 q$$

and ended at the Debye cut-off of 1·09 Å. They calculated the attenuation using equation (4.4), curve A of figure 29 and by calculating the Γ_1 explicitly and using equation (4.3). The result, curve B of figure 29, shows that the change from $\bar{\Gamma}$ to Γ_1 makes a considerable difference to the results but that $\alpha/2A\omega T^4$ is still decreasing with increasing T. Curve C of figure 29 was obtained by calculating the first term in the infinite series for the vertex corrections, as in figure 30(b). The result is in excellent accord with the experimental results.

Recently this work has been extended by Maris (1972) who has assumed that the dispersion relation is given by

$$\omega(q) = c_0 q(1-\gamma q^2) \tag{4.7}$$

with $\gamma = -8\times 10^{37}\ \mathrm{g^{-2}\,cm^{-2}\,s^2}$, and has solved the integral equation for the vertex corrections selfconsistently. His results for the attenuation are shown in figure 31, and give very satisfactory agreement with experiment.

Unfortunately neither of these calculations are entirely convincing because of the assumed form of the dispersion relations. The pressure dependence of the attenuation demonstrates that beyond some critical wave vector q_c the velocity is less than c_0, and that this critical wave vector is comparable with those excited thermally. Consequently it is unreasonable to expect equation (4.6) to be a valid description of the dispersion relation over the region of interest. In particular Klein and Wehner (1971) have used equation (4.3) for the attenuation and calculated Γ_1 from equations (4.6) and (4.2). They suggest that the value of A determined from the pressure dependent attenuation cannot be compared with theory as we have done in figure 27, because at the temperature and frequency of the measurements the second term in curly brackets in equation (4.3) is small and not $-\pi/2$. At present we must treat this result with caution, both because of the unsatisfactory form of the assumed dispersion relation, and because of the failure to include the vertex corrections which may well make Γ_1 much smaller.

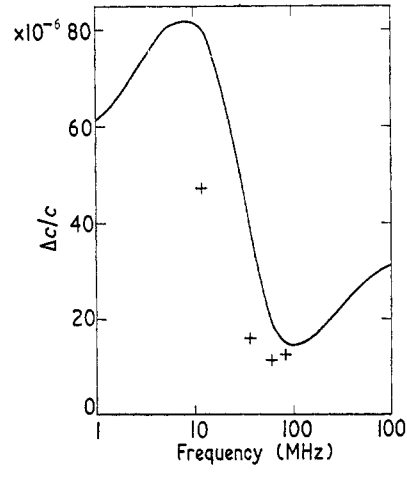

Figure 32. The theoretical frequency dependence of the velocity at 0·35 K compared with the data of Abraham *et al* (1969). From Maris (1972).

The theory of the change in velocity with temperature and frequency is similar to that of the attenuation. The result for the change in velocity equivalent to equation (4.4) is

$$\Delta c = Ac^2 T^4 \ln\left(\frac{1+(\omega/\bar{\Gamma})^2}{1+\{\omega(c_0-\bar{c})/2c_0\bar{\Gamma}\}^2}\right).$$

This result is in approximate agreement with the experimental results, figure 25, in that at low temperature and large ω, the results are largely independent of ω and vary approximately as T^4. In detail, however, there are discrepancies; in particular the theory predicts that c increases with increasing ω, whereas in practice, for frequencies greater that 12 MHz, it decreases. Cheung (1970) calculated the first-order vertex correction for the sound velocity using a linear dispersion relation and found this did not improve agreement with experiment, whereas Maris (1972), in his calculation in which he solved the integral equation and used the dispersion relation given by equation (4.7), obtained the curve shown in figure 32. Clearly the agreement is greatly improved.

In summary therefore, considerable progress has been made in understanding the ultrasonic properties of liquid helium below 0·6 K. The simple three-phonon process gives a qualitative account of the experimental results if we have anomalous dispersion at low wave vectors, and a critical wave vector beyond which the velocity is less than c_0. It has been shown that vertex corrections make an important change in the results but we must await detailed calculations of these corrections, based on a more realistic dispersion relation, before the situation is entirely satisfactory.

4.3.2. *Attenuation above* 0·6 K. In view of all the difficulties encountered in the theory of the ultrasonic attenuation below 0·6 K, it is not surprising that far less work has been done on the theory above 0·6 K. Above 0·6 K there are two difficulties which arise. Firstly, the perturbation theory we used in the previous section is valid only when $\omega\tau \gg 1$, and this no longer holds above 0·6 K. It is then necessary either to treat the vertex corrections in detail, or to solve the appropriate Boltzmann equation. The second difficulty is that below 0·6 K the theory could be developed ignoring the rotons, whereas above 0·6 K this is no longer adequate. Despite these difficulties Khalatnikov and Chernikova (1966b) have made immense progress in calculating the ultrasonic attenuation above 0·6 K. In this section we shall review their development in the light of our now more complete understanding of the low temperature properties and of the phonon–phonon scattering.

Khalatnikov and Chernikova introduce density distribution functions for both the phonons and the rotons. The kinetic equations for these distribution functions are Boltzmann equations describing the way these distributions vary in space and time. The most difficult part of the development is in describing the three scattering processes in which the phonons are scattered by each other, and by the rotons, and the rotons are scattered by other rotons.

The roton–roton scattering (Khalatnikov 1965) is described by an interaction which is a delta function of the distance between a pair of rotons. When two rotons interact they are scattered with conservation of energy and momentum into two other rotons. The roton–roton scattering time is then evaluated by integrating over all the rotons and the phase space of the scattered rotons, with the result

$$1/\tau_{\mathrm{RR}} = 1{\cdot}2 \times 10^{13}\, T^{1/2} \exp(-\Delta/k_{\mathrm{B}}\, T)\ \mathrm{s}^{-1}$$

where Δ is the roton energy and the strength of the roton–roton interactions is determined from viscosity measurements. We discuss roton–roton scattering in more detail in § 5.3.4.

The roton–phonon interaction is a scattering process whereby a phonon collides with a roton to give another roton of a different energy and wave vector. The interaction may be obtained from the pressure dependence of the roton energy, and leads to a phonon–roton scattering time of (Abraham *et al* 1969)

$$1/\tau_{\mathrm{PR}} = 1{\cdot}3 \times 10^{12}\, T^{9/2} \exp(-\Delta/k_{\mathrm{B}}\, T)\ \mathrm{s}^{-1}.$$

In their work on phonon–phonon scattering Khalatnikov and Chernikova (1966b) assumed that the dispersion relation was given by

$$\omega(q) = c_0\, q(1-\gamma q^2)$$

with γ positive. If the width of the phonons is neglected the three-phonon process, which was discussed in the previous section, cannot occur, and it is necessary to consider more complex scattering. All of the scattering processes tend to have small energy denominators when all the phonons are travelling in the same direction.

These processes then establish equilibrium amongst the phonons with parallel wave vectors but do not distribute the energy in different directions. Khalatnikov and Chernikova discuss four- and five-phonon scattering processes which lead to three different relaxation times. A four-phonon scattering, in which two phonons scatter to give two other phonons travelling in the same direction, establishes thermodynamic equilibrium among the phonons travelling in one direction, but does not alter the total number of phonons. It gives rise to a scattering time of

$$1/\tau_{\mathrm{PP}}^{(1)} = 1{\cdot}4 \times 10^8\, T^7\ \mathrm{s}^{-1}.$$

A five-phonon process, in which two phonons collide to give three phonons or three collide to give two, changes the number of phonons, and keeps the phonon number in equilibrium. It has a relaxation time of

$$1/\tau_{\mathrm{PP}}^{(2)} = 8 \times 10^7\, T^9\ \mathrm{s}^{-1}.$$

In both of these processes the largest contribution to the scattering arises when all the phonons have nearly parallel wave vectors. The scattering of the energy away from that direction is a slower process, and the contribution to the wide-angle scattering from the four-phonon process is

$$1/\tau_{\mathrm{PP}}^{(3)} = 3{\cdot}0 \times 10^7\, T^9\ \mathrm{s}^{-1}.$$

Since Khalatnikov and Chernikova used a dispersion relation with $\gamma > 0$, whereas in fact, at least at low pressures, the dispersion is anomalous, all of these relaxation times are in error. With the present lack of knowledge about the form of the dispersion relation at small q, however, it is not possible to recalculate the necessary results. Nevertheless, with the anomalous dispersion at small q the three-phonon process is allowed, and will both establish equilibrium among the phonons travelling in one direction and also keep the phonon number in equilibrium. The relaxation times $\tau_{\mathrm{PP}}^{(1)}$ and $\tau_{\mathrm{PP}}^{(2)}$ are both probably shorter and more similar to one another than the results given above. Jackle and Kehr (1971b) have calculated the three-phonon contribution to $1/\tau_{\mathrm{PP}}^{(1)}$ and $1/\tau_{\mathrm{PP}}^{(2)}$ as $7 \times 10^9\, T^5\ \mathrm{s}^{-1}$ using anomalous dispersion. Likewise it is to be expected that there will be an additional contribution to the wide-angle scattering rate. It is of interest that the wide-angle scattering rate deduced from heat conduction and heat pulse experiments by Jackle and Kehr (1971b) varies as T^5, and not as T^9 which is given by the theory with normal dispersion.

Khalatnikov and Chernikova then observe that below 1·2 K, $\tau_{\mathrm{PP}}^{(1)}$, $\tau_{\mathrm{PP}}^{(2)}$ and τ_{RR} are less than τ_{PR}. Both the phonon and roton distributions are therefore in thermodynamic equilibrium with a local space, direction and time dependent temperature. They solve the two coupled Boltzmann equations for these distributions with the aid of the equations of motion and continuity, to give the attenuation as

$$\alpha = \frac{\pi^2 k_{\mathrm{B}}^4 \omega T^4}{45\hbar^3 \rho^2 c^6}\, \mathrm{Im}\,(\Phi). \tag{4.8}$$

In this expression

$$\begin{aligned}\Phi = Z_{\mathrm{R}} - 3[\![u^2 \ln a + [2uZ_{\mathrm{R}} + Z_{\mathrm{R}}^2\{1-\beta(1-Z_{\mathrm{R}})\} + 3u^2(1-Z_{\mathrm{P}})] \\ \times\{-2+(Z_{\mathrm{R}}+Z_{\mathrm{P}}-1)\ln a\}]\!] \times [2+\{1-Z_{\mathrm{P}}+(1-\beta)(1-Z_{\mathrm{R}})\}\ln a \\ +3(1-Z_{\mathrm{P}})\{1-\beta(1-Z_{\mathrm{R}})\}\{-2\times(Z_{\mathrm{P}}-Z_{\mathrm{R}}-1)\ln a\}]^{-1}\end{aligned} \tag{4.9}$$

where

$$a = (Z_P + Z_R)/(Z_P + Z_R - 2)$$

$$\beta = 3k_B T/\mu c^2$$

$$Z_P = 1 - 1/i\omega\tau_{PP}^{(3)}$$

and

$$Z_R = 1 - 1/i\omega\tau_{PR}$$

while μ is the effective mass of the rotons.

This formula looks and is very complicated, but in the limit as $\omega\tau_{PP}^{(3)} \ll 1$, α is proportional to ω^2 whereas at high frequencies, α is proportional to ω. This is borne out by experiment as shown in figure 23.

At low temperatures $\tau_{PR} \gg \tau_{PP}^{(3)}$ and equation (4.8) reduces to equation (4.4) with the omission of the second term, and the replacement of $\bar{\Gamma}$ by $1/\tau_{PP}^{(3)}$. The omission arises because equation (4.9) was calculated neglecting the dispersion in the velocity, which can be easily included. The replacement of $\bar{\Gamma}$ by $1/\tau_{PP}^{(3)}$, the wide-angle relaxation time, arises because the Boltzmann equation approach includes the effect of the vertex corrections, at least approximately, as discussed in § 4.3.1.

Khalatnikov and Chernikova suggest that, above 0·9 K $\tau_{PR} \ll \tau_{PP}^{(3)}$ so that equation (4.8) may again be simplified. Since the three-phonon scattering gives rise to an additional contribution to $1/\tau_{PP}^{(3)}$ this may not be an appropriate approximation. Likewise, above 1·2 K they suggest that $\tau_{PR} \ll \tau_{PP}^{(2)}$ so that the phonon distribution in a given direction cannot reach equilibrium. They introduce a chemical potential for these phonons to allow for this, and deduce a new equation for α. The three-phonon scattering will reduce $\tau_{PP}^{(2)}$, however, so that this situation may not occur in practice, in which case equation (4.8) may be a better approximation throughout the whole temperature region than the use of Khalatnikov and Chernikova's results above 1·2 K.

In summary the theory of the ultrasonic properties of liquid helium above 0·6 K is a very complicated subject. Khalatnikov and Chernikova have, however, been successful in developing an exceedingly detailed theory, but the forms they have used for the phonon–phonon scattering and the roton–roton scattering (§ 5.3.4) are probably inadequate in the light of recent developments. There is a definite need for this part of the theory to be reworked and a detailed comparison made with the available experimental results.

5. Light scattering measurements

5.1. *Experimental techniques*

The principle behind the light scattering measurements is very similar to that of the neutron scattering measurements described in § 2 and is illustrated in figure 33. A beam of monochromatic light with wave vector, $\boldsymbol{k}_0$, frequency, ω_0 and plane of polarization, $\boldsymbol{E}_0$, is incident upon the liquid helium and scattered to produce a beam of wave vector, $\boldsymbol{k}_s$, frequency, ω_s, and polarization, $\boldsymbol{E}_s$. Conservation of wave vector and energy then gives the wave vector transfer and frequency transfer through the equations

$$\left.\begin{aligned} \boldsymbol{k}_0 - \boldsymbol{k}_s &= \boldsymbol{Q} \\ \omega_0 - \omega_s &= \omega. \end{aligned}\right\} \tag{5.1}$$

Since the wave vector of the light used in these experiments is typically about 10^{-3} Å^{-1}, it is only possible to satisfy equations (5.1) for the creation of single excitations if the excitations are phonons. In liquid helium the frequencies of these phonons are about 700 MHz and the scattering is known as Brillouin scattering. Alternatively the equations may be satisfied if the scattering occurs by the creation of two or more excitations in the helium. Since these excitations will usually have a wave vector considerably larger than 10^{-3} Å^{-1}, the wave vector transfer in these experiments may be taken as zero. This latter type of scattering is known as Raman scattering.

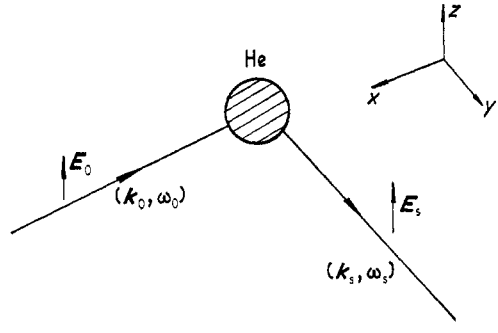

Figure 33. A schematic diagram showing a Raman scattering experiment in which the beam is incident along x, scattered along y and both electric vectors are polarized along z. This arrangement is denoted configuration (zz).

Both of these two types of scattering have been studied experimentally by a group at MIT (Greytak and Yan 1969, 1971, Greytak *et al* 1970) and by a group at RRE, Malvern and the University of Birmingham (Pike *et al* 1970, Pike and Vaughan 1971). Both of these groups have used essentially the same techniques. The monochromatic incident light was obtained from an argon ion laser and the scattered light was collected in an angular range of about 0·05 sr at 90° scattering. Two different approaches were used to detect the frequency change of the scattered light. For the Raman scattering measurements both groups have used a double grating spectrometer, while for the Brillouin scattering measurements and some high resolution measurements of the Raman scattering, a scanning Fabry–Pérot etalon has been used. The interferometric technique has the advantage of much greater accuracy, but the disadvantage that the different orders are all superposed. This difficulty does not occur with the grating spectrometer. Finally, the light is detected by a cooled photomultiplier with a dark count of as low as one count per second.

Considerable difficulty is experienced with scattered light, and the cell containing the liquid helium is carefully constructed to minimize the problem. Absorption of the laser power at dust particles may produce local boiling and hence scattering. This is reduced in the MIT experiments by filling the cell through a superfluid leak, and in the RRE experiments by pressurization to 1·45 atm and the use of low laser powers.

Optical techniques have also been used to detect the generation of first sound and second sound in liquid helium. The former experiments by Woolf *et al* (1966) were described in §4.1. The first sound was generated by ultrasonics and diffraction of a laser beam from the density fluctuations gave the velocity and

attenuation of the sound wave. A similar approach was used by Cunsolo *et al* (1971) to determine the velocity of second sound close to the λ point. In both of these experiments the results were in agreement with those obtained with more conventional techniques and will not be discussed further.

5.2. *Experimental results*

5.2.1. *Brillouin scattering.* The Brillouin scattering from liquid helium has been reported by Pike *et al* (1970) and Pike (1972) and some typical spectra are shown in figure 34. The peaks at finite frequency correspond to the scattering by the

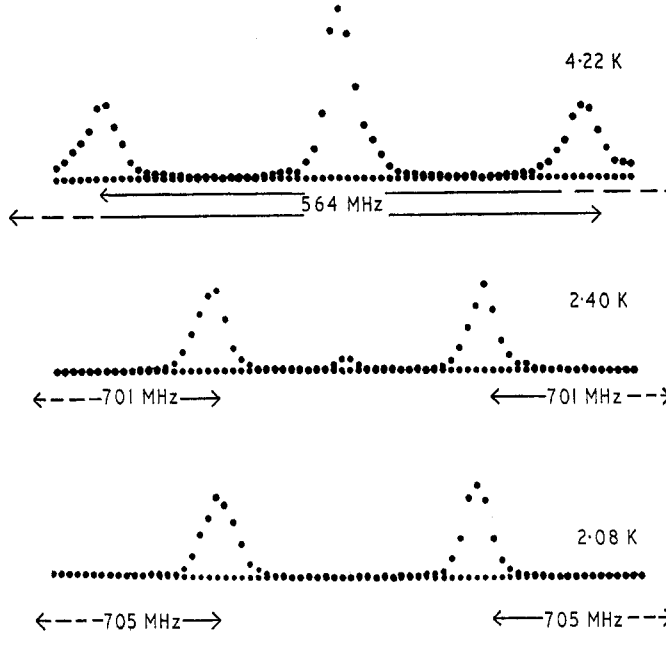

Figure 34. The Brillouin scattering spectrum of liquid helium at three temperatures. The incident laser frequency is at the centre and dispersion is about 5·8 MHz/channel. The Brillouin lines overlap about $1\frac{1}{2}$ orders of the interferometer. After Pike (1972).

sound waves and the centres of the peaks give the ultrasonic frequencies. In figure 35 we show the temperature dependence of these frequencies and the results are clearly in excellent accord with those obtained by ultrasonic techniques. Unfortunately the results are not of adequate precision to give detailed information comparable to that obtained with ultrasonic methods. The temperature dependence of the intensity of the scattering by the Brillouin lines is approximately proportional to temperature.

The peak in the centre of figure 34 arises from the scattering by the temperature fluctuations in the liquid. It is known as the Rayleigh scattering and above the λ point the scattering is quasi-elastic. The intensity of this scattering has been measured relative to that of the Brillouin lines and the results are shown in figure 36; the intensity of the Rayleigh component increases dramatically as the temperature is raised.

Below the λ point the temperature fluctuations propagate with the second sound velocity. As shown, however, in figure 34 the intensity at low pressures is very low and these fluctuations have not as yet been observed. The intensity, as described later, may be enhanced by performing the experiments at elevated

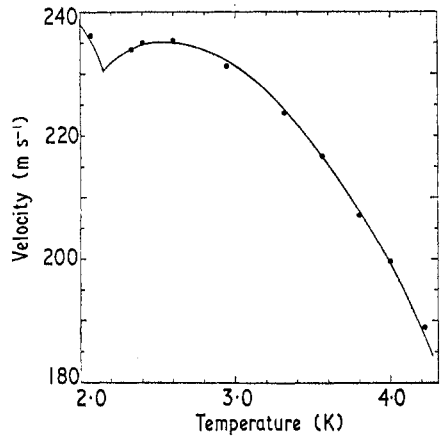

Figure 35. The velocity of first sound at a pressure of 1·4 atm. The points are from Brillouin scattering measurements by Pike (1972) and the full line is taken from ultrasonic measurements. From Pike (1972).

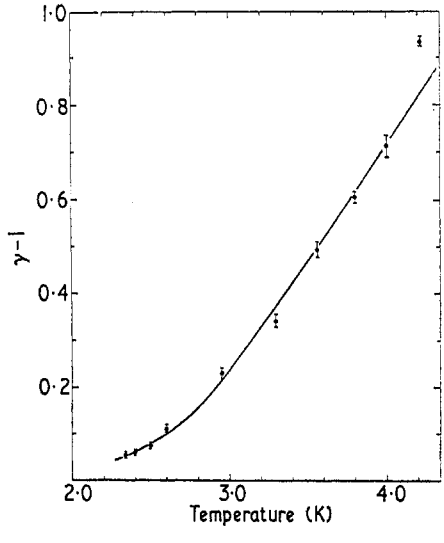

Figure 36. The ratio of the intensity of the Rayleigh to the Brillouin scattering (points) compared with $\gamma-1$ (where $\gamma = C_p/C_v$) derived from thermodynamic data (line) from Pike (1972).

pressures and second sound has been observed in this way by Greytak (1972 unpublished). Alternatively in a ^{3}He–^{4}He mixture the concentration fluctuations give rise to an enhancement of the second sound cross section (Gorkov and Pitaevskii 1958, Ganguly and Griffin 1968) and this has been observed by Palin *et al* (1971).

5.2.2. *Raman scattering.* The Raman scattering was first observed by Greytak and Yan (1969) and their results are shown in figure 37. At low temperatures there is a sharp peak at about 17 K above which there is a much smaller subsidiary maximum at 36 K and a long high frequency tail. Detailed measurements of the

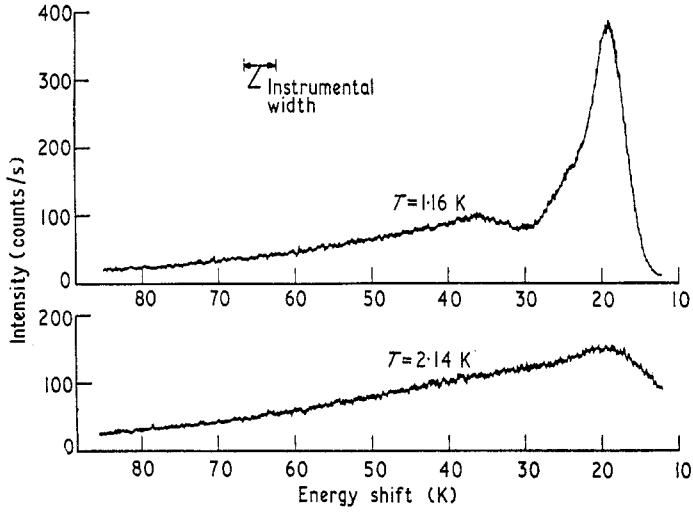

Figure 37. The Raman spectra of liquid helium at two temperatures. After Greytak and Yan (1969).

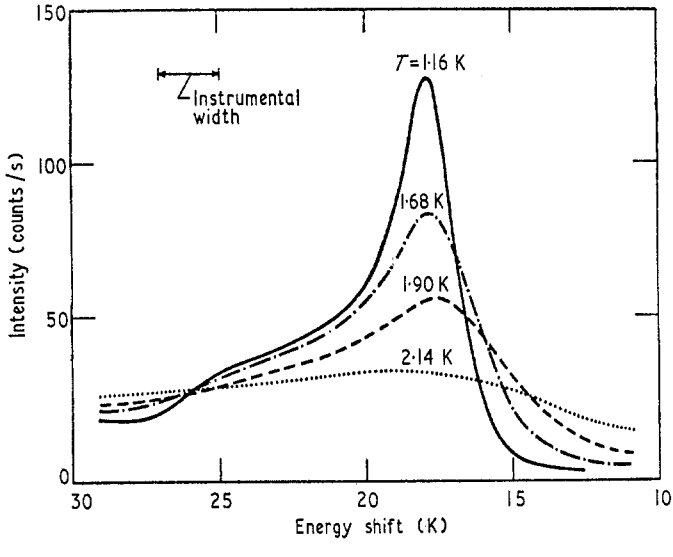

Figure 38. The temperature dependence of the two-roton peak in the Raman scattering from liquid helium. From Greytak and Yan (1969).

temperature dependence of the sharp peak are shown in figure 38 and the intensity is seen to decrease rapidly as the temperature is raised. Above the λ point the spectra, figure 39 (Pike and Vaughan 1971), have broad maxima at about 30 K. The detailed shape of the sharp peak at low temperatures was studied by Greytak

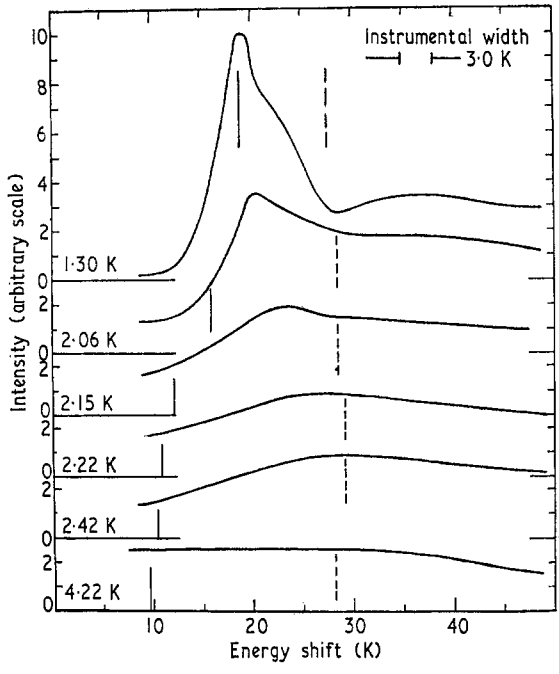

Figure 39. The temperature dependence of the Raman spectra in liquid helium at a pressure of 1·15 atm. The full vertical lines show the positions of twice the roton energy and the broken vertical lines twice the maximum energy of the dispersion curve. From Pike and Vaughan (1971).

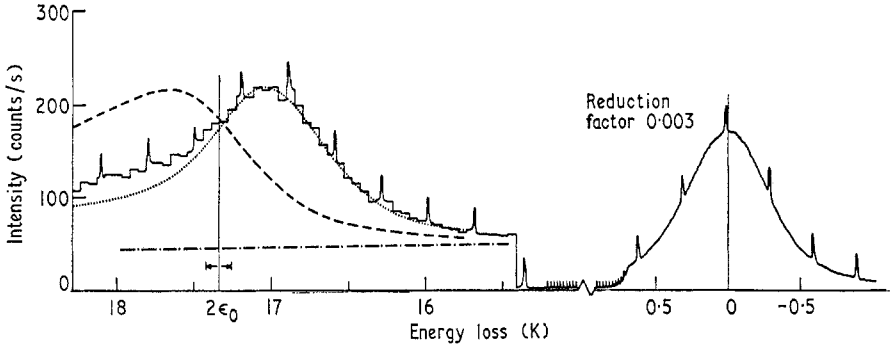

Figure 40. The Raman spectrum of liquid helium at 1·2 K. The strong peak at zero energy transfer is the Brillouin scattering. The dotted curve is a theoretical fit based on a model with roton–roton interactions and the broken line a similar model without these interactions. From Greytak *et al* (1970).

et al (1970) using interferometric techniques. Their results are shown in figure 40. The maximum in the spectrum was determined to be at $17{\cdot}022 \pm 0{\cdot}027$ K.

The form of the high frequency part of the spectrum was studied by Pike and Vaughan (1971) with the results shown in figure 41. The results show the spectra at 1·15 atm and three different temperatures and are compared with the analogous spectra from ^{4}He gas at 0·96 atm and 4·22 K. The results show that gaseous ^{4}He at 4·22 K gives an exponential spectrum, similar to that found in gaseous krypton

and argon by Gerstein *et al* (1970) and McTague and Birnbaum (1968) and with a characteristic width of 19 ± 3 K. At 4·22 K the liquid has a similar exponential form for frequency transfers above 45 K with a characteristic width of 29 ± 3 K. The slope of the line decreases as the temperature is decreased.

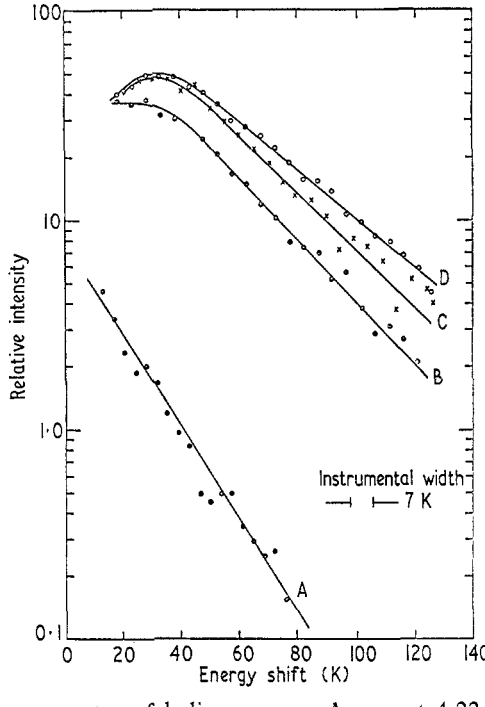

Figure 41. The Raman spectra of helium: curve A, gas at 4·22 K and 0·96 atm; curve B, liquid at 4·22 K and 1·15 atm; curve C, liquid at 3·31 K and 1·15 atm; curve D, liquid at 2·42 K and 1·15 atm. From Pike and Vaughan (1971).

Table 1. The ratio of the intensities for Raman scattering in the configuration ($\alpha\beta$)†

Configurations	Gas (Pike and Vaughan 1972)	Liquid at 4·2 K (Pike and Vaughan 1972)	Liquid at 1·3 K (Greytak and Yan 1969)	Theory s component	Theory d component
$(zx)/(zz)$	$0{\cdot}75 \pm 0{\cdot}16$	$0{\cdot}66 \pm 0{\cdot}09$	$0{\cdot}9 \pm 0{\cdot}2$	0	0·75
$(zy)/(yx)$	$1{\cdot}0 \pm 0{\cdot}2$	$1{\cdot}1 \pm 0{\cdot}2$	$0{\cdot}85 \pm 0{\cdot}2$	0/0	1·0
$(yz)/(zz)$	$0{\cdot}72 \pm 0{\cdot}1$	$0{\cdot}77 \pm 0{\cdot}1$		0	0·75
$(yz+yx)/(zz+zx)$			$0{\cdot}84 \pm 0{\cdot}08$	0	0·86

† α is the direction of E_0 and β of E_s; see figure 33.

The polarization properties of the spectra have been measured for the liquid and gas at 4·2 K and for the liquid at 1·3 K. The results using the geometry described by figure 33 are collected in table 1. The spectra occur in all polarizations and, furthermore, the shape of the spectra does not change with the polarization.

5.3. *Theoretical analysis*

5.3.1. *Interaction of light with the helium excitations.* The spectrum of the light scattered by a system is dependent upon the interaction between the light and the

excitations and secondly on the properties of these excitations. In this section we consider the first part of this problem and leave the second until §§ 5.3.2 and 5.3.3. The interaction of light with liquid helium was discussed by Halley (1969); the electric field of the incident light polarizes a helium atom which then interacts with its neighbours so as to polarize them, and hence to give rise to scattering. Halley developed the theory by explicitly introducing the electronic coordinates required to describe the polarizability of the helium atoms. We shall not follow this approach but describe the more straightforward, but similar, approach taken by Stephen (1969). A similar theory has been given by Nakajima (1971).

In Stephen's theory the polarizability of the crystal is expressed in terms of the fluctuations in the atomic density. If $\rho(\boldsymbol{r})$ is the atomic density at $\boldsymbol{r}$ and ρ_0 is the uniform density

$$\rho(\boldsymbol{r}) = \rho_0 + \delta\rho(\boldsymbol{r}).$$

Since the excitations are most readily described in wave vector space we shall also require the Fourier transform of $\rho(\boldsymbol{r})$ which is written $\rho(\boldsymbol{q})$.

The polarization produced at any point within the liquid by the incident field, $\boldsymbol{E}_0(\boldsymbol{r})$, assumed to vary with wave vector $\boldsymbol{k}_0$, is the product of the atomic polarizability, the atomic density and the field at that point within the liquid;

$$\boldsymbol{P}(\boldsymbol{r}) = \alpha\rho(\boldsymbol{r})\,\boldsymbol{E}(\boldsymbol{r}). \tag{5.2}$$

In the scattering experiment the scattered wave has a wave vector $\boldsymbol{k}_s$, which is radiated by the electric polarization wave in the helium with this wave vector.

There are two components to the electric field, $\boldsymbol{E}(\boldsymbol{r})$; the incident field, $\boldsymbol{E}_0(\boldsymbol{r})$, and the effective field $\boldsymbol{E}'(\boldsymbol{r})$ produced by the dipole moments on all the atoms other than the one at $\boldsymbol{r}$. These fields will be produced by the fluctuating parts of the density, $\delta\rho(\boldsymbol{r})$, and since electromagnetic waves travel through helium much faster than density fluctuations we may calculate the field from these fluctuations in the static approximation

$$E'_\alpha(\boldsymbol{r}) = \alpha \sum_\beta \int_r V_{\alpha\beta}(\boldsymbol{r}-\boldsymbol{r}')\,\delta\rho(\boldsymbol{r}')\,E_\beta(\boldsymbol{r}')\,\mathrm{d}\boldsymbol{r}' \tag{5.3}$$

where $V_{\alpha\beta}(\boldsymbol{r})$ is the electric field produced in the α direction due to a dipole in the β direction a distance $\boldsymbol{r}$ away. The integral $\int_r \ldots \mathrm{d}\boldsymbol{r}'$ is an integral over all the atoms other than the one at $\boldsymbol{r}$.

The lowest order solution to equation 5.3 is given by neglecting the fluctuating part of the electric field on the right hand side when equation 5.3 may be Fourier transformed to give

$$E'_\alpha(\boldsymbol{q}+\boldsymbol{k}_0) = \alpha \sum_\beta f_{\alpha\beta}(\boldsymbol{q})\,E_\beta(\boldsymbol{k}_0). \tag{5.4}$$

The magnitude of a polarization wave of wave vector $\boldsymbol{k}_s$, produced by an incident electric field of wave vector, $\boldsymbol{k}_0$, is obtained from the polarizability which may be written as

$$P_{\alpha\beta} = P^{(0)}_{\alpha\beta} + P^{(1)}_{\alpha\beta}\,\rho(Q) + \frac{1}{N}\sum_{\boldsymbol{q}} P^{(2)}_{\alpha\beta}(\boldsymbol{q})\,\rho(\boldsymbol{q})\,\rho(-\boldsymbol{q}) + \ldots \tag{5.5}$$

where

$$P^{(0)}_{\alpha\beta} = \alpha\rho_0\,\delta_{\alpha\beta} \quad \text{when } Q = 0$$
$$P^{(1)}_{\alpha\beta} = \alpha\delta_{\alpha\beta}$$
$$P^{(2)}_{\alpha\beta}(\boldsymbol{q}) = \alpha^2 f_{\alpha\beta}(\boldsymbol{q}).$$

The light scattering cross section is given, for a frequency transfer ω and an incident and scattered polarization given by the unit vectors $\boldsymbol{p}^0$ and $\boldsymbol{p}^s$, by (Born Huang 1954)

$$\sigma(\omega) = \frac{c^2 k_0^2}{2\pi} \sum_{\alpha\beta\gamma\delta} I_{\alpha\beta\gamma\delta}(\omega)\, p^0_\alpha p^s_\beta p^0_\gamma p^s_\delta$$

where the fourth rank tensor is given by the correlation function

$$I_{\alpha\beta\gamma\delta}(\omega) = \frac{1}{2\pi}\int_{-\infty}^{\infty} \langle P_{\alpha\beta}(0)\, P^*_{\gamma\delta}(t)\rangle \exp(\mathrm{i}\omega t)\, \mathrm{d}t.$$

The Brillouin scattering is then determined by the tensor

$$I^{(1)}_{\alpha\beta\gamma\delta}(\omega) = \alpha^2(\boldsymbol{p}^0 . \boldsymbol{p}^s)^2\, S(\boldsymbol{Q}, \omega) \tag{5.6}$$

where $S(\boldsymbol{Q}, \omega)$ is the same function as measured by neutron scattering techniques and described in §§2 and 3. We are unaware of any published results which confirm the polarization dependence, although Greytak *et al* (1970) imply that the result is at least approximately satisfied.

The two-excitation scattering occurs from the third term in equation (5.5) and gives rise to a two-density correlation function

$$I^{(2)}_{\alpha\beta\gamma\delta}(\omega) = \frac{\alpha^4}{N} \sum_{\boldsymbol{q}} \sum_{\boldsymbol{q}_1} f_{\alpha\beta}(\boldsymbol{q})\, f_{\gamma\delta}(\boldsymbol{q}_1)\, H_{\alpha\beta\gamma\delta}(\boldsymbol{q}\boldsymbol{q}_1, \omega) \tag{5.7}$$

where

$$H_{\alpha\beta\gamma\delta}(\boldsymbol{q}\boldsymbol{q}_1, \omega) = \frac{1}{2\pi}\int_{-\infty}^{\infty} \langle \rho(\boldsymbol{q}, 0)\, \rho(-\boldsymbol{q}, 0)\, \rho^+(\boldsymbol{q}_1, t)\, \rho^+(-\boldsymbol{q}_1, t)\rangle \exp(\mathrm{i}\omega t)\, \mathrm{d}t$$

and we have neglected the wave vector transfer $\boldsymbol{Q}$, compared with $\boldsymbol{q}$ and $\boldsymbol{q}_1$. The form of the correlation function depends on $(\alpha\beta\gamma\delta)$ through the angular dependence of the f factors as will be more apparent when we discuss its form in detail in §5.3.3.

Since liquid helium is isotropic and $I_{\alpha\beta\gamma\delta}(\omega)$ is a fourth rank tensor with the same symmetry properties as the elastic constant tensor, there are only two independent components. These are usually referred to as the s and d components and result from the s and d parts of the interaction $V_{\alpha\beta}(\boldsymbol{R})$. When an average over all the possible directions of the wave vectors $\boldsymbol{q}$ and $\boldsymbol{q}_1$ has been performed, the scattering separates into (Iwamoto 1970)

$$I_s(\omega) = \frac{\alpha^4}{N} \sum_{\boldsymbol{q}} \sum_{\boldsymbol{q}_1} (\boldsymbol{p}^0 . \boldsymbol{p}^s)^2\, f_s(\boldsymbol{q})\, f_s(\boldsymbol{q}_1)\, H_s(\boldsymbol{q}\boldsymbol{q}_1, \omega) \tag{5.8}$$

and

$$I_d(\omega) = \frac{6\alpha^4}{5N} \sum_{\boldsymbol{q}} \sum_{\boldsymbol{q}_1} \{1 + \tfrac{1}{3}(\boldsymbol{p}^0 . \boldsymbol{p}^s)^2\}\, f_d(\boldsymbol{q})\, f_d(\boldsymbol{q}_1)\, H_d(\boldsymbol{q}\boldsymbol{q}_1, \omega) \tag{5.9}$$

where the factors f and H are not dependent on the polarization vectors.

The functions $f_s(\boldsymbol{q})$ and $f_d(\boldsymbol{q})$ may be calculated once we assume a model for the interaction potential, $V_{\alpha\beta}(\boldsymbol{r})$. This interaction describes how a dipole at $\boldsymbol{r}$ interacts with one at the origin and from classical electrostatics the field is

$$V_{\alpha\beta}(\boldsymbol{r}) = \left(\frac{3r_\alpha r_\beta/\boldsymbol{r}^2 - \delta_{\alpha\beta}}{|\boldsymbol{r}|^3}\right).$$

Stephen (1969) then evaluated the Fourier transform of this function, and took account of the exclusion of the atom at r from the integral in equation (5.3) by cutting off the transform when $r = a$. Since this interaction is entirely d-like it contributes only to $f_{\mathrm{d}}(q)$ which is then

$$f_{\mathrm{d}}(q) = 4\pi\left(\frac{\sin(qa)}{(qa)^3} - \frac{\cos(qa)}{(qa)^2}\right).$$

In figure 42 we show this function for $a = 1{\cdot}57$ Å.

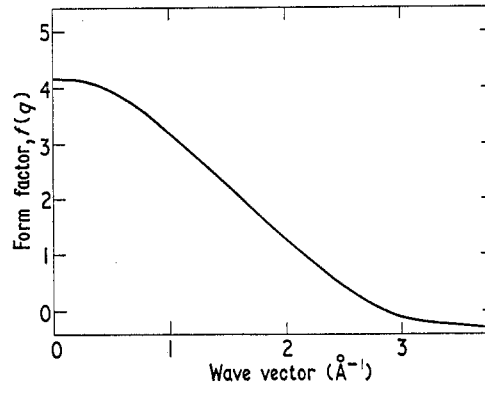

Figure 42. The form factor $f(q)$ for Stephen's model of the Raman scattering, for $a = 1{\cdot}57$ Å.

Stephen's theory then predicts that the two excitation scattering will be entirely d-like. In table 1 we list the experimental results for various polarization ratios and the predictions for s and d symmetries. Clearly the observed intensity is largely d-like although improved accuracy might show a small s-like component. This result is a very convincing test of Stephen's theory and also possibly surprising in that a large part of the field $V_{\alpha\beta}(r)$ probably arises from nearest neighbour interactions, and this might well have a short range overlap interaction in addition to the classical electrostatic field. A short range overlap contribution would give rise to s symmetry scattering, and it would therefore be of considerable interest to measure this.

5.3.2. *Brillouin scattering.* The cross section for Brillouin scattering is dependent upon the Van Hove correlation function $S(\boldsymbol{Q}, \omega)$ as shown by equation (5.6). Since the wave vector $\boldsymbol{Q}$ is typically about 10^{-3} Å^{-1}, the scattering arises from the phonon part of the dispersion relation. The experiments have so far been conducted above 1·0 K and so are in the hydrodynamic region and the theory is most appropriately described by a hydrodynamic model. Since we are not treating the two-fluid model in detail we shall describe the behaviour in this region only qualitatively.

The density fluctuations in a liquid are dependent upon changes in pressure and entropy

$$\Delta\rho = \left(\frac{\partial\rho}{\partial p}\right)_S \Delta p + \left(\frac{\partial\rho}{\partial S}\right)_p \Delta S.$$

Now the fluctuations in the pressure and temperature will, for He I, be uncorrelated

and the magnitude of the fluctuations given by the fluctuation-dissipation theorem as

$$(\overline{\Delta p^2}) = -\frac{k_B T}{(\partial V/\partial p)_S}$$

while

$$(\overline{\Delta S^2}) = \frac{k_B T}{(\partial T/\partial S)_p}.$$

The intensity of the light scattered by the pressure fluctuations or sound waves is

$$I_p = -\left(\frac{\partial \rho}{\partial p}\right)_S^2 \left(\frac{\partial p}{\partial V}\right)_S k_B T$$

while that scattered by the entropy fluctuations, which are entirely damped by the thermal conductivity, is known as the Rayleigh scattering and is given by

$$I_S = \left(\frac{\partial \rho}{\partial S}\right)_p^2 \left(\frac{\partial S}{\partial T}\right)_p k_B T.$$

The ratio of these intensities, as first shown by Landau and Placzek (1934) and derived in detail by Frenkel (1946), is given by

$$\frac{I_s}{I_p} = \gamma - 1 \tag{5.10}$$

where γ is the ratio of specific heats C_p/C_v. The results shown in figure 37 are in excellent accord with this theory and give further support to Stephen's theory of the light scattering in liquid helium. If the scattering arose not only from density fluctuations, but also from explicit temperature fluctuations, the intensities and shapes would be quite different, as shown in the case of solids by Wehner and Klein (1972).

Below the λ transition the pressure and entropy fluctuations are coupled, and the entropy fluctuations propagate with the speed of second sound. The theory must then be developed by use of the two-fluid hydrodynamic model, but, as shown by Vinen (1971), the ratio of the intensities above 1·3 K is still given to good accuracy by equation (5.10). In particular he shows from thermodynamic data that C_p/C_v differs from unity at high pressures and predicts the ratio I_S/I_p for a series of pressures in He II.

Unfortunately Brillouin scattering measurements have not yet been conducted at lower temperature and at a variety of pressures with sufficient accuracy to determine the form of the velocity and attenuation in a frequency range different from that attainable by conventional ultrasonic measurements. Such measurements might well clarify the uncertainties described in § 4 about the interpretation of the ultrasonic measurements.

5.3.3. *Raman scattering.* The form of the Raman scattering is dependent upon the two-excitation correlation function defined by equation (5.7). The simplest form of this function assumes that there is no interaction between the excitations and

$$\sum_{q_1} \langle \rho(\boldsymbol{q}, 0)\, \rho(-\boldsymbol{q}, 0)\, \rho^+(\boldsymbol{q}_1, t)\, \rho^+(-\boldsymbol{q}_1, t)\rangle$$
$$= \langle \rho(\boldsymbol{q}, 0)\, \rho^+(\boldsymbol{q}, t)\rangle \langle \rho(-\boldsymbol{q}, 0)\, \rho^+(-\boldsymbol{q}, t)\rangle$$

so that

$$H(\boldsymbol{q}\boldsymbol{q}_1, \omega) = \int_{-\infty}^{\infty} S(\boldsymbol{q}, \omega')\, S(-\boldsymbol{q}, \omega - \omega')\, \mathrm{d}\omega'. \tag{5.11}$$

The low frequency part of the scattering is then dominated by the one-phonon part of $S(q, \omega)$, namely $Z(q)\,\delta(\omega - \omega(q))$ from equation (2.11) to give

$$H(\boldsymbol{q}\boldsymbol{q}_1, \omega) = Z(\boldsymbol{q})^2\, \delta(\omega - 2\omega(\boldsymbol{q}))\, \delta_{\boldsymbol{q}\boldsymbol{q}_1}.$$

The Raman scattering for the d-wave scattering is then

$$I_{\mathrm{d}}(\omega) = \frac{6\alpha^4}{10\pi^2}\left(1 + \frac{(\boldsymbol{p}^0 \cdot \boldsymbol{p}^{\mathrm{s}})^2}{3}\right) \int M(\boldsymbol{q})\, \delta(\omega - 2\omega(\boldsymbol{q}))\, \mathrm{d}\boldsymbol{q} \tag{5·12}$$

where

$$M(\boldsymbol{q}) = (Z(\boldsymbol{q})\, f_{\mathrm{d}}(\boldsymbol{q}))^2.$$

The two-excitation Raman scattering is therefore a modulation of the two-excitation density of states. In particular near the roton minimum the excitation energies are given by equation (1.3) and if we neglect $M(\boldsymbol{q})$ the remainder of the integral in equation (5.12) may be performed analytically to give the density of states for ω close to 2Δ as

$$N_2(\omega) = 4\pi q_0^2 \left(\frac{\mu}{\omega - 2\Delta}\right)^{1/2} \qquad \omega > 2\Delta$$

where Δ and μ are the parameters of the roton dispersion curve, equation (1.3).

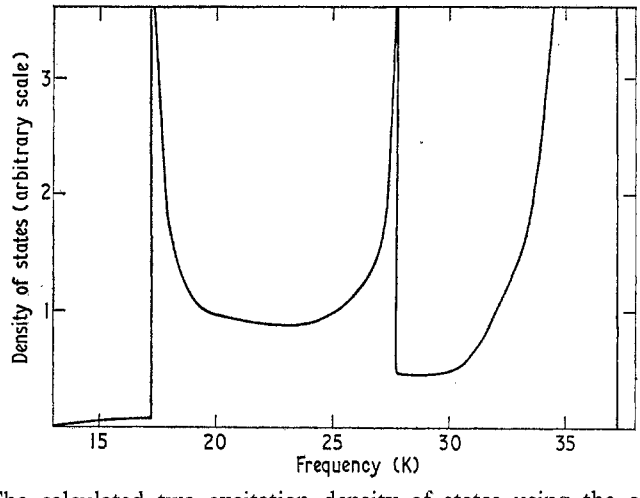

Figure 43. The calculated two excitation density of states using the observed dispersion relation for $0 < q < 3{\cdot}6$ Å^{-1}. The singularities occur at the frequencies of the roton minimum, the maximum for $q \simeq 1$ Å^{-1} and the end of the dispersion relation.

This result shows that the density of states has a square root singularity at $\omega = 2\Delta$. In the same way the maximum in the dispersion relation for a wave vector $q \approx 1{\cdot}0$ Å^{-1} gives a square root singularity at a frequency of 27·6 K. Halley (1969) therefore predicted that the Raman spectrum would consist of two sharp peaks corresponding to these two singularities. Iwamoto (1970) also suggested that the flat portion of the dispersion relation for wave vectors larger than 3·0 A^{-1} would also give rise to a singularity. In figure 43 we show a calculation of the two-excitation density of states.

In the experiments, figure 37, only one peak is observed instead of the three peaks shown in figure 43. In large part this is because of the effect of the coefficient modifying the form of the scattering. In figure 44 we show a calculation of the Raman spectrum using equation (5.12) (Cowley 1972). The calculation includes the effect of the resolution function appropriate to the experiments of figures 38 and 40 and has been normalized to give the same peak height as both experiments. The agreement between experiment and theory is clearly quite reasonable especially for the lower resolution experiment shown in part (*a*) of the figure; the high frequency peaks in figure 43 are almost wholly eliminated by the function $M(\boldsymbol{q})$.

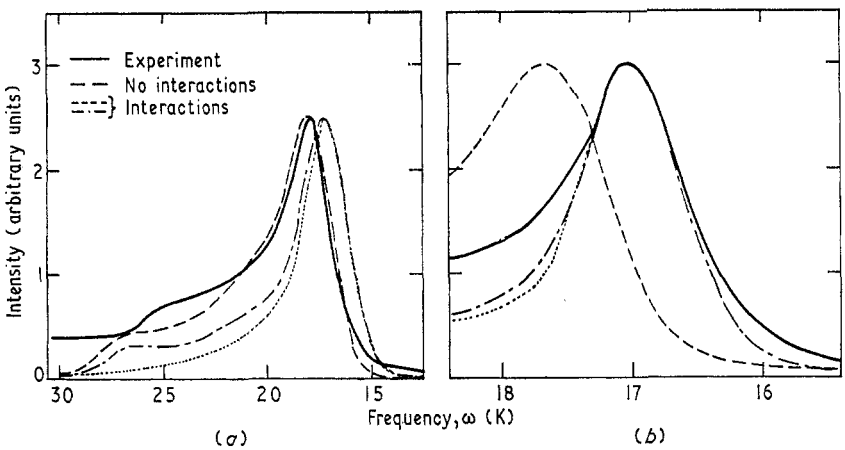

Figure 44. The Raman scattering from liquid helium as measured experimentally (full line) by (*a*) Greytak and Yan (1969) and by (*b*) Greytak *et al* (1970), and as calculated from equation (5.12) neglecting roton–roton interactions (broken lines). The dotted and chain lines are calculated with roton–roton interactions assuming g_4 constant and V_R constant respectively. In all of the calculations $\Gamma_R = 0{\cdot}15$ K and allowance has been made for the instrumental resolution function.

At the higher frequencies there are appreciable discrepancies between the theory and experiment but these may well result from the multiphonon part of $S(\boldsymbol{Q}, \omega)$ which has not been included in these calculations.

The effect of the roton lifetime may be included in these calculations by replacing the delta function in equation (5.12) by a lorentzian with half-width Γ_R, the inverse lifetime of the rotons. This leads to a decrease in the peak height as Γ_R increases and by fitting Γ_R to the results of figure 38 Greytak *et al* (1971) were able to obtain Γ_R as a function of temperature, as shown in figure 45.

Despite the considerable success of the theory as shown by figure 44(*a*), it is inconsistent with the results of Greytak *et al* (1970) as shown in figures 40 and 44(*b*). In both Greytak's calculations and ours the peak of the spectrum for non-interacting excitations occurs at 17·65 K, whereas his observed maximum is at 17·022 K. This discrepancy is apparently well outside the errors in the frequency measurements both of his experiment and of the basic neutron scattering results which we have used in the calculations ($2\Delta = 17{\cdot}34 \pm 0{\cdot}08$ K). Greytak *et al* interpret this discrepancy as evidence for a two-roton bound state.

Ruvalds and Zawadowski (1970) initially introduced attractive roton–roton interactions in order to account for the suppression of the high frequency peaks in the density of states, figure 43, in the observed Raman scattering. As a result

of this they predicted that a two-roton bound state might occur with an energy below 2Δ. As we have seen the suppression of the peaks in the Raman scattering results largely from the $M(\boldsymbol{q})$ function but nevertheless Ruvalds and Zawadowski's consequent prediction of a two-roton bound state provides a mechanism to understand the presence of Raman scattering below 2Δ. The theory of this effect is discussed in detail by Iwamoto (1970) and by Zawadowski *et al* (1972), and we will quote their important results.

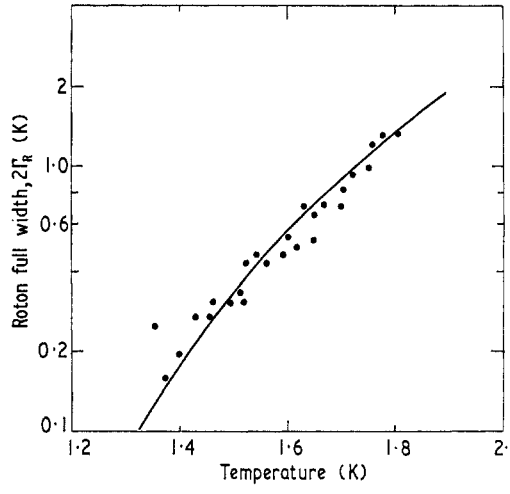

Figure 45. The roton full width at half-height, $2\Gamma_R$, as a function of temperature from Greytak and Yan (1971). The full line is the best fit obtained with the theory of Landau and Khalatnikov (1949). See also figure 13.

The Raman scattering produces pairs of density fluctuations which may interact with one another. If the light produces a pair of fluctuations with wave vector $\boldsymbol{q}$ they will be scattered to a wave vector $\boldsymbol{q}_1$ by the interaction given by

$$\frac{1}{2N}\sum_{\boldsymbol{q}\boldsymbol{q}_1} V(\boldsymbol{q},\boldsymbol{q}_1)\,\rho(\boldsymbol{q})\,\rho(-\boldsymbol{q})\,\rho^{+}(\boldsymbol{q}_1)\,\rho^{+}(-\boldsymbol{q}_1).$$

Since the two-excitation Raman scattering has a definite symmetry there will be definite angular correlations occurring both in the incident and scattered waves. The interaction depends therefore on the magnitude of the wave vectors and the symmetry, s- or d-like, of the Raman scattering. The interaction may therefore be rewritten as

$$V(\boldsymbol{q},\boldsymbol{q}_1) = V^{\mathrm{s}}(\boldsymbol{q},\boldsymbol{q}_1) + V^{\mathrm{d}}(\boldsymbol{q},\boldsymbol{q}_1)$$

with the appropriate interaction to be chosen for the different symmetries of the Raman scattering.

Furthermore the problem is intractable if the interactions are dependent on both $\boldsymbol{q}$ and $\boldsymbol{q}_1$ unless the form is separable $V(\boldsymbol{q}\boldsymbol{q}_1) = V'(\boldsymbol{q})\,V'(\boldsymbol{q}_1)$. The Raman scattering is then given by equation (5.9) but with

$$\begin{aligned} H_{\mathrm{d}}(\boldsymbol{q}\boldsymbol{q}_1,\omega) &= \frac{1}{\pi}\,\mathrm{Im}\,\{F(\boldsymbol{q})\}\,\delta_{\boldsymbol{q}\boldsymbol{q}_1} \\ &\quad + \frac{1}{\pi N}\,\mathrm{Im}\left\{F(\boldsymbol{q})\,V'(\boldsymbol{q})\left(1-\frac{1}{N}\sum_{\boldsymbol{q}_2} V'(\boldsymbol{q}_2)^2 F(\boldsymbol{q}_2)\right)^{-1} V'(\boldsymbol{q}_1)\,F(\boldsymbol{q}_1)\right\} \end{aligned} \tag{5.13}$$

where the function $F(\boldsymbol{q})$ is

$$F(\boldsymbol{q}) = \lim_{\varepsilon \to 0^+} \frac{(Z(\boldsymbol{q}))^2}{\omega - \mathrm{i}\varepsilon - 2\omega(\boldsymbol{q})}.$$

The importance of equation (5.13) is that it permits scattering to occur when

$$1 = \frac{1}{N} \sum_{\boldsymbol{q}_2} V'(\boldsymbol{q}_2)^2 F(\boldsymbol{q}_2).$$

The two-excitation density of states has a singularity when $\omega = 2\Delta$, as shown in figure 43. In a similar manner, for $\omega < 2\Delta$ and $\omega \to 2\Delta$, an integral over $\boldsymbol{q}_2$ gives

$$\mathrm{Re}\left(\sum_{\boldsymbol{q}} F(\boldsymbol{q})\right) = -\frac{q_0^2 Z_{\mathrm{R}}^2 \mu}{2\pi} |2\Delta - \omega|^{-1/2}.$$

Since the dominant excitations in this sum are all rotons we may approximate $V'(\boldsymbol{q})^2$ as V_{R}. A two-roton bound state is then obtained if V_{R} is negative at a frequency given by

$$\omega = 2\Delta - \left(\frac{V_{\mathrm{R}} q_0^2 Z_{\mathrm{R}}^2}{2\pi}\right)^2 \mu^2. \tag{5.14}$$

This result differs from that of Ruvalds and Zawadowski (1970) and Zawadowski *et al* (1972) by the presence of Z_{R}. This arises because we have assumed that the interactions occur between density fluctuations whereas they have assumed interactions between rotons; their $g_4 = Z_{\mathrm{R}}^2 V_{\mathrm{R}}$. In numerical calculations we need to know how $V'(\boldsymbol{q}, \boldsymbol{q}_1)$ varies with $\boldsymbol{q}$ and $\boldsymbol{q}_1$, and we have made two approximations. One is identical to the theory of Ruvalds and Zawadowski (1970) and $V(\boldsymbol{q}, \boldsymbol{q}_1) = g_4/Z(\boldsymbol{q})Z(\boldsymbol{q}_1)$ and in the other $V(\boldsymbol{q}, \boldsymbol{q}_1)$ has been taken as a constant.

The roton–roton interactions not only give rise to a bound state, but also drastically modify the form of the two-excitation band. This is illustrated in figure 46(*b*) where the Raman spectra are calculated with a roton–roton interaction to give the observed frequency of the bound state. The observed spectra, which are then convolutions of these spectra with the experimental resolution, are shown in figure 44. The comparison with the Greytak and Yan experiment, figure 44(*a*), shows that the model neglecting roton–roton interactions is most satisfactory. The frequency of the peak and the intensity at $\omega \simeq 20$ K are both more satisfactory than for the interacting models. The comparison with the high resolution experiments, shown in figure 44(*b*), shows that there is an error in the peak frequency for the noninteracting model, while those including interactions fall significantly below the observed curves for ω about 18 K. These calculations are essentially the same as those of Greytak *et al* (1970) shown in figure 40 except they include the $M(\boldsymbol{q})$ factor.

Greytak and Yan (1969) and Greytak *et al* (1970) report measurements of the spectra with three different resolution functions which give peak frequencies which increase as the resolution width increases as shown in table 2. This effect also arises in the calculation performed with noninteracting excitations because the spectrum, figure 46(*a*), is asymmetric about 2Δ. On the other hand when the interactions are introduced with sufficient strength to account for the results shown in figure 44(*b*), the spectrum is very sharp in frequency, figure 46(*b*), and the peak frequency almost independent of the resolution function, table 2. The theory and the experimental results are therefore inconsistent; the peak frequency occurring

below 2Δ in figure 46(*b*) cannot be understood simultaneously with the resolution dependence of the peak frequency shown in table 1. Pike and Vaughan (1971), figure 39, also measured the spectrum with somewhat worse resolution than Greytak *et al* and obtained an even larger peak frequency.

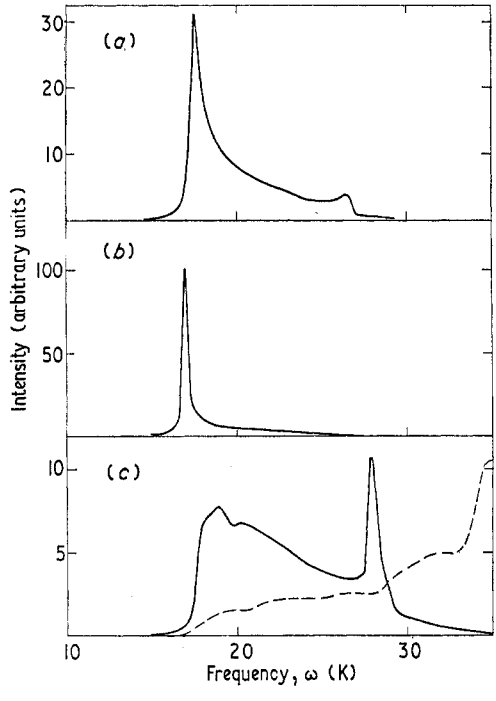

Figure 46. The Raman scattering calculated (*a*) with no interactions, (*b*) with attractive interactions of a strength to produce the measured bound state energy, and (*c*) with repulsive interactions ten times larger in magnitude. The solid curves assume g_4 is a constant after Ruvalds and Zawadowski (1970) and the broken curve that $V(\boldsymbol{q}\boldsymbol{q}_1)$ is a constant. The corresponding curve for (*b*) is indistinguishable from the solid curve. The roton width Γ_R is taken throughout as 0·15 K after Greytak *et al* (1970). The calculations (*b*) are chosen to represent the spectra for d symmetry and (*c*) for s symmetry.

Table 2. Peak frequencies (in kelvins) for the Raman spectra as observed experimentally and as calculated

Resolution width		4·2 K	2·1 K	0·7 K
Experiment		18·7 †	17·85‡	17·02†
Theory	$g_4 = 0$	18·75	18·00	17·64
	$g_4 = -12$	17·10	17·06	17·02
	$g_4 = -6$	18·10	17·70	17·40

† Greytak and Yan (1969).
‡ Greytak *et al* (1970).

The shape of the peak is also dependent upon the strength of the interactions and figure 46(*a*) indicates that the agreement is most satisfactory for the model without interactions. Although this result is dependent upon the detailed shape of the resolution function, the $\boldsymbol{q}$ dependence of the interactions and the form factor $M(\boldsymbol{q})$, we believe that this and the resolution dependence of the peak frequency indicate that the interactions between the rotons are considerably smaller than

suggested by Greytak *et al* (1970). The binding energy of the bound state is less than 0·1 K with an interaction g_4 of less than 6×10^{-40} erg cm^{-3}. The results for the peak frequencies obtained with this interaction are shown in table 2. Since this interpretation fails to give the peak frequency for the high resolution experiment of figure 46(*b*) correctly, we must discuss the possible origin of this discrepancy.

The neutron scattering experiment on which the calculations were based was conducted at 1·1 K whereas the Raman scattering measurements were made at 1·2 K. An increase in temperature does reduce Δ, § 3.4.2, but the reduction is not sufficient to account for the discrepancy. The roton energy is also pressure dependent, § 3.4.2, but both neutron and Raman scattering measurements were obtained at the saturated vapour pressure. It is apparent from the pressure dependence of Δ, see § 3.4.1, that if the pressure in the Raman scattering measurements were 1 atm, then the discrepancy would be almost removed. The determination of Δ in the neutron scattering experiments is possibly in error by 0·17 K, but an error of this magnitude would destroy the agreement found in figure 44(*a*). We conclude that there is at present a significant discrepancy between the theory of the Raman scattering and the available experimental results, which prevents us from being confident of the existence of a bound two-roton state. The present evidence suggests that if it exists at all it has a binding energy of less than 0·1 K.

No attempts have as yet been made to understand the very high frequency part of the Raman scattering. Its similarity to that observed in gases suggests that a collision theory similar to that used for gases (Gerstein *et al* 1970) might be appropriate.

5.3.4. *Roton–roton interactions.* The theory of the Raman scattering from liquid helium has introduced a roton–roton interaction to explain the two-roton bound state but also requires an interaction to explain the roton lifetime Γ_R. The results of Greytak and Yan (1971) show that the roton lifetime may be written as

$$\Gamma_R = 2 \times 10^{10} N_R \text{ s}^{-1}$$

where N_R is the roton density at any given temperature. This result appears to be in agreement both with the neutron scattering measurements of the lifetime, § 3.4.2 and figure 13, and also with Brewer and Edwards' (1962) measurements of the viscosity of helium.

Khalatnikov (1965) discusses roton–roton scattering using the theory of Landau and Khalatnikov (1947) by assuming a repulsive interaction between two rotons, $V_R\,\delta(\boldsymbol{r}_1 - \boldsymbol{r}_2)$, and calculating the scattering by the 'golden rule' of perturbation theory. The theory then agrees with the experiments for Γ_R if

$$V_R = 2 \times 10^{-38} \text{ erg cm}^{-3}.$$

The roton bound state in the Raman scattering is not given by the Khalatnikov potential because it does not contain any d-like components. The binding energy of the rotons suggests that this component is $V_R^d = -1{\cdot}2 \times 10^{-39}$ erg cm^{-3}. The discrepancy between these results has led to a recent reinvestigation of roton–roton scattering by Yau and Stephen (1971), Nagai *et al* (1972) and Solana *et al* (1972).

The first two authors suggest that at large distances rotons interact through the backflow fields and that this interaction is of a dipole or d-like form. They show that this form of interaction is capable of explaining the value of V_R^d.

The calculation of Γ_R by Khalatnikov (1965) is criticized by all the authors. Yau and Stephen and Nagai *et al* show that for the strength of interaction the Born

approximation, and hence the golden rule, is invalid, and that a more complete T matrix theory gives much less scattering for a repulsive interaction and more scattering for an attractive interaction. They suggest that the scattering of the rotons must arise from the short but finite range interaction between the rotons of the form $V(r) = V_0 \exp(-r^2/b^2)$, for example, with b about 1–2 Å. Solana *et al* use a Green function treatment in which they improve on Khalatnikov's approach by using the density of states calculated by including the attractive roton–roton interactions. The roton lifetime is then calculated selfconsistently. In contrast Yau and Stephen say that since the roton binding energy, at most 0·34 K, is less than the temperature of the measurements of Γ_R, about 1·5 K, the bound state has little effect on the cross section.

Clearly further theoretical work and measurements are required before roton–roton scattering is fully understood. If, as suggested by Yau and Stephen, the s part of the roton–roton interaction is repulsive and ten times stronger than the d part it will have a large effect on the s-like part of the Raman scattering. This has been calculated, and is shown by figure 46(*c*), using the same $M(\boldsymbol{q})$ factors as for the d part of the scattering. This is very likely a poor approximation and the intensity is probably further reduced as a result. Despite this problem, however, the s part of the scattering, if observable, might well provide very useful information about roton–roton interactions.

6. Theories of liquid helium

It is the purpose of this section to review the theory of the structure and excitations of liquid helium. Since there is not a wholly convincing theory available despite the enormous amount of work which has been expended on this problem, it is necessary to describe a variety of different approaches. We shall not, however, attempt a fully inclusive review of the theory but merely describe those approaches which seem to us, largely subjectively, to be the most promising. We begin with the most ambitious approach; namely a full microscopic theory which introduces a pair potential between the atoms and attempts to calculate the properties from this. Despite considerable formal progress, it has not yet been developed to give a detailed description of liquid helium. The next section discusses a variety of variational calculations for the structure factor $S(Q)$. These are considerably more successful in that they are able to reproduce the experimental curve quite satisfactorily. We then describe less ambitious theories for the scattering function, $S(Q, \omega)$. These theories are based either on a phenomenological form for the hamiltonian, or on a parametrized form of $S(Q, \omega)$ with the parameters obtained from moment relations.

6.1. *Microscopic theory*

6.1.1. *Formalism and exact results.* Most of the recent microscopic theories of liquid helium have made use of many-body techniques as described, for example, by Abrikosov *et al* (1964). It is not our intention to review either the use of these techniques in detail, or their particular application to liquid helium, but merely to point out what seem to us to be the most important developments.

In a gas of noninteracting bosons, the ground state at absolute zero has all the particles in the same state with momentum zero. This macroscopic occupation of a particular state leads to difficulties in the application of many-body techniques to

liquid helium, but these were overcome by Beliaev (1958) and by Hugenholtz and Pines (1959). The hamiltonian for N helium atoms is the sum of the kinetic energy, T, and the potential energy, V. These may be written in terms of particle creation $a^+(\boldsymbol{q})$ and destruction $a(\boldsymbol{q})$ operators, where $\boldsymbol{q}$ is the wave vector of the particle. The kinetic energy is given by

$$T = \sum_{\boldsymbol{q}} \frac{\hbar^2 q^2}{2M} a^+(\boldsymbol{q})\, a(\boldsymbol{q}).$$

If the potential is a two-body pair potential the potential energy is

$$V = \tfrac{1}{2} \sum_{\boldsymbol{q}} V(\boldsymbol{q})\, \rho^+(\boldsymbol{q})\, \rho(\boldsymbol{q})$$

where $V(\boldsymbol{q})$ is the Fourier transform of the interaction and $\rho(\boldsymbol{q})$ is the density operator which is given by

$$\rho(\boldsymbol{q}) = \sum_{\boldsymbol{k}} a^+(\boldsymbol{k})\, a(\boldsymbol{k}+\boldsymbol{q}).$$

If there is a macroscopic occupation of the state with $q = 0$, the operators $a^+(0)$ and $a(0)$ will only change the number of particles in that state, $n(0)$, by a fractionally infinitesimal amount. They may therefore be replaced by the number $n(0)^{1/2}$. The density operator is then

$$\rho(\boldsymbol{q}) = n(0)^{1/2}(a(\boldsymbol{q}) + a^+(-\boldsymbol{q})) + \sum_{\boldsymbol{k}\neq 0} a^+(\boldsymbol{k})\, a(\boldsymbol{k}+\boldsymbol{q}). \tag{6.1}$$

The part of the potential energy which depends on the particles outside the condensate is

$$V = V_2 + V_3 + V_4$$

where

$$\begin{aligned} V_2 = \frac{n(0)}{2} \sum_{\boldsymbol{q}} [V(\boldsymbol{q})\{a(\boldsymbol{q})\, a^+(\boldsymbol{q}) + a^+(\boldsymbol{q})\, a(\boldsymbol{q}) + a(\boldsymbol{q})\, a(-\boldsymbol{q}) \\ + a^+(\boldsymbol{q})\, a^+(-\boldsymbol{q})\} + V(0)\{a^+(\boldsymbol{q})\, a(\boldsymbol{q}) + a(\boldsymbol{q})\, a^+(\boldsymbol{q})\}] \end{aligned} \tag{6.2}$$

$$V_3 = n(0)^{1/2} \sum_{\boldsymbol{k},\boldsymbol{q}} V(\boldsymbol{q})\{a^+(\boldsymbol{q})\, a^+(\boldsymbol{k})\, a(\boldsymbol{k}+\boldsymbol{q}) + a(\boldsymbol{q})\, a(\boldsymbol{k})\, a^+(\boldsymbol{k}+\boldsymbol{q})\} \tag{6.3}$$

and

$$V_4 = \tfrac{1}{2} \sum_{\boldsymbol{k}_1,\boldsymbol{k}_2,\boldsymbol{q}} V(\boldsymbol{q})\, a^+(\boldsymbol{k}_1)\, a(\boldsymbol{k}_1+\boldsymbol{q})\, a^+(\boldsymbol{k}_2)\, a(\boldsymbol{k}_2-\boldsymbol{q}). \tag{6.4}$$

The theory is then developed by introducing the Green's functions for the particles not in the condensate. Since, however, the hamiltonian for these particles does not conserve the number of particles, it is necessary to use an effective hamiltonian, $H - \mu N$, where μ is the chemical potential, and, further, to introduce four Green's functions instead of the one needed for normal systems. These Green's functions are defined by

$$\left.\begin{aligned} G_{11}(\boldsymbol{q},\omega) &= -\mathrm{i} \int \mathrm{d}t \exp(\mathrm{i}\omega t) \langle T a^+(\boldsymbol{q},t)\, a(\boldsymbol{q},0)\rangle \\ G_{12}(\boldsymbol{q},\omega) &= -\mathrm{i} \int \mathrm{d}t \exp(\mathrm{i}\omega t) \langle T a^+(\boldsymbol{q},t)\, a^+(-\boldsymbol{q},0)\rangle \\ G_{21}(\boldsymbol{q},\omega) &= -\mathrm{i} \int \mathrm{d}t \exp(\mathrm{i}\omega t) \langle T a(-\boldsymbol{q},t)\, a(\boldsymbol{q},0)\rangle \\ G_{22}(\boldsymbol{q},\omega) &= -\mathrm{i} \int \mathrm{d}t \exp(\mathrm{i}\omega t) \langle T a(-\boldsymbol{q},t)\, a^+(-\boldsymbol{q},0)\rangle \end{aligned}\right\} \tag{6.5}$$

where T is the time ordering operator. These Green's functions may then be calculated using the normal techniques of many-body theory with an effective hamiltonian given by

$$H' = \sum_q (E(q) - \mu)\, a^+(q)\, a(q) + V_2 + V_3 + V_4 \tag{6.6}$$

and with $E(q) = \hbar^2 q^2/2M$. The rules for the calculation of the terms in the diagrammatic perturbation theory are given by Abrikosov *et al* (1964), and the diagrams are similar to those of a normal fermion system except for the presence of the interactions V_2 and V_3. In representing these diagrams $n(0)^{1/2}$ is represented by a dotted line with an arrow at the end. The Green's functions (6.5) may be obtained

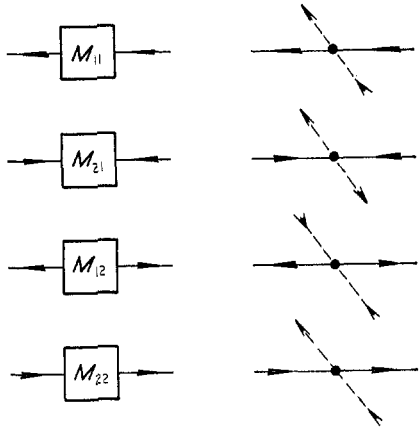

Figure 47. The four different self-energy diagrams are shown in general with a particular example of each type.

from the effective hamiltonian (6.6) by treating the unperturbed part of the hamiltonian as the leading term and the potential terms as perturbations. There are then four types of self-energies as shown schematically in figure 47. Beliaev (1958) obtained the Dyson equation for the Green functions (6.5) in the form

$$(\hbar\omega\tau_\alpha - E(q) + \mu)\, G_{\alpha\gamma}(q, \omega) = \delta_{\alpha\gamma} + \sum_\beta M_{\alpha\beta}(q, \omega)\, G_{\beta\gamma}(q, \omega) \tag{6.7}$$

where $\tau_\alpha = 1, -1$ when $\alpha = 1, 2$ and $M_{\alpha\beta}(q, \omega)$ is the self-energy matrix which satisfies

$$M_{11}(q, \omega) = M_{22}(q, -\omega),$$
$$M_{12}(q, \omega) = M_{21}(q, \omega).$$

The Green's function is therefore

$$G_{11}(q, \omega) = (\hbar\omega + E(q) - \mu + M_{22}(q, \omega))/D, \tag{6.8}$$

where

$$D = (\hbar\omega - E(q) + \mu - M_{11}(q, \omega))\,(\hbar\omega + E(q) - \mu + M_{22}(q, \omega)) + (M_{12}(q, \omega))^2.$$

Translational symmetry shows that for $q = 0$ and $\omega = 0$ equation (6.8) must have a solution with $D = 0$. This imposes the condition that

$$(\mu - M_{11}(0, 0))^2 = M_{12}(0, 0)^2$$

and Hugenholtz and Pines (1959) showed that from the two solutions to this

equation the correct solution is

$$\mu = M_{11}(0,0) - M_{12}(0,0).$$

This result gives a relation between the self-energy and the chemical potential. A relation may also be obtained between $n(0)$ and the Green's functions by use of number conservation;

$$N - n(0) = \frac{1}{2\pi} \sum_{q} \int_{-\infty}^{0} \operatorname{Im}\{G_{11}(q, \omega - \mathrm{i}0^{+})\}\, \mathrm{d}\omega. \tag{6.9}$$

The scattering cross section is not dependent on the one-particle Green's function but on the density–density correlation function. If we define

$$F(q, \omega) = -\mathrm{i} \int \mathrm{d}t \exp(\mathrm{i}\omega t) \langle T\rho(q, t)\, \rho^{+}(q, 0)\rangle \tag{6.10}$$

the Van Hove structure factor is given by

$$S(q, \omega) = \frac{1}{\pi N} \operatorname{Im}\{F(q, \omega)\}.$$

In the diagrammatic analysis for $F(q, \omega)$, there are certain terms which contain the single particle Green's function as a factor. These are known as the singular part, $F_{\mathrm{s}}(q, \omega)$, because the imaginary parts of these terms will be peaked near the poles of the one-particle Green's function. The contribution of these terms to the scattering may be written as

$$F_{\mathrm{s}}(q, \omega) = \sum_{\alpha\beta} \Lambda_{\alpha}(q, \omega)\, G_{\alpha\beta}(q, \omega)\, \Lambda_{\beta}(q, \omega) \tag{6.11}$$

where $\Lambda_{\alpha}(q, \omega) = n(0)^{1/2} + P_{\alpha}(q, \omega)$ is the summation of all those processes by which the density operator $\rho(q)$ couples to the single particle operator $a^{+}(q)$, or $a(q)$, as represented in figure 48. The remaining part of $F(q, \omega)$ is known as the

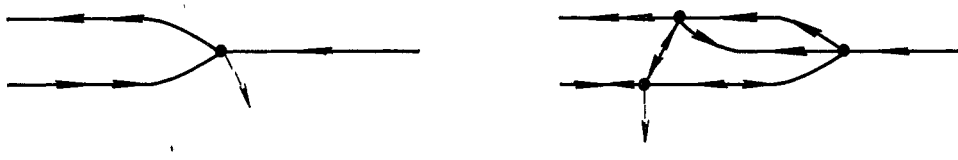

Figure 48. Two diagrams contributing to $P_1(q, \omega)$. The Green's functions of the internal lines are described by two arrows: $\leftarrow\leftarrow$ = G_{11}, $\rightarrow\leftarrow$ = G_{21}, etc.

regular part $F_{\mathrm{R}}(q, \omega)$ and consists of all those diagrams which at all points have two or more single particle lines.

The result given by equation (6.11) is of great importance because it shows that the poles of the single particle Green's functions will also be poles of the density–density response function. The frequencies observed for the sharp peaks in the neutron scattering experiments are therefore the frequencies of the poles in the single particle functions. It is, however, important to note that although some of the poles in $G_{\alpha\beta}(q, \omega)$ and $F(q, \omega)$ occur at the same frequencies, their residues may and usually will be different, and also that any broad features in the spectral responses may be quite different in the different Green's functions. It is therefore necessary to distinguish between calculations of the density–density Green's function, which may be directly compared with neutron scattering experiments,

and calculations of the single particle Green's function which may have the same poles but may not be compared with these experiments in detail.

These results are very general, but in most cases it is necessary to make approximations to proceed further. The only exact results which have been obtained are in the long wavelength and low frequency region where a very careful diagrammatic analysis by Gavoret and Nozieres (1964) gave results for the Green's functions at $T = 0$ as

$$\lim_{q,\omega\to 0} G_{\alpha\alpha}(q,\omega) = -\lim_{q,\omega\to 0} G_{\alpha\beta}(q,\omega)$$
$$= \frac{n(0)\,Mc^2}{N\hbar^2(\omega^2 - c^2q^2 + \mathrm{i}0^+)} \tag{6.12}$$

and for the density–density Green's function as

$$\lim_{q,\omega\to 0} F(q,\omega) = \frac{q^2}{M(\omega^2 - c^2q^2 + \mathrm{i}0^+)} \tag{6.13}$$

showing that both functions have only a single pole, corresponding to the macroscopic sound velocity, and that this pole is the only contribution to the spectral responses as q and ω become small. Similar conclusions were obtained by Hohenberg and Martin (1965) and Huang and Klein (1964).

6.1.2. *The Bogoliubov approximation.* The classic work of Bogoliubov (1947) on the dilute weakly interacting gas is equivalent to considering only the first term in the potential energy; namely V_2 of equation (6.2). The self-energies are then given by

$$\left.\begin{aligned} M_{11}(q,\omega) &= n(0)\,(V(0) + V(q)) \\ M_{12}(q,\omega) &= n(0)\,V(q) \end{aligned}\right\} \tag{6.14}$$

giving the chemical potential $\mu = n(0)\,V(0)$. The one-particle Green's functions then have only a single pole at the frequencies given by

$$\hbar^2\omega_{\mathrm{B}}(q)^2 = E(q)^2 + 2E(q)\,n(0)\,V(q) \tag{6.15}$$

and the Green's function is given by

$$G_{11}(q,\omega) = \frac{\hbar\omega + E(q) + n(0)\,V(q)}{\hbar^2(\omega^2 - \omega_{\mathrm{B}}(q)^2)}. \tag{6.16}$$

The occupation of the zero-momentum state, $n(0)$, is then obtained self-consistently from equations (6.16) and (6.9).

If we compare this result with the exact result (6.12), they are equivalent as q and $\omega \to 0$ if $n(0)\,V(0)/M = c^2$ and $n(0)/N = 1$. The Bogoliubov approximation is therefore a satisfactory approximation only if $n(0)/N$ is very close to unity, which in turn is equivalent to assuming that the interactions are very weak.

The density–density response function is obtained by neglecting $P_\alpha(q,\omega)$ in comparison with $n(0)^{1/2}$ in equation (6.11) when the singular part of $F(q,\omega)$ is

$$F_{\mathrm{s}}(q,\omega) = n(0)\sum_{\alpha\beta} G_{\alpha\beta}(q,\omega).$$

When q, $\omega \to 0$, this result is again equivalent to the exact result (6.13) provided that the difference between $n(0)$ and N is neglected.

The Bogoliubov approximation is therefore a small V approximation, but nevertheless is inconsistent with the known exact results. Its great triumph is that it shows that if the potential is repulsive, that is if $V(0)$ is positive, the dispersion relation is linear with q (equation (6.15)). It fails to be consistent, however, because this of necessity implies that $n(0) < N$ when the theory fails to give the correct results for either $G_{\alpha\beta}$ or F as q and $\omega \to 0$.

6.1.3. *The T matrix approximation.* The Bogoliubov approximation is dependent upon the potential being sufficiently weak that first-order perturbation theory is adequate. Since it is impossible for two helium atoms to be at the same point at

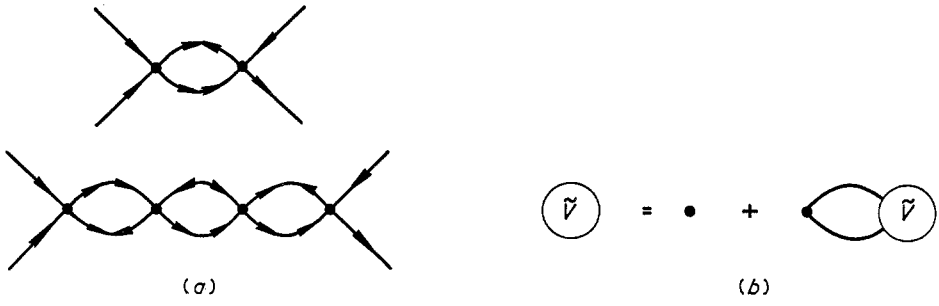

Figure 49. Two ladder diagrams, shown in (*a*), for the effective interaction $\tilde{V}$ which is given by the integral equation shown in (*b*).

the same time the potential is certainly not weak at short distances. Brueckner and Sawada (1957) developed a theory allowing for strong repulsive interactions by assuming that the liquid was dilute. They showed that if the strong potential is of radius a then a suitable expansion parameter is (ρa^3) where ρ is the density.

Basically the approximation is to replace the interaction in the Bogoliubov approximation by the series of ladder diagrams shown in figure 49(*a*). The effective interaction is then dependent upon the wave vectors and possibly the frequencies associated with the four lines involved in the interaction, and is given by the integral equation, figure 49(*b*),

$$\tilde{V}(\boldsymbol{q}_1, \boldsymbol{q}_2, \boldsymbol{q}_3, \boldsymbol{q}_4) = V(\boldsymbol{q}_1 - \boldsymbol{q}_3) + \mathrm{i} \sum_{\boldsymbol{k}} \int \frac{\mathrm{d}\omega}{2\pi} V(\boldsymbol{q}_1 - \boldsymbol{k})\, G(\boldsymbol{k}, \omega)\, G(\boldsymbol{q}_1 + \boldsymbol{q}_2 - \boldsymbol{k}, \omega) \times \tilde{V}(\boldsymbol{k}, \boldsymbol{q}_1 + \boldsymbol{q}_2 - \boldsymbol{k}, \boldsymbol{q}_3, \boldsymbol{q}_4).$$

Brueckner and Sawada were able to solve this equation by making the centre-of-mass approximation, when V is independent of $\boldsymbol{q}_1 + \boldsymbol{q}_2$ and the frequencies $\tilde{V}$ associated with the particle lines. Parry and ter Haar (1962) have estimated the error produced by this approximation to be only about 3%. Brueckner and Sawada then suggested that the Green's functions in the integral equation could be approximated by neglecting the off-diagonal parts of the self-energy $M_{12}(\boldsymbol{q}, \omega)$ when it is unnecessary to distinguish between the different components V_{11}, V_{12} etc. Finally they assumed that the scattering was dominated by the s-wave part of the scattering potential.

Once the effective interaction T matrix has been obtained the quasiparticle spectrum, $n(0)$, and $G_{\alpha\beta}(\boldsymbol{q}, \omega)$ are all obtained from the expressions deduced by the Bogoliubov theory but with $V(\boldsymbol{q})$ replaced by $\tilde{V}(0, 0, \boldsymbol{q}, -\boldsymbol{q})$.

Calculations have been performed with this theory by Goble and Trainor (1968) who used various hard-core radii and solved the equations selfconsistently for $n(0)$ and the excitation spectrum. They found that $n(0)/N$ varied from 0·37 to 0·79 as the hard-core radius was altered from 3·0 to 1·0 Å. Byckling (1966) performed similar calculations, but allowing for all partial waves, for a hard-core potential of radius 2·6 Å and for a Lennard–Jones potential. He was unable to obtain $n(0)$ selfconsistently but the calculated excitation curves were qualitatively similar to the experimental results. The value of $n(0)$ calculated from these curves was however in both cases larger than N.

Singh and Kumar (1967, 1970) have extended the theory to include a weak attractive interaction in addition to the repulsive core. The attractive interaction is treated by first-order perturbation theory and the repulsive interaction by a T matrix. They also consider higher-order diagrams for the self-energy.

All of these theories give results which at low frequencies reduce to the Bogoliubov approximation with a modified form of potential. They will therefore only be consistent with the exact result (6.12) if $n(0)/N \simeq 1$. In all the numerical calculations the spectra which agree even qualitatively with the experimental results give $n(0)/N$ very different from unity. We conclude therefore that although T matrix corrections are important to take account of the strong correlations produced by the repulsive interactions at short distances, it is also necessary to include more complex diagrams to obtain a theory of liquid helium.

6.1.4. *The shielded potential approximation.* Another approach to approximating the self-energies for liquid helium has been that of Tserkovnikov (1965, 1967), Pines (1966a,*b*), Etters (1966) and of Cheung and Griffin (1970, 1971) who have attempted to apply the same approximations as those inherent in the random phase approximation of an electron gas. Initially it is useful to distinguish between proper and improper contributions to the functions $G_{\alpha\beta}$, F and Λ defined in §6.1.1. (Kondor and Szepfalusy 1968). The proper parts of these functions, denoted by $\mathscr{G}_{\alpha\beta}$, etc, are those parts which cannot be separated into two by cutting a single interaction vertex in two. In terms of the proper parts of the functions it then follows immediately that

$$F_{\mathrm{R}}(\boldsymbol{q},\omega) = \mathscr{F}_{\mathrm{R}}(\boldsymbol{q},\omega)/(1-V(\boldsymbol{q})\mathscr{F}_{\mathrm{R}}(\boldsymbol{q},\omega))$$

$$F(\boldsymbol{q},\omega) = \mathscr{F}(\boldsymbol{q},\omega)/(1-V(\boldsymbol{q})\mathscr{F}(\boldsymbol{q},\omega))$$

$$\Lambda_{\alpha}(\boldsymbol{q},\omega) = \mathscr{L}_{\alpha}(\boldsymbol{q},\omega)/(1-V(\boldsymbol{q})\mathscr{F}_{\mathrm{R}}(\boldsymbol{q},\omega))$$

$$\mathscr{F}_{\mathrm{s}}(\boldsymbol{q},\omega) = \sum_{\alpha\beta} \mathscr{L}_{\alpha}(\boldsymbol{q},\omega)\,\mathscr{G}_{\alpha\beta}(\boldsymbol{q},\omega)\,\mathscr{L}_{\beta}(\boldsymbol{q},\omega)$$

and

$$M_{\alpha\beta}(\boldsymbol{q},\omega) = \mathscr{M}_{\alpha\beta}(\boldsymbol{q},\omega) + \mathscr{L}_{\alpha}(\boldsymbol{q},\omega)\,V(\boldsymbol{q})\,\mathscr{L}_{\beta}(\boldsymbol{q},\omega).$$

These results are exact and important because they enable us to make a further connection between structure in the density–density function and in the single particle functions. In §6.1.1, we showed that the poles in $G_{\alpha\beta}(\boldsymbol{q},\omega)$ occurred in $F(\boldsymbol{q},\omega)$ through $F_{\mathrm{s}}(\boldsymbol{q},\omega)$. The regular part of $F(\boldsymbol{q},\omega)$, $F_{\mathrm{R}}(\boldsymbol{q},\omega)$, has a pole when $(1-V(\boldsymbol{q})\mathscr{F}_{\mathrm{R}}(\boldsymbol{q},\omega))$ has a zero. Since the same denominator occurs in $\Lambda_{\alpha}(\boldsymbol{q},\omega)$ and hence in $M_{\alpha\beta}(\boldsymbol{q},\omega)$ the one-particle self-energy will have a singularity at the same frequency as the pole of $F_{\mathrm{R}}(\boldsymbol{q},\omega)$. Structure in the single particle self-energy will therefore be mirrored in the regular part of the density–density Green's function.

Approximations are needed before detailed calculations can be performed with this formalism. The approximation used in the shielded potential approximation is to include only those terms which correspond to the Bogoliubov approximation, but to replace the bare interaction with the shielded interaction. This corresponds to neglecting the proper self-energy, $\mathscr{M}$ and writing $\Lambda_\alpha = n(0)^{1/2}$ when

$$M_{\alpha\beta}(\boldsymbol{q}, \omega) = n(0)\, V_s(\boldsymbol{q}, \omega)$$

where

$$V_s(\boldsymbol{q}, \omega) = V(\boldsymbol{q})/(1 - V(\boldsymbol{q})\, \mathscr{F}_R(\boldsymbol{q}, \omega)),$$

and

$$\mathscr{F}_s(\boldsymbol{q}, \omega) = \frac{2E(\boldsymbol{q})\, n(0)}{\hbar^2 \omega^2 - E(\boldsymbol{q})^2}.$$

In figure 50 we show a graphical representation of M, F_R and F_s in the shielded

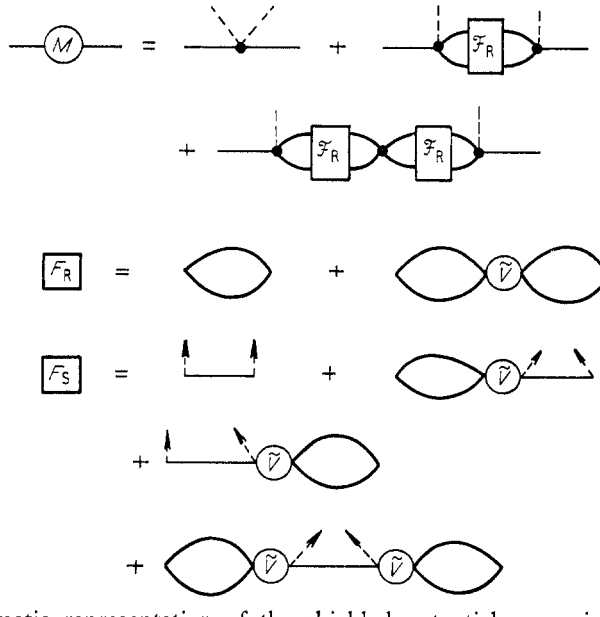

Figure 50. Schematic representation of the shielded potential approximations for M, F_R and F_S.

potential approximation. Using these results both the single particle and density–density correlation functions may be obtained for a particular approximation to $\mathscr{F}_R(\boldsymbol{q}, \omega)$.

The simplest approximation is to assume that $\mathscr{F}_R(\boldsymbol{q}, \omega)$ is given by a simple polarization bubble, namely,

$$\mathscr{F}_R(\boldsymbol{q}, \omega) = \sum_\alpha \sum_{\boldsymbol{p}} \int \frac{d\omega'}{2\pi} G_{1\alpha}(\boldsymbol{p}, \omega')\, G_{\alpha 1}(\boldsymbol{q} - \boldsymbol{p}, \omega - \omega'). \tag{6.17}$$

Strictly the theory should now be made self-consistent by using $G_{\alpha\beta}(\boldsymbol{q}, \omega)$ calculated from the self-energy (Tserkovnikov 1967). Cheung and Griffin (1970) suggested replacing the Green's functions on the right hand side of equation (6.17) for $F_R(\boldsymbol{q}, \omega)$ by free boson Green's functions, but this leads to difficulties at absolute zero because $\mathscr{F}_R(\boldsymbol{q}, \omega)$ then vanishes.

Although the theory has not as yet been applied in full detail it has several appealing features. Firstly the self-energies are complex functions of $\boldsymbol{q}$ and ω, unlike the real functions of the T matrix approximations. The Green's functions are not therefore single poles but may exhibit more structure. This is clearly a great improvement if the theory is to explain the neutron scattering results of § 3.

On a more quantitative level the results give a more satisfactory result for the velocity of sound at finite temperatures. Etters (1966) approximates $F(\boldsymbol{q},\omega)$ by $F_{\mathrm{R}}(\boldsymbol{q},\omega)$ and then calculates $\mathscr{F}_{\mathrm{R}}(\boldsymbol{q},\omega)$ using free boson Green's functions. $F_{\mathrm{R}}(\boldsymbol{q},\omega)$ has a pole when

$$V(\boldsymbol{q})\sum_{\boldsymbol{p}}\frac{n(\boldsymbol{p})-n(\boldsymbol{q}+\boldsymbol{p})}{\hbar\omega-E(\boldsymbol{p}+\boldsymbol{q})+E(\boldsymbol{p})}=1 \tag{6.18}$$

where $n(\boldsymbol{p})$ is the Bose occupation number. On expanding this function for large ω a dispersion relation is obtained for small $\boldsymbol{q}$

$$\omega^2=c^2q^2\left(1+\frac{\hbar^2q^2}{M\omega^2}\langle\boldsymbol{p}^2\rangle+\ldots\right)$$

where the velocity c is given by

$$c^2=\sum_{\boldsymbol{p}}n(\boldsymbol{p})\,V(0)/M$$

and $\langle\boldsymbol{p}^2\rangle$ is the mean value of $\boldsymbol{p}^2$. This result shows that the velocity is not dependent upon $n(0)$ as given by the Bogoliubov approximation but upon $\sum_{\boldsymbol{p}}n(\boldsymbol{p})$. In the former case the velocity would be expected to be strongly temperature dependent (Hohenberg and Martin 1964) whereas in practice, as described in § 3.4.2, it is largely independent of temperature. Although in our derivation of the velocity the $\sum_{\boldsymbol{p}}n(\boldsymbol{p})$ excludes the particles in the zero momentum state, by including the appropriate part of $F_{\mathrm{s}}(\boldsymbol{q},\omega)$, the sum may be extended over all the particles to give a result which is largely independent of temperature in agreement with the experimental results § 3.4.2. This theoretical development is certainly not accurate because of the use of the free Bose Green functions to calculate $\mathscr{F}_{\mathrm{R}}(\boldsymbol{q},\omega)$ and because of the high frequency expansion. In practice the average kinetic energy of those particles which are not in the condensate is sufficiently large that this expansion is invalid. Despite these difficulties the results are strongly suggestive that the screened potential approximation is useful.

Tserkovnikov (1967) and Cheung and Griffin (1970) have also examined the zeros of the function $(1-V(\boldsymbol{q})\mathscr{F}_{\mathrm{R}}(\boldsymbol{q},\omega))$ with different approximate forms for $\mathscr{F}_{\mathrm{R}}(\boldsymbol{q},\omega)$. Both sets of workers conclude that at small ω and $\boldsymbol{q}$ there are two sets of solutions. One corresponds to the normal sound waves propagating with velocity, c, and the other to a new sound-like wave propagating with a velocity c_2 which is proportional to $n(0)^{1/2}$. They suggest that the one-particle Green's functions $G_{\alpha\beta}(\boldsymbol{q},\omega)$ may have two poles corresponding to these two branches of the excitation spectrum, but that the new branch may be overdamped. In contrast in the density–density response, $F(\boldsymbol{q},\omega)$, this new mode has negligible weight so that it could not be observed by neutron scattering experiments. These authors conclude that this new excitation is a form of collisionless second sound, in contrast to the normal second sound mode which occurs in the thermodynamic regime. The existence of this branch is certainly one of the interesting predictions of the theory. Unfortunately we cannot at present rule out the possibility that it arises from the

approximations used to evaluate $\mathscr{F}_{\mathrm{R}}(\boldsymbol{q}, \omega)$. In particular at absolute zero, $\mathscr{F}_{\mathrm{R}}(\boldsymbol{q}, \omega)$, cannot have an imaginary part for small $\boldsymbol{q}$ when $\omega < cq$. The new mode, if it exists, must be well defined in this limit. The large damping found by Cheung and Griffin (1970) arises from their use of the free Bose Green's functions in calculating $\mathscr{F}_{\mathrm{R}}(\boldsymbol{q}, \omega)$. It remains an open and very interesting question whether this collisionless second sound exists or whether it results from the approximations in the theory.

Ma *et al* (1971) and Gould and Wong (1971) have used a similar theory and examined the poles of the $F(\boldsymbol{q}, \omega)$ through the equation

$$1 = V(\boldsymbol{q})\mathscr{F}(\boldsymbol{q}, \omega).$$

Since they were primarily interested in the $q \to 0$ limit, it was technically advantageous to rewrite $\mathscr{F}(\boldsymbol{q}, \omega)$ in terms of the current–current Green's function. They then evaluated these expressions by approximating $\mathscr{F}_{\mathrm{R}}(\boldsymbol{q}, \omega)$ by the simple bubble diagram of equation (6.17) and also considering the first two terms in the expansion of $\Lambda_{\alpha}(\boldsymbol{q}, \omega)$. In this way they selected all those diagrams for which there was one closed ring of single particle lines.

All of these contributions contain terms involving two Green's functions such as given in equation (6.17) and in their approximation they treated these Green's functions within the Bogoliubov approximation. Expressions for the $\boldsymbol{q}$ dependence of the excitation frequency, $\omega(\boldsymbol{q})$, were obtained by expanding these terms in a power series in $\boldsymbol{q}$. The most unexpected feature is that some of the integrals over $\boldsymbol{p}$ diverge as $p \to 0$. In this region the expansion for small $\boldsymbol{q}$ is clearly invalid but the divergence led Gould and Wong (1971) to suggest that the dispersion relation is given by

$$\omega(q) = q\{c_0 + c_2 q^2 + c_4 q^4 \ln(1/q)\}$$

and they obtained expressions for the coefficients c_0, c_2 and c_4 in terms of the interaction between the helium atoms. Ma *et al* (1971) obtained a similar result for the temperature dependence of the sound velocity namely

$$\mathrm{Re}\left(\frac{\omega}{qc_0}\right) = 1 + A_1 T^4 + BT^4 \ln(1/T) + \ldots.$$

Both of these results are clearly of interest in comparison with the power series expansions used to describe the experimental results at small q (§ 3.3.3).

The difference between these results and those obtained by calculating $\mathscr{F}_{\mathrm{R}}(\boldsymbol{q}, \omega)$ with free Bose propagators emphasizes the importance of making appropriate approximations in the theory. Neither of the approaches has been made self-consistent and there is no proof that it is adequate to approximate $\mathscr{F}_{\mathrm{R}}(\boldsymbol{q}, \omega)$ by the leading term. In all of these theories, as emphasized by Cheung and Griffin (1970) and by Ma *et al* (1971), the potential $V(\boldsymbol{q})$ should be replaced by the T matrix or effective potential, $\tilde{V}(\boldsymbol{q}_1, \boldsymbol{q}_2, \boldsymbol{q}_3, \boldsymbol{q}_4)$, as introduced in § 6.1.3. The strong repulsive interactions at short distances do not then give rise to divergent results in the summations over wave vector. Clearly we must await further developments of this theory before it is possible to assess whether some low order approximation to $\mathscr{F}_{\mathrm{R}}(\boldsymbol{q}, \omega)$ gives a satisfactory theory of liquid helium, or whether it is necessary to include such complex diagrams that the theory becomes unmanageable.

6.1.5. *Other developments.* Several theories of liquid helium have exploited the similarity between the λ transition of liquid helium and the superconducting phase transition in metals and have suggested that there is a similar pairing in liquid

helium. In the original pairing theories of Valatin and Butler (1958), Girardeau and Arnowitt (1959), Luban (1962), Kobe (1968) and Brown and Coopersmith (1969), a macroscopic occupation of the zero momentum state was assumed and the Bogoliubov transformation performed. The remainder of the hamiltonian was, however, truncated so that it could be diagonalized in a similar manner to that used in the theory of superconductivity. There seems to be no justification for this truncation in practice, unlike the case of superconductors.

Recently pairing theories have been developed in which there is no macroscopic occupation of the zero momentum state, but an effective attractive interaction between the particles to produce a pair condensation (Congilio *et al* 1969, Evans and Imry 1969). This variant of the theory is unrealistic. A repulsive interaction must exist between helium atoms because they cannot occupy the same position in space and also because the liquid has a positive compressibility. In superconductors the exclusion principle provides the effective repulsion to keep the particles apart, and the interaction may be attractive, but in helium the interaction must be effectively repulsive.

A related but somewhat different formalism to that described above has been developed by Brandow (1969, 1971). He suggests that instead of using the many-body theory developed by Beliaev (1958) and by Hugenholtz and Pines (1959) it is preferable to treat helium as a fermi system with infinite spin degeneracy. The infinite spin degeneracy permits the condensation of all the particles into a single spatial state, and has the advantage that the techniques developed by Goldstone (1957) for fermi systems may be taken over directly to liquid helium. This obviates the need to introduce a chemical potential and enables conservation of particles to be enforced rigorously at all stages in the development.

He then suggests that the important contributions to the energy and self-energy of the particles arise from the short range correlations in the motions of the particles as found by Bethe (1965, 1967) in nuclear matter. It is of interest that the development distinguishes between those terms in the self-energy which may be represented as an effective potential and hence summed, and those terms which are energy dependent and far more difficult to treat. In the anharmonic theory of solid helium (Werthamer 1969) the success of the selfconsistent theory shows that inclusion of the former terms and neglect of the latter is a reasonable approximation. We must await further results however before we can assess Brandow's theory in detail.

Finally the theory we have described has been largely restricted to absolute zero. As shown for example by Abrikosov *et al* (1964), there is no difficulty in extending the techniques to finite temperature, and the development has been pursued by many authors. In view, however, of the lack of success in quantitatively calculating the properties of liquid helium at absolute zero, it is not appropriate to review these developments here.

6.2. *Calculations of* $S(Q)$

By far the most successful calculations of the structure factor of liquid helium have been made by use of variational techniques and an approximate form of the wavefunction. The hamiltonian of the system is given by

$$H = -\sum_i \frac{\hbar^2}{2M}\nabla_i^2 + \sum_{ij} V(\boldsymbol{r}_{ij})$$

where $V(\boldsymbol{r})$ is the two-body potential function which in the case of liquid helium may be reasonably taken be to a Lennard-Jones potential

$$V(r) = 4E\left\{\left(\frac{\sigma}{r}\right)^{12} - \left(\frac{\sigma}{r}\right)^{6}\right\}$$

with $E = 10{\cdot}22$ K and $\sigma = 2{\cdot}556$ Å as determined by de Boer and Michels (1938).

Since this potential is large whenever two particles are close together, the trial wavefunction must be taken to be of a form such that it is small whenever pairs of particles approach. This is most simply achieved with a Jastrow function

$$\Psi = \sum_{i<j} \exp\left(U(\boldsymbol{r}_{ij})/2\right).$$

On substituting this wavefunction into the Schrödinger equation, the ground state energy per particle is

$$E_0 = \frac{1}{2v}\int\left(\frac{\hbar^2}{4M}\frac{\mathrm{d}g(\boldsymbol{r})}{\mathrm{d}r}\frac{\mathrm{d}U(\boldsymbol{r})}{\mathrm{d}r} + g(\boldsymbol{r})\,V(\boldsymbol{r})\right)\mathrm{d}\boldsymbol{r} \tag{6.19}$$

where v is the volume of liquid and $g(\boldsymbol{r})$ the pair distribution function, which in terms of the wavefunction, is given by

$$g(\boldsymbol{r}_1 - \boldsymbol{r}_2) = \frac{v^2\int|\Psi(\boldsymbol{r}_1, \ldots, \boldsymbol{r}_N)|^2\,\mathrm{d}\boldsymbol{r}_3 \ldots \mathrm{d}\boldsymbol{r}_N}{\int|\Psi(\boldsymbol{r}_1, \ldots, \boldsymbol{r}_N)|^2\,\mathrm{d}\boldsymbol{r}_1 \ldots \mathrm{d}\boldsymbol{r}_N} \tag{6.20}$$

which in turn is related to $S(Q)$ by

$$S(Q) = 1 + \frac{N}{v}\int(g(\boldsymbol{r}) - 1)\exp(\mathrm{i}\boldsymbol{Q}\,.\,\boldsymbol{r})\,\mathrm{d}\boldsymbol{r}.$$

The one-particle density matrix may also be defined in terms of the wavefunction by

$$n(\boldsymbol{r} - \boldsymbol{r}') = \frac{N\int\Psi(\boldsymbol{r}, \boldsymbol{r}_2, \ldots, \boldsymbol{r}_N)\,\Psi(\boldsymbol{r}', \boldsymbol{r}_2, \ldots, \boldsymbol{r}_N)\,\mathrm{d}\boldsymbol{r}_2 \ldots \mathrm{d}\boldsymbol{r}_N}{\int|\Psi(\boldsymbol{r}_1, \ldots, \boldsymbol{r}_N)|^2\,\mathrm{d}\boldsymbol{r}_1 \ldots \mathrm{d}\boldsymbol{r}_N}.$$

For large $\boldsymbol{r} - \boldsymbol{r}'$, Penrose and Onsager (1956) showed that $n(\boldsymbol{r} - \boldsymbol{r}')$ approaches $n(0)$ the occupation of the condensed zero momentum state. The occupation numbers for the other states are obtained from

$$n(\boldsymbol{q}) = \int(n(\boldsymbol{r}) - n(0))\exp(i\boldsymbol{q}\,.\,\boldsymbol{r})\,\mathrm{d}\boldsymbol{r}.$$

Hence, once the wavefunction has been found the energy, $S(Q)$, and the occupation numbers can be found.

There have been two approaches adopted to obtain the wavefunctions from equations (6.19) and (6.20). The direct method is difficult numerically because equation (6.20) contains a multidimensional integral for each of the helium atoms. McMillan (1965) and Schiff and Verlet (1967) have both adopted the direct procedure, however. They approximated $U(r)$ by

$$U_{\mathrm{S}}(r) = -(a/r)^n \tag{6.21}$$

and calculated the integrals for a variety of values of a and n. McMillan (1965) performed the integrals with a Monte Carlo procedure and a system of either 32 or 108 helium atoms. The minimum energy, density and $n(0)/N$ are listed in table 3 and occurred when $a \simeq 2{\cdot}7$ Å and $n \simeq 5$. Schiff and Verlet (1967) evaluated the

integrals for 864 particles by using the techniques of molecular dynamics. Their results are listed in table 3 and shown in figure 51. The minimum was obtained with $a \simeq 2{\cdot}9$ Å and $n \simeq 5$. The values of $n(q)$ obtained by McMillan (1965) are shown in figure 52.

Table 3. The values of the density $N_{\min}/N$ (fractions of the density at $T = 0$), the minimum energy $E_{\min}$, the energy E at density N, and the fraction of particles in the zero momentum state, $n(0)/N$

	$N_{\min}/N$	$E_{\min}$	E	$n(0)/N$
McMillan (1965)	$0{\cdot}89 \pm 0{\cdot}01$	$-5{\cdot}9$	$-5{\cdot}66$	$0{\cdot}11 \pm 0{\cdot}01$
Schiff and Verlet (1967)	$0{\cdot}9 \pm 0{\cdot}1$	$-5{\cdot}95$	$-5{\cdot}73$	$0{\cdot}105 \pm 0{\cdot}005$
Massey and Woo (1967)		$-6{\cdot}06$	$-6{\cdot}02$	
Campbell and Feenberg (1969)			$-6{\cdot}7$	
Francis *et al* (1970)				
Short range only	0·97	$-6{\cdot}29$		0·131
Total $U(r)$	1·035	$-6{\cdot}77$	$-6{\cdot}72$	0·101
Experiment	1·0	$-7{\cdot}14$	$-7{\cdot}14$	

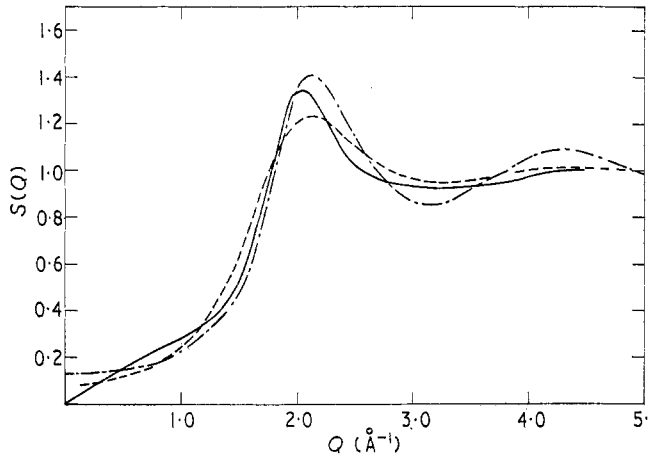

Figure 51. The structure factor $S(Q)$: ——, experimental results from Achter and Meyer (1969); – – – –, calculations by Schiff and Verlet (1967); —·—·—, calculations with a hard sphere model from Reatto and Chester (1967).

The alternative approach to performing the integrals in equation (6.20) is to obtain another relation between $g(r)$ and $U(r)$ which is more convenient computationally. Several equations of this type have been found in the theory of classical liquids (Egelstaff 1967), and the results may be adapted to liquid helium without difficulty. For example, the BBGKY equation, known by the initials of its originators, was derived by Wu and Feenberg (1962), in the form

$$\frac{\mathrm{d}U(r)}{\mathrm{d}r} - \frac{\mathrm{d}g(r)}{\mathrm{d}r}\frac{1}{g(r)} = -N\int g(r')\,U(r')\{g(|\boldsymbol{r}-\boldsymbol{r}'|)-1\}\cos(\boldsymbol{r}\boldsymbol{r}')\,\mathrm{d}\boldsymbol{r}'$$

where $\cos(\boldsymbol{r}\boldsymbol{r}')$ is the cosine of the angle between $\boldsymbol{r}$ and $\boldsymbol{r}'$.

This equation is only approximate and other approximate equations connecting $g(r)$ and $U(r)$ have been derived, and are known as the hypernetted chain (HNC)

equation, the Percus–Yevick equation (Feenberg 1970) and the modified Percus–Yevick equation (PY2XS) (Francis *et al* 1970). *A priori* it is by no means clear which of these equations will give the most satisfactory results in any particular instance.

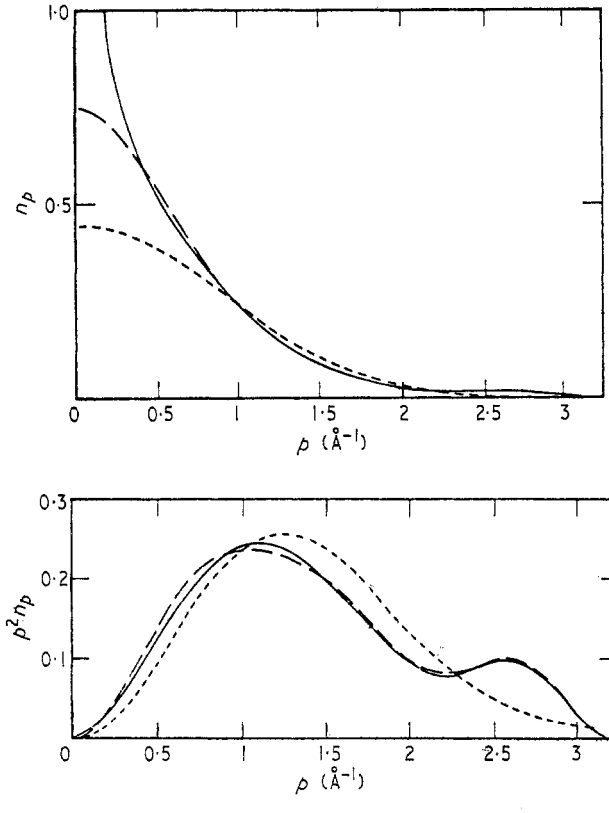

Figure 52. The distribution of particles $n_p(= n(p)/N)$ and $p^2 n_p$: — — —, as calculated by McMillan (1965); ———, an empirical fit including the correct behaviour as $p \to 0$ by Gersch and Smith (1971); - - - - -, a single gaussian fit giving the same average kinetic energy as McMillan.

Lee (1969) used the HNC equation and equation (6.21) for $U(r)$. The BBGKY equation was used by Massey (1966) and by Massey and Woo (1967) to obtain $S(Q)$ for liquid helium. The pair distribution function was chosen to have a complex form involving five parameters which were varied to find the minimum energy. The results for the Lennard-Jones potential are listed in table 3, and are similar to those obtained with the other technique. Their results for $g(r)$ are also very similar.

All of these calculations gave a nonzero result for $S(Q)$ when $Q = 0$ in contradiction to the exact result, equation (6.13). Reatto and Chester (1967) showed that the discrepancy arose from the inadequacy of the assumed form of $U(r)$. The virtual phonons in liquid helium give rise to long range correlations in the ground state wavefunction and Reatto and Chester calculated this correlation with the aid of a phonon model. They suggested that

$$U(r) = U_{\mathrm{L}}(r) + U_{\mathrm{S}}(r)$$

where $U_S(r)$ is the form used before and

$$U_L(r) = -\frac{cM}{\pi^2 N\hbar}(r^2 + k_c^{-2})$$

with k_c an arbitrary cut-off wave vector for the phonon model. This result shows that the long range correlations in the ground state fall off as $1/r^2$, and this makes the numerical work involved in the calculations for all of the methods more difficult. An approximate form for $S(Q)$ may be obtained by taking advantage of the different range of $U_L(r)$ and $U_S(r)$ to give

$$S(Q) = S^0(Q)/(1 + NU_L(Q)\,S^0(Q))$$

where $U_L(Q)$ is the Fourier transform of $U_L(r)$ and $S^0(Q)$ is $S(Q)$ calculated with $U(r) = U_S(r)$. This result suggests that these long range correlations will only be of importance for small wave vectors, Q.

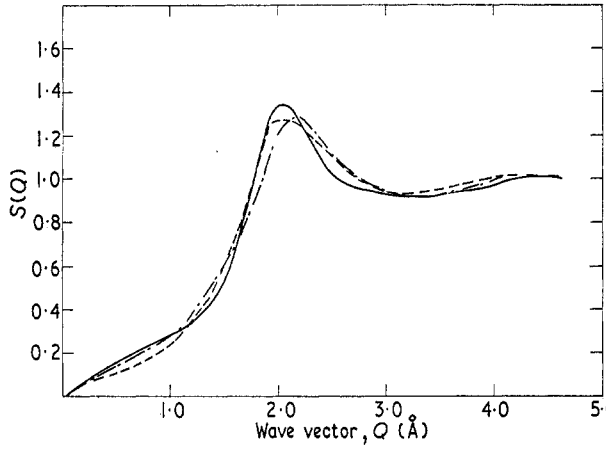

Figure 53. Calculations of $S(Q)$ by Francis *et al* (1970) (– – – –) and by Campbell and Feenberg (1969) (—·—·—) as compared with the measurements of Achter and Meyer (1969) (———).

Schiff and Verlet (1967) discuss the importance of $U_L(r)$ by including it as a small perturbation in their molecular dynamics approach. Their results show that the energy decreases as k_c increases and they conclude that the inclusion of $U_L(r)$ improves $S(Q)$ at small Q without appreciably changing the other results. Francis *et al* (1970) developed the PY2XS equation in order to minimize the computational difficulties of using the full $U(r)$ throughout the calculation. They chose the values of $a = 2{\cdot}9$ Å and $n = 5$ for $U_S(r)$ and then varied k_c to obtain the results listed in table 3. In figure 53 we show their results for $S(Q)$ as compared with experimental results, and in figure 52 the correction to $n(q)$ resulting from the different behaviour as $q \to 0$. The inclusion of the long-range part of $U(r)$ largely changes the curve for $n(q)$ at small q, where $n(q)$ is a constant if $U_L(r)$ is neglected but varies as $1/q$ for the full $U(r)$.

The long-range effects were incorporated into $U(r)$ in a somewhat *ad hoc* manner by Reatto and Chester (1967). A more systematic way of including these effects is to use the technique of improving Ψ developed by Jackson and Feenberg (1961) and applied by Campbell and Feenberg (1969). They considered a subspace

spanned by the ground state and all two-phonon wavefunctions, and then carried out a Bogoliubov transformation in this subspace to obtain an improved wavefunction. The transformation generates an equation which maximizes that improvement, and enables an improved $S(Q)$ to be found. With this new $S(Q)$, $g(r)$ and $U(r)$ are calculated using the normal integral equations. The procedure may then be repeated with the new $U(r)$ to obtain a yet further improved $S(Q)$ until convergence is obtained. In their calculations Campbell and Feenberg (1969) initially took $U(r)$ from the work of Massey and Woo (1966) and then used their formalism to obtain an improved $S(Q)$. Convergence was obtained after only one cycle. The energy of the ground state decreased as shown in table 3 and the structure factor $S(Q)$ changed slightly as shown in figure 53 and also was somewhat dependent upon the integral equation used to obtain $U(r)$ from $S(Q)$.

The results of all these workers give quite good agreement ($\simeq 15\%$) between experiment and theory for the ground state energy and $S(Q)$. The fraction of helium atoms in the zero momentum state, $n(0)/N$, is given by all the methods as about $0{\cdot}11 \pm 0{\cdot}02$. Although the agreement with $S(Q)$ is very gratifying it is unfortunately not unexpected. $S(Q)$ has a very similar form for all one component liquids and in figure 51 we show the exact solution (Wertheim 1963) to the Perus–Yevick equation for liquid helium at its equilibrium density and with a hard sphere potential

$$V = \infty \qquad r < 2{\cdot}9 \text{ Å}$$

$$V = 0 \qquad r > 2{\cdot}9 \text{ Å}.$$

The results (Reatto and Chester 1967) are also in reasonable agreement with the experimental results and suggest that the form of $S(Q)$ is comparatively insensitive to the details of the potential and probably the wavefunction. The agreement shown in figures 51 and 53 should not therefore be interpreted as particularly strong evidence that the ground state wavefunction is well represented by a Jastrow form.

Despite these qualms, the success of the calculations of $S(Q)$ compared with the lack of comparable success with the microscopic calculations described in § 6.1 has prompted a comparison of the two theories in the hope that the Jastrow function approach will suggest suitable approximations in the microscopic theory. Sim *et al* (1970) have applied both the microscopic approach and the Jastrow function approach to obtain the energy of the dilute Bose gas. They show that both approaches give identical results for those terms involving the potential $(V)^m$ for m less than 4. In the terms of order $(V)^4$, the Jastrow function approach as optimized by Campbell and Feenberg (1969) gives correctly all the single ring diagrams (*a*) and simple ladder diagrams (*e*), which are shown in figure 54. It fails to give either the mixed diagrams or cross-bar diagrams (*b*)–(*d*) of figure 54 correctly. These may be obtained, however, if corrections to the Jastrow function theory are included in low-order perturbation theory. On the basis of this analysis, and the success of the Jastrow function approach, Sim *et al* suggest firstly that the Jastrow function approach sums ring and simple ladder diagrams to all orders, and secondly that this might be a good approximation in the microscopic theory. Brandow (1971) in his microscopic theory makes similar suggestions (§6.1.5).

6.3. *Direct calculations of the density fluctuations*

In § 6.1 we described the microscopic theory of liquid helium and emphasized the difference between the one-particle response functions and the density response

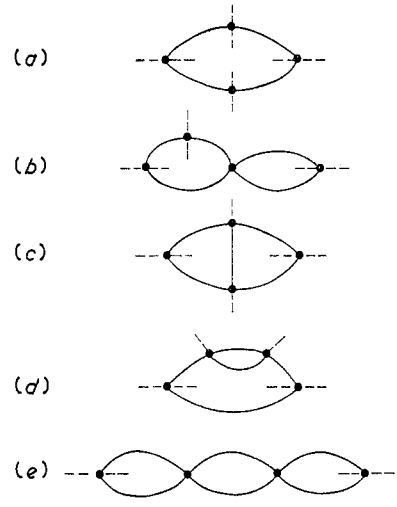

Figure 54. Diagrams contributing to the energy of a dilute Bose gas of order $(V)^4$. The ring diagrams (*a*) and the ladder diagram (*e*) are given exactly by the Jastrow function technique as developed by Campbell and Feenberg (1969). This technique gives the mixed diagram (*b*), the cross-bar diagram (*c*) and the side loop diagram (*d*) only approximately.

functions which may be measured directly. One way of developing the theory is to eliminate the single particle properties from consideration, and to recast the whole theory in terms of the density operator. There have been two approaches to this problem; one of these approaches is to eliminate all reference to the single particle properties in the hamiltonian and hence to rewrite it in terms of the density operators directly. This approach is described in § 6.3.1. The other approach is more akin to the calculations of $S(Q)$ and introduces approximate wavefunctions for the excited state and then evaluates corrections to these wavefunctions and energies as described in § 6.3.2. In the final sections we describe various aspects of the solutions to these equations.

6.3.1. *The hamiltonian in density fluctuations.* The hamiltonian for liquid helium consists of a kinetic energy term, T, and a two-body potential energy term. The latter is directly given in terms of the density operator $\rho(\boldsymbol{q})$ as

$$V = \sum_{\boldsymbol{q}} V(\boldsymbol{q})\,\rho(\boldsymbol{q})\,\rho(-\boldsymbol{q}).$$

The kinetic energy is given by

$$T = -\frac{\hbar^2}{2M}\int \nabla\Psi^*(\boldsymbol{r}).\nabla\Psi(\boldsymbol{r})\,\mathrm{d}\boldsymbol{r}$$

and presents more difficulty to rewrite in terms of the density. The difficulties have been overcome by Sunakawa *et al* (1969) and by Bierter and Morrison (1969), by introducing a momentum density operator

$$\boldsymbol{p}(\boldsymbol{r}) = -\frac{\mathrm{i}\hbar}{2}(\Psi^*(\boldsymbol{r})\,\nabla\Psi(\boldsymbol{r}) - \nabla\Psi^*(\boldsymbol{r})\,\Psi(\boldsymbol{r}))$$

and introducing the density operator, $\rho(\boldsymbol{r}) = \Psi^*(\boldsymbol{r})\,\Psi(\boldsymbol{r})$ into the expression for T

to give

$$T = -\frac{\hbar^2}{2M}\int \frac{\nabla\Psi^*(\boldsymbol{r})\,\Psi(\boldsymbol{r})\,\Psi^*(\boldsymbol{r}).\nabla\Psi(\boldsymbol{r})}{\rho(\boldsymbol{r})}\,\mathrm{d}\boldsymbol{r}.$$

Taking the gradient of the density operator gives

$$\mathrm{i}\hbar\nabla\rho(\boldsymbol{r}) = 2\mathrm{i}\hbar\nabla\Psi^*(\boldsymbol{r})\,\Psi(\boldsymbol{r}) - 2\boldsymbol{p}(\boldsymbol{r})$$

which on substitution into the kinetic energy yields

$$T = \frac{\hbar^2}{8M}\int\left(\nabla\rho(\boldsymbol{r}) + \frac{2\mathrm{i}\boldsymbol{p}(\boldsymbol{r})}{\hbar}\right)\frac{1}{\rho(\boldsymbol{r})}\left(\nabla\rho(\boldsymbol{r}) - \frac{2\mathrm{i}\boldsymbol{p}(\boldsymbol{r})}{\hbar}\right)\mathrm{d}\boldsymbol{r}.$$

The Fourier transform of the operators ρ and $\boldsymbol{p}$ obey the commutation relations

$$[\rho(\boldsymbol{q}), \rho(\boldsymbol{q}')] = 0$$

$$[\boldsymbol{p}(\boldsymbol{q}), \rho(\boldsymbol{q}')] = \hbar\boldsymbol{q}\rho(\boldsymbol{q}'-\boldsymbol{q})$$

and

$$[p_\alpha(\boldsymbol{q}), p_\beta(\boldsymbol{q}')] = \hbar(p_\alpha(\boldsymbol{q}+\boldsymbol{q}')\,q_\beta - p_\beta(\boldsymbol{q}+\boldsymbol{q}')\,q_\alpha).$$

The analysis proceeds by considering the perturbations in the density, $\rho(\boldsymbol{q})$ with $\boldsymbol{q}\neq 0$, and expanding T in a power series in these perturbations. Unfortunately the commutation relations are more complex than those for a canonical set of dynamical variables. In particular the second relation is not zero even when $\boldsymbol{q} = \boldsymbol{q}'$. Sunakawa *et al* (1969) overcome this difficulty by introducing a new variable

$$\boldsymbol{h}(\boldsymbol{q}) = \boldsymbol{p}(\boldsymbol{q}) - \frac{1}{N}\sum_{\boldsymbol{p}\neq\boldsymbol{q}}\rho(\boldsymbol{p}-\boldsymbol{q})\,\boldsymbol{h}(\boldsymbol{q})$$

which commutes with $\rho(\boldsymbol{q}')$ when $\boldsymbol{q}\neq\boldsymbol{q}'$, and furthermore they show that the commutation relations $[\boldsymbol{h}(\boldsymbol{r}), \rho(\boldsymbol{r}')]$ and $[\boldsymbol{h}(\boldsymbol{r}), \boldsymbol{h}(\boldsymbol{r}')]$ are identical with those assumed by Landau (1941) in his theory of quantum hydrodynamics.

If vortex motion is neglected these commutation relations become

$$[\boldsymbol{h}(\boldsymbol{q}), \rho(\boldsymbol{q}')] = \hbar\boldsymbol{q}\delta(\boldsymbol{q}-\boldsymbol{q}')$$

and

$$[\boldsymbol{h}(\boldsymbol{q}), \boldsymbol{h}(\boldsymbol{q}')] = 0,$$

which are appropriate to canonical dynamical variables. The hamiltonian may now be expanded in a power series in the operators $\rho(\boldsymbol{q})$ and $\boldsymbol{h}(\boldsymbol{q})$ to give

$$\begin{aligned} H = H_0 &+ \sum_{\boldsymbol{q}}\left\{\frac{1}{2M}\boldsymbol{h}(\boldsymbol{q}).\boldsymbol{h}(\boldsymbol{q}) + \left(\frac{\hbar^2 q^2}{8M} + NV(\boldsymbol{q})\right)\rho(\boldsymbol{q})\,\rho(-\boldsymbol{q})\right\} \\ &+ \frac{1}{N^{1/2}}\sum_{\substack{\boldsymbol{p},\boldsymbol{q},\\ \boldsymbol{p}+\boldsymbol{q}\neq 0}}\left\{\frac{1}{2M}\boldsymbol{h}(\boldsymbol{p}).\boldsymbol{h}(\boldsymbol{q})\,\rho(\boldsymbol{p}+\boldsymbol{q})\right. \\ &\qquad \left. + \frac{\hbar^2}{8M}(\boldsymbol{p}.\boldsymbol{q})\,\rho(\boldsymbol{p})\,\rho(\boldsymbol{q})\,\rho(-\boldsymbol{p}-\boldsymbol{q})\right\} + \ldots \end{aligned} \tag{6.21}$$

This hamiltonian is further reduced by diagonalizing the quadratic part with a transformation to the creation and destruction operators for the density excitations

$A^*(\boldsymbol{q})$ and $A(\boldsymbol{q})$ such that

$$\rho(\boldsymbol{q}) = (d(\boldsymbol{q}))^{1/2}(A(\boldsymbol{q}) + A^*(-\boldsymbol{q}))$$

and

$$\boldsymbol{h}(\boldsymbol{q}) = \frac{\hbar \boldsymbol{q}}{2(d(\boldsymbol{q}))^{1/2}}(A(-\boldsymbol{q}) - A^*(\boldsymbol{q}))$$

when the quadratic part of the hamiltonian becomes

$$\sum_{\boldsymbol{q}} \hbar\omega_0(\boldsymbol{q})\, A^*(\boldsymbol{q})\, A(\boldsymbol{q})$$

with

$$\omega_0(\boldsymbol{q}) = \frac{\hbar^2 q^2}{2Md(\boldsymbol{q})} \tag{6.22}$$

and

$$d(\boldsymbol{q}) = \frac{q^2}{\{q^2 + (4MN/\hbar^2)\, V(q)\}^{1/2}}.$$

Equation (6.22) for the energy of the excitations may be compared with equation (6.15) for the energy of the single particle excitations in the Bogoliubov approximation. They are identical apart from the replacement of $n(0)$ by the total particle number N, and hence the lowest order theory is far less temperature dependent. The cubic term in the hamiltonian may be rewritten in terms of the density excitation operators as

$$\begin{aligned} H_{\mathrm{I}} = \sum_{\boldsymbol{p},\boldsymbol{q}} [V_1(\boldsymbol{p},\boldsymbol{q})\{&A^*(\boldsymbol{p})\, A^*(\boldsymbol{q})\, A^*(-\boldsymbol{p}-\boldsymbol{q}) + A(\boldsymbol{p})\, A(\boldsymbol{q}) \\ &\times A(-\boldsymbol{p}-\boldsymbol{q}) + A^*(\boldsymbol{p})\, A^*(\boldsymbol{q})\, A(\boldsymbol{p}+\boldsymbol{q}) + A^*(\boldsymbol{p}+\boldsymbol{q})\, A(\boldsymbol{p})\, A(\boldsymbol{q})\} \\ &+ V_2(\boldsymbol{p},\boldsymbol{q})\{A^*(-\boldsymbol{q})\, A^*(\boldsymbol{p}+\boldsymbol{q})\, A(\boldsymbol{p}) + A^*(\boldsymbol{p}) \\ &\times A(\boldsymbol{p}+\boldsymbol{q})\, A(-\boldsymbol{q})\}] + \ldots \end{aligned} \tag{6.23}$$

where

$$V_1(\boldsymbol{p},\boldsymbol{q}) = \frac{\hbar^2}{8MN^{1/2}}\left(\frac{\mathrm{d}(\boldsymbol{p}+\boldsymbol{q})}{\mathrm{d}(\boldsymbol{p})\,\mathrm{d}(\boldsymbol{q})}\right)^{1/2}(1 + \mathrm{d}(\boldsymbol{p})\,\mathrm{d}(\boldsymbol{q}))\,(\boldsymbol{p}\cdot\boldsymbol{q})$$

$$V_2(\boldsymbol{p},\boldsymbol{q}) = -\frac{\hbar^2}{4MN^{1/2}}\left(\frac{\mathrm{d}(\boldsymbol{p}+\boldsymbol{q})}{\mathrm{d}(\boldsymbol{p})\,\mathrm{d}(\boldsymbol{q})}\right)^{1/2}(1 - \mathrm{d}(\boldsymbol{p})\,\mathrm{d}(\boldsymbol{q}))\,(\boldsymbol{p}\cdot\boldsymbol{q}).$$

The formalism enables the calculation of the structure factor $S(Q,\omega)$ in terms of the density excitations and their mutual interactions. It is of course an open question as to whether the perturbation theory is convergent.

6.3.2. *An approximate wavefunction for density fluctuations*

In §6.2 we showed that considerable progress has been achieved by using variational techniques for the calculation of the static structure factor $S(Q)$. Similar approaches have been adopted in treating the density excitations. The first approach was that of Bijl (1940). Feynman suggested on the basis of plausible arguments that an appropriate wavefunction for a single excitation of wave vector $\boldsymbol{q}$ is given by

$$|\boldsymbol{q}\rangle = (S(\boldsymbol{q}))^{-1/2}\,\rho(\boldsymbol{q})\,\Psi \tag{6.24}$$

where $\rho(\boldsymbol{q})$ is the density operator and Ψ is the wavefunction of the ground state. With this wavefunction the excitation energy of the system is given by

$$\omega_{\mathrm{F}}(\boldsymbol{q}) = \langle \boldsymbol{q} | H | \boldsymbol{q} \rangle - \langle \Psi | H | \Psi \rangle$$
$$= \frac{\hbar^2 q^2}{2MS(q)}. \tag{6.25}$$

Since the phonon wavefunction was not proven but merely guessed, equation (6.25) is expected to give an energy which is larger than that of the real excitations. This is indeed the case as shown in figure 55. It is also of interest to comment on the

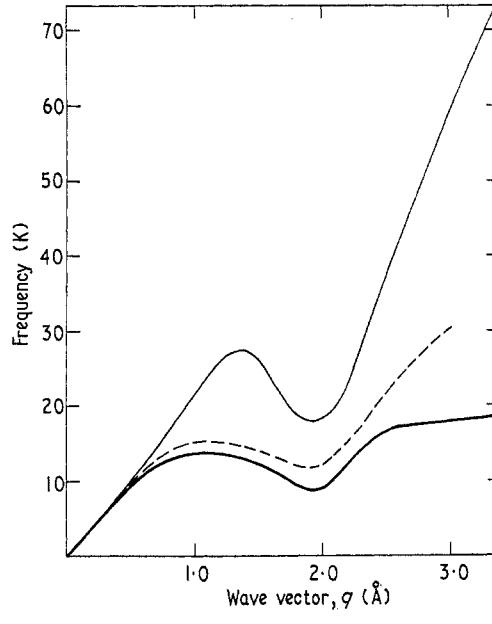

Figure 55. The energy of the elementary excitations in liquid helium: ———, the experimental curve (figure 9); ———, the Feynman excitation curve $\omega_{\mathrm{F}}(\boldsymbol{q})$; - - - -, the curve obtained by Jackson and Feenberg (1962) using the matrix elements, equation (6.27) and Brillouin perturbation theory.

similarity between equations (6.25) and (6.22); $S(q)$ of the former plays the role of $d(q)$ in the latter. Since the Feynman expression for the energy of an excitation is approximately twice as large as that found experimentally near the roton minimum, it is pertinent to examine improvements to the wavefunction (6.24). Feynman and Cohen (1956) introduced backflow in order to improve the wavefunction. This is equivalent to the introduction of interactions between the Feynman excitations (Miller *et al* 1962). The theory of these interactions was developed systematically by Jackson and Feenberg (1961, 1962).

If we introduce a Feynman excitation creation operator by $A^*(\boldsymbol{q}) = (S(\boldsymbol{q}))^{1/2}\rho(\boldsymbol{q})$, then the Feynman theory is equivalent to the use of an effective hamiltonian $H_0 + H_{\mathrm{F}}$, where H_0 is the hamiltonian in the absence of excitations and

$$H_{\mathrm{F}} = \sum_{\boldsymbol{q}} \hbar\omega_{\mathrm{F}}(\boldsymbol{q})\, A^*(\boldsymbol{q})\, A(\boldsymbol{q}).$$

The remainder of the hamiltonian gives rise to interactions between the excitations.

Jackson and Feenberg (1962) suggest that the most important terms in $H-H_0-H_F = \delta H$, give rise to a coupling between a single excitation ($\boldsymbol{q}$) and pairs of excitations with wave vectors $\boldsymbol{p}$ and ($\boldsymbol{q}-\boldsymbol{p}$). Alternatively δH may be rewritten in the form

$$\delta H = \sum_{\boldsymbol{q},\boldsymbol{p}} V(\boldsymbol{q},\boldsymbol{p})\{A^*(\boldsymbol{p})A^*(\boldsymbol{q}-\boldsymbol{p})A(\boldsymbol{q})+A^*(\boldsymbol{q})A(\boldsymbol{p})A(\boldsymbol{q}-\boldsymbol{p})\}.$$

The analysis of Jackson and Feenberg is then concerned with evaluation of $V(\boldsymbol{q},\boldsymbol{p})$. The part of the matrix elements dependent on $H-H_0$ may be evaluated directly to give

$$\langle \boldsymbol{p},\boldsymbol{q}-\boldsymbol{p}|H-H_0|\boldsymbol{q}\rangle = \frac{\hbar^2}{2MN^{1/2}}\{S(\boldsymbol{q})S(\boldsymbol{p})S(\boldsymbol{q}+\boldsymbol{p})\}^{-1/2} \times\{\boldsymbol{q}.(\boldsymbol{q}-\boldsymbol{p})S(\boldsymbol{p})+\boldsymbol{q}.\boldsymbol{p}S(\boldsymbol{q}-\boldsymbol{p})\} \tag{6.26}$$

but the remainder which is dependent upon H_F gives rise to a three-particle correlation function. If this is decoupled by the convolution approximation then

$$\langle \boldsymbol{p},\boldsymbol{q}-\boldsymbol{p}|H_F|\boldsymbol{q}\rangle = \frac{\hbar\omega_F(\boldsymbol{q})}{N^{1/2}}\{S(\boldsymbol{q})S(\boldsymbol{p})S(\boldsymbol{q}+\boldsymbol{p})\}^{1/2}.$$

Adding these two results and using equation (6.25) for $\omega_F(\boldsymbol{q})$ gives

$$V(\boldsymbol{q},\boldsymbol{p}) = \frac{\hbar^2}{2MN^{1/2}}\{S(\boldsymbol{p})S(\boldsymbol{q})S(\boldsymbol{p}+\boldsymbol{q})\}^{-1/2} \times\{\boldsymbol{q}.(\boldsymbol{q}-\boldsymbol{p})S(\boldsymbol{p})+\boldsymbol{q}.\boldsymbol{p}S(\boldsymbol{q}-\boldsymbol{p})-q^2S(\boldsymbol{q}-\boldsymbol{p})S(\boldsymbol{p})\}. \tag{6.27}$$

This result is analogous to the form of the interaction deduced in equation (6.23) and we shall discuss the similarity in more detail in the next section.

Lee (1967) and Lai *et al* (1970) have further developed this approach and have derived expressions for the term in the hamiltonian involving four excitations with the aid of the convolution approximation, and have also taken account of the lack of orthogonality between the different states. They have specifically applied their results to an evaluation of the dispersion relation in the small q limit.

In view of the interest in the interactions between four rotons, § 5.3.4, it is worthwhile to calculate the roton–roton interactions from their expressions. The result is particularly simple if we consider the scattering of rotons with wave vectors ($\boldsymbol{p}+\boldsymbol{Q}/2$) and ($-\boldsymbol{p}+\boldsymbol{Q}/2$) into two rotons with wave vectors ($\boldsymbol{p}'+\boldsymbol{Q}/2$) and ($-\boldsymbol{p}'+\boldsymbol{Q}/2$). Their interaction then reduces to

$$\frac{3\hbar^2 Q^2}{2MN}(1-S(q_R))S(q_R).$$

Since $S(q_R)$, the value of $S(q)$ at the roton minimum, is larger than unity this interaction is attractive and depends only on the total wave vector of the pair of rotons. In particular for the pairs created in a Raman scattering experiment, $Q \simeq 0$, there is no interaction between the excitations, cf § 5.3.3. For a total wave vector $Q = 1$ Å^{-1}, the interaction is attractive with a strength of $\simeq 6\times 10^{38}$ erg cm^{-3}, which is the same order of magnitude as that discussed in § 5.3.4 but somewhat larger than expected. The detailed form of this interaction is quite different from that deduced from the backflow models of Yau and Stephen (1971) and Nagai *et al* (1972) and we must await further developments before we can accurately calculate roton–roton interactions. In particular, although the interaction obtained by

Lai *et al* is attractive for rotons, when the excitations have wave vectors which differ appreciably from the roton wave vector, q_R, the interaction becomes repulsive.

6.3.3. *The self-energy of the density response.* The self-energy for the density fluctuations may be obtained from the hamiltonians deduced either by Sunakawa *et al* (1969), equation (6.23), or by Jackson and Feenberg (1962), equation (6.26). In the latter case the self-energy is given by

$$M(\boldsymbol{q},\omega) = \frac{1}{2}\sum_{\boldsymbol{p}} |V(\boldsymbol{q},\boldsymbol{p})|^2 \left(\frac{1}{\omega-\omega_F(\boldsymbol{p})-\omega_F(\boldsymbol{q}-\boldsymbol{p})} + i\pi\delta(\omega-\omega_F(\boldsymbol{p})-\omega_F(\boldsymbol{q}-\boldsymbol{p}))\right). \tag{6.28}$$

In the former case the interaction term is more complicated and in particular the terms containing A^*A^*A appear with different coefficients from the $A^*A^*A^*$ terms so that the two self-energy diagrams shown in figure 56 must be treated

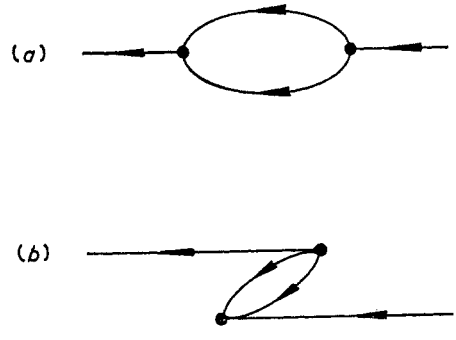

Figure 56. The two distinct self-energy diagrams which contribute in the theory of Sunakawa *et al* (1969). Only diagram (*a*) contributes in the Jackson and Feenberg (1962) theory.

separately. The self-energy is then obtained from equation (6.23) after some algebra to give equation (6.28) but with $\omega_F(\boldsymbol{p})$ replaced by $\omega_0(\boldsymbol{p})$ and the matrix element $V(\boldsymbol{p}-\boldsymbol{q})$ replaced by

$$V_s(\boldsymbol{p}\cdot\boldsymbol{q}) = \frac{\hbar^2}{2MN^{1/2}}\{d(\boldsymbol{p})\,d(\boldsymbol{q})\,d(\boldsymbol{q}-\boldsymbol{p})\}^{-1/2}\{\boldsymbol{q}\cdot\boldsymbol{p}d(\boldsymbol{q}-\boldsymbol{p})+\boldsymbol{q}\cdot(\boldsymbol{q}-\boldsymbol{p})\,d(\boldsymbol{p})\}. \tag{6.29}$$

This result is very similar to the Jackson and Feenberg result, equation (6.28), except that firstly $d(\boldsymbol{q})$ replaces the structure factor $S(\boldsymbol{q})$ throughout and secondly the final term in equation (6.27) is missing in equation (6.29). In equation (6.27) this term arose because it was necessary to subtract the quadratic part of the hamiltonian to obtain that part of H which acts as a perturbation, whereas in the theory of Sunakawa *et al* we have directly computed the perturbation. We believe that Sunakawa *et al* are in error in their development of perturbation theory at this point. Likewise their statement that conventional perturbation theory diverges with their interaction is also incorrect, possibly because of their incorrect evaluation of the two diagrams shown in figure 56.

The Van Hove structure factor $S(\boldsymbol{q},\omega)$ is then obtained in terms of the self-energy as

$$S(\boldsymbol{q},\omega) = \frac{1}{\pi}\,\mathrm{Im}\left(\frac{1}{\omega-\omega(\boldsymbol{q})-M(\boldsymbol{q},\omega)}\right) \tag{6.30}$$

where $\omega(\boldsymbol{q})$ is the excitation energy, $\omega_0(\boldsymbol{q})$, equation (6.22), in the theory of Sunakawa *et al* and the Feynman energy, $\omega_F(\boldsymbol{q})$, equation (6.25), in the theory of Jackson and Feenberg.

The complex self-energy therefore determines the dynamic structure factor and evaluation of the lowest order term (6.28) is dependent upon a knowledge of both the matrix elements and the frequencies $\omega(\boldsymbol{p})$. We have seen above that both the theories developed for the matrix elements give similar results and so we may have some confidence in their form. The dependence of the structure factor on the density of two-phonon states has recently been discussed by Iwamoto (1970), Jackson (1971) and by Zawadowski *et al* (1972). Unfortunately Iwamoto and Zawadowski *et al* discuss their results using the microscopic theory and with the Bogoliubov approximation of § 6.1.2. Since this is certainly an inadequate theory we believe, following Griffin (1972), that it is preferable to consider their theories and density theories. The hamiltonian represents the density fluctuations and their interactions, which do not then bear any simple relationship to the interactions between atoms.

In particular there is no simple relation connecting the cubic and quartic terms in the hamiltonian (g_3 and g_4 of Zawadowski *et al* (1972)).

Iwamoto (1970) discusses the form of $M(\boldsymbol{q}, \omega)$ in a qualitative manner and concludes that it is possible for the theory to produce a sharp response corresponding to well defined excitations and a broad continuum as found experimentally.

Zawadowski *et al* (1972) make the reasonable assumption that the perturbation theory will be improved if $\omega_F(\boldsymbol{p})$ etc in equation (6.28) is replaced by the observed excitation frequencies $\omega(\boldsymbol{q})$. They then further assume that the integrals over $\boldsymbol{p}$ are dominated by the contributions from the rotons and furthermore that the roton dispersion relation is a parabola. They then show that

$$\left.\begin{aligned} \operatorname{Re}\{M(q,\omega)\} &= \left(\frac{K}{q}\right)\Big/\ln\left|\frac{\omega-2\Delta}{2D}\right| \\ \operatorname{Im}\{M(q,\omega)\} &= \left(\frac{K}{q}\right)\pi \qquad \omega > 2\Delta \\ &= 0 \qquad\qquad \omega < 2\Delta \end{aligned}\right\} \tag{6.31}$$

where K is a constant and the dispersion relation for the rotons is parabolic up to frequencies of $\Delta + D$.

The real part of the self-energy diverges logarithmically as $\omega \to 2\Delta$. Equation (6.30) then shows that as ω increases there will always be a solution for ω less than 2Δ and that for increasing $\omega(q)$ the solution will approach closer to 2Δ. This result led Pitaevskii (1959) to suggest that the dispersion relation would approach 2Δ exponentially. Zawadowski *et al* (1972) discuss the effect on equation (6.31) of both a finite roton lifetime and of attractive roton–roton interactions. The former suppresses the singularity in the real part of $M(\boldsymbol{q}, \omega)$ and, is of importance when $|\omega - 2\Delta|$ is comparable with the roton half-width. Attractive roton–roton interactions give rise to a marked change in the two-roton continuum, as shown in figure 57, and also, for any nonzero attractive roton–roton interaction, to a bound state. Zawadowski *et al* then proceed to calculate the dynamic structure factor with this model for various different values of the parameters in the theory and to show that roton–roton interactions and the magnitude of the coefficient K, which is determined

by the strength of the interaction between three excitations, both have a considerable influence on the form of $S(q, \omega)$. In figure 58 we show the results of some of their calculations.

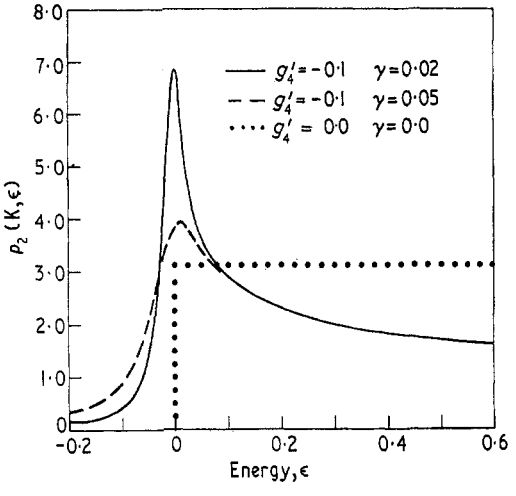

Figure 57. The approximate two-roton density of states at finite momentum q, plotted against energy, $\epsilon = (\omega - 2\Delta)/2D$. The dotted curve is the unperturbed result while the full and broken curves include both roton–roton attractive interactions, g_4', and a roton linewidth γ. From Zawadowski *et al* (1972).

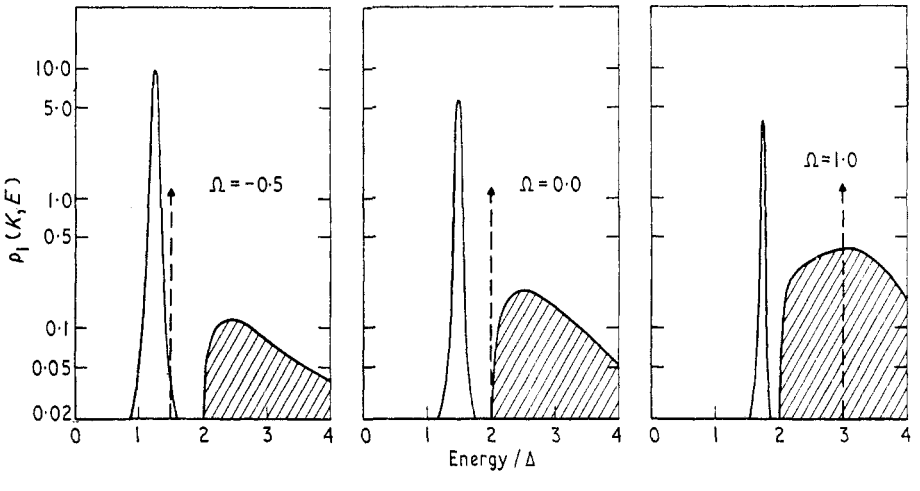

Figure 58. The theoretical $S(q, \omega)$, $\rho_1(K, E)$ for various values of $\omega_F(q) = (\Omega + 2\Delta)/\Delta$. The vertical broken lines show the delta functions which would occur if $M(q, \omega) = 0$, and the calculations include both roton–roton interactions and a finite roton lifetime. The unshaded regions correspond to the one-phonon scattering of § 3 and the shaded regions to the multiphonon scattering. From Zawadowski *et al* (1972).

Although Zawadowski *et al* (1972) have certainly demonstrated that roton–roton interactions may play an important role in determining $S(q, \omega)$, they have by no means proved this. The effects of including the $\boldsymbol{p}$ and $\boldsymbol{q}$ dependent matrix

elements, $V(\boldsymbol{q}, \boldsymbol{p})$, are largely unknown, as are the effect on their results of using a more realistic form for the dispersion relation. Despite these deficiencies the work of Zawadowski *et al* (1972) is certainly the most promising line of progress at present towards even a phenomenological theory of $S(q, \omega)$ in liquid helium.

Jackson (1969) has used a similar approach to discuss the behaviour of $S(q, \omega)$ at very large momentum transfers. He uses the form of interaction between the excitations given by equation (6.28) and then calculates the self-energy $M(q, \omega)$ with the aid of approximate Green's functions for $S(q, \omega)$. He then uses these approximate Green's functions to further improve the original calculation until selfconsistency is obtained. A completely selfconsistent calculation is impractical and he finds it necessary to make some approximations. His results show, however, that $S(q, \omega)$ is peaked around $\omega = \hbar q^2/2M$, that the width of the spectrum is proportional to q, and that the calculated shape of the spectrum has large wings before decreasing exponentially as $|\omega - \hbar q^2/2M|$ increases. Even though the widths of the spectra are only about one third that obtained experimentally, the results are important because they stress the importance of performing a selfconsistent calculation. The perturbation theory result without selfconsistency yields a width which is independent of q. The theory is, therefore, qualitatively but not quantitatively in accord with the results of § 3.

6.3.4. *Results of the theory and temperature dependence of the roton spectrum.* Numerical calculations of the spectrum of elementary excitations have been made using this formalism by Jackson and Feenberg (1962), Lee (1967) and Lai *et al* (1970). The last two sets of authors concentrated on the small q limit and on the evaluation of the dispersion parameter γ', defined by the equation

$$\omega(q) = \frac{\hbar q^2}{2MS(q)}(1 - \gamma' q^2). \tag{6.32}$$

Evaluation of the second-order perturbation result as described in the previous section together with $S(q)$ obtained from Campbell and Feenberg (1969) leads to $\gamma' = 0{\cdot}46$ Å^2. Lai *et al* (1970) also evaluate the contribution of six higher order terms in perturbation theory and find that their contribution to γ' is considerably smaller, namely $0{\cdot}133$ Å^2, suggesting that the perturbation theory for the density fluctuations is not rapidly convergent.

The experimental results described in § 3.3.2 give $\gamma' = 1{\cdot}5 \pm 0{\cdot}2$ Å^2, considerably larger than any of the calculations.

Jackson and Feenberg (1962) calculated the excitation spectrum for the density fluctuations by solving the implicit equation

$$\omega(q) = \omega_{\mathrm{F}}(q) + M(q, \omega(q))$$

and using the Feynman excitation frequencies in their evaluation of equation (6.28) for $M(q, \omega)$. The static structure factor was obtained from the measurements of Goldstein and Reekie (1955). The results, which are shown in figure 55, show that the agreement between theory and experiment is not very good. Lee (1967) reports on similar calculations with Massey's (1966) theoretical $S(q)$ which give somewhat larger discrepancies with experiment.

In a recent series of papers Ruvalds (1971), Jackle (1972), Takeno (1972) and Nagai (1973) have studied the temperature dependence of the roton energies,

§ 3.4.2. The theory considers the effect of attractive roton–roton interactions between four rotons. This arises from the quartic term in the expansion of the hamiltonian in terms of creation and destruction operators for density fluctuations and was also discussed in § 5.3.4. Ruvalds, Jackle and Takeno all calculate the effect of this term using first-order perturbation theory performed selfconsistently and find reasonable agreement with the experimental results, if the interaction is attractive and has a strength of about 5×10^{-38} erg cm^{-3}, which is considerably larger than the strength estimated in § 5.3.3. Nagai discusses the same problem with a T matrix multiple scattering formalism, but finds it difficult to obtain a form of interaction which is consistent with both the line width and frequency of the rotons as a function of temperature.

All of these calculations have neglected the effect of the cubic term in the expansion of the hamiltonian discussed in the preceding few sections. The calculation of the self-energy in § 6.3.3 was performed at absolute zero but may be readily extended to finite temperature when additional terms occur which are proportional to the occupation numbers of the excitations. This contribution will tend to decrease the frequency of the rotons with increasing temperature. Furthermore, since the calculations of Jackson and Feenberg (1962), figure 55, show that at absolute zero the self-energy correction arising from the cubic term is about 10·0 K, whereas the binding energy of a bound two-roton state is certainly less than 0·5 K, it would seem more likely that the temperature dependence of the rotons arises from changes in the cubic rather than in the quartic contribution to the self-energy.

The cubic term will also give rise to a contribution to the line width of the rotons, but in view of the difficulty in conserving both energy and momentum, it is quite likely that the dominant contribution to the roton line width arises from the quartic terms. In conclusion we can see no reason for the neglect of the cubic interactions in the treatments of Ruvalds, Jackle, Takeno and Nagai, and expect that in fact a large part of the temperature dependence arises from the cubic interactions, as discussed at $T = 0$ by Jackson and Feenberg (1962).

Ruvalds (1971) and Jackle (1972) then proceed to calculate the thermodynamic properties of liquid helium with their model. They obtain reasonable agreement presumably because their models accurately describe the temperature dependence of the rotons. Ruvalds also suggests that the rotons may act as a 'soft-mode' for the superfluid–normal phase transition. This seems to us to be incorrect because it is known that the second sound velocity becomes zero at this phase transition so that second sound is the 'soft-mode'.

7. Conclusions

Despite all the work described in this article, the most certain conclusion must be that liquid helium will continue to fascinate both experimental and theoretical physicists for many years. We have shown in §§ 2 and 3 that there are certainly more detailed and extensive x ray and neutron scattering measurements available for liquid helium than for any other material. At about 1·1 K and the saturated vapour pressure both $S(Q)$ and $S(Q, \omega)$ have been measured with greater precision than for any other material. For example the measurements provide reasonable confirmation of the zero and first sum rules and extend from $Q \simeq 0{\cdot}3$ Å^{-1} to $Q \simeq 20$ Å^{-1}, that is from the long wavelength collective region to the very short

wavelength independent particle region. Furthermore certain aspects of the scattering have been studied as a function of temperature and pressure.

Likewise ultrasonic measurements have been performed, as described in §4, in more detail than for any other material. The frequency, pressure and temperature dependences have all been accurately measured. The light scattering has also been studied although not so extensively because its history is only three years old instead of the twenty or more years for the other techniques.

In view of this wealth of experimental information it would not be surprising if experimental work ceased, but we know this will not be the case. Both the Chalk River and Brookhaven neutron scattering groups are planning further experiments to study the pressure and temperature dependence of $S(Q,\omega)$ more carefully. We hope that the x ray scattering measurements of $S(Q)$ will be performed as a function of pressure and temperature. Likewise as we indicated in §5.3.3, there is an urgent need for more Raman scattering measurements in order to elucidate the magnitude of the interactions between the rotons in liquid helium. Further measurements of the Raman scattering at higher pressures would also be informative.

The theory of the excitations in liquid helium is far less satisfactory. Despite all the experimental information and the numerous theoretical discussions there is still no convincing theory of the excitations which begins with the known interaction between helium atoms. Several elegant formalisms have been developed but in any detailed application some approximations must be made, and a suitable set of approximations are still unknown. In the same way that the BCS theory of superconductivity picked out the important terms for the origin of superconductivity the theory of superfluidity is still in need of the insight required to pick out the terms of importance in liquid helium.

A large part of the theoretical work on liquid helium adopts a less ambitious approach and employs a semi-phenomenological hamiltonian for the excitations and their interactions. Liquid helium then provides a very suitable system for testing theories of the interactions between excitations. Using this approach considerable progress has been made in understanding $S(Q,\omega)$, the Raman scattering and the ultrasonic attenuation. Unfortunately further work is needed in all of these examples because of the failure of different workers to consider all possible effects. In the ultrasonic attenuation, §4, it is now known that both anomalous dispersion of the phonon dispersion curve at low pressure and multiple scattering vertex corrections play important roles, but theoretical work has as yet concentrated on one or other of these problems and there is not a completely satisfactory theoretical treatment of both effects.

Likewise in the theory of the Raman scattering, the shape of the spectrum may be dependent upon both the interaction between the light and the excitations and on the interactions between the excitations. As described in §5 theoretical work has tended to concentrate on one of these explanations of the results to the exclusion of the other.

There is therefore in almost all aspects of the confrontation between experiment and theory in liquid helium more work to be done in order to clarify the theoretical position. In many cases this work requires a detailed consideration of several different explanations of the observed results and a careful discussion of their relative importance. Further a much clearer distinction needs to be made between the genuinely microscopic theories and the phenomenological Landau theories of

the excitations. Clearly we can anticipate considerable progress in our understanding of the structure, excitations and their interactions during the next few years, and hope that this review will provide at least some stimulation for that progress.

Acknowledgments

We have benefitted from discussions about aspects of liquid helium with many friends and colleagues to whom we are grateful. A large part of this article was written while one of us (RAC) was a summer visitor to Atomic Energy of Canada Limited whose support and hospitality he is pleased to acknowledge.

References

Abraham B M *et al* 1969 *Phys. Rev.* **181** 347–73
Abraham B M *et al* 1970 *Phys. Rev.* A **1** 250–7
Abrikosov A A, Gorkov L P and Dyzaloshinski I E 1964 *Methods of Quantum Field Theory in Statistical Physics* (Englewood Cliffs, NJ: Prentice-Hall)
Achter E K and Meyer L 1969 *Phys. Rev.* **188** 291–300
Ambegaokar V, Conway J M and Baym G 1965 *Lattice Dynamics* ed R F Wallis (Oxford: Pergamon Press) pp261–4
Anderson C H and Sabisky E S 1972 *Phys. Rev. Lett.* **28** 80–2
Barmatz M and Rudnick I 1968 *Phys. Rev.* **170** 224–38
Beaumont C F A and Reekie J 1955 *Proc. R. Soc.* A **228** 363–76
Beliaev S T 1958 *Sov. Phys.-JETP* **7** 289–98, 299
Bendt P J, Cowan R D and Yarnell J L 1959 *Phys. Rev.* **113** 1386–95
Bethe H A 1965 *Phys. Rev.* **138B** 804–22
—— *Phys. Rev.* **158** 941–7
Bierter W and Morrison H L 1969 *J. Low Temp. Phys.* **1** 65–72
Bijl A 1940 *Physica* **7** 869
de Boer J and Michels A 1938 *Physica* **5** 945–57
Bogoliubov N N 1947 *J. Phys. USSR* **11** 23–32
Born M and Huang K 1954 *Dynamical Theory of Crystal Lattices* (London: Oxford University Press)
Brandow B H 1969 *Phys. Rev. Lett.* **22** 173–96
—— 1971 *Ann. Phys. NY* **64** 21–99
Brewer D F and Edwards D O 1962 *Proc. 8th Int. Conf. Low Temperature Physics* ed R O Davies (London: Butterworths) p96
Brockhouse B N 1961 *Inelastic Scattering of Neutrons in Solids and Liquids* (Vienna: International Atomic Energy Agency) pp113–51
Brockhouse B N *et al* 1960 *Atomic Energy of Canada Ltd* Report AECL 1103
Brockhouse B N, Hauteler S and Stiller H 1964 *The Interaction of Radiation with Solids* ed R Strumane, J Nikoul, R Gevers and S Amelinckx) (Amsterdam: North-Holland) p580
Brown G V and Coopersmith M H 1969 *Phys. Rev.* **178** 327–44
Brueckner K A and Sawada K 1957 *Phys. Rev.* **106** 1117–27, 1128–35
Brugger R M 1965 *Thermal Neutron Scattering* ed P A Egelstaff (London and New York: Academic Press) p54–97
Byckling E 1966 *Phys. Rev.* **145** 71–5
Campbell C E and Feenberg E 1969 *Phys. Rev.* **188** 396–409
Chase C E 1953 *Proc. R. Soc.* A **220** 116
Chase C E and Herlin M A 1955 *Phys. Rev.* **97** 1447–52
Cheung T H 1970 *Phys. Lett.* **32A** 211–2
Cheung T H and Griffin A 1970 *Can. J. Phys.* **48** 2135–54

CHEUNG T H and GRIFFIN A 1971 *Phys. Rev.* A **4** 237–45
COHEN M and FEYNMAN R P 1957 *Phys. Rev.* **107** 13–24
CONIGLIO A, MANCINI F and MATURI M 1969 *Nuovo Cim.* B **63** 227–35
CONSOLO S, GRILLO G and JACUCCI G 1971 *Proc. 12th Int. Conf. Low Temperature Physics* ed E Kanda (Kyoto: Academic Press) pp49–50
COWLEY R A 1972 *J. Phys.* C: *Solid State Phys.* **5** L287–91
COWLEY R A and WOODS A D B 1968 *Phys. Rev. Lett.* **21** 787–9
—— 1971 *Can. J. Phys.* **49** 177–200
DIETRICH O W, GRAF E H, HUANG C H and PASSELL L 1972 *Phys. Rev.* A **5** 1377–91
DISATNIK Y 1967 *Phys. Rev.* **158** 162–9
DONNELLY R 1972 *Phys. Lett.* **39A** 221–2
DRANSFELD K, NEWELL J A and WILKS J 1958 *Proc. R. Soc.* A **243** 500–17
EGELSTAFF P A 1967 *An Introduction to the Liquid State* (London: Academic Press)
ETTERS R P 1966 *Phys. Rev. Lett.* **16** 119–22
EVANS W A B and IMRY Y 1969 *Nuovo Cim.* B **63** 155–84
FEENBERG E 1970 *Am. J. Phys.* **38** 684–704
—— 1971 *Phys. Rev. Lett.* **26** 301–3
FERRELL R A *et al* 1967 *Phys. Rev. Lett.* **18** 891–4
FERNANDEZ J F and GERSCH H A 1969 *Phys. Lett.* **30A** 261–2
FEYNMAN R P 1954 *Phys. Rev.* **94** 264–77
FEYNMAN R P and COHEN M 1956 *Phys. Rev.* **102** 1189–204
FINDLAY J C, PITT A, GRAYSON-SMITH H and WILHELM J O 1938 *Phys. Rev.* **54** 506–9
FRANCIS W P, CHESTER G V and REATTO L 1970 *Phys. Rev.* A **1** 86–97
FRENKEL J 1946 *Kinetic Theory of Liquids* (London: Oxford University Press) p244
FURUKAWA K 1962 *Rep. Prog. Phys.* **25** 395–440
GANGULY B N and GRIFFIN A 1968 *Can. J. Phys.* **46** 1895–1903
GAVORET J and NOZIERES P 1964 *Ann. Phys., NY* **28** 349–99
GERSCH H A and SMITH P N 1971 *Phys. Rev.* A **4** 281–90
GERSTEIN J I, SLUSHER R E and SURKO C M 1970 *Phys. Rev. Lett.* **25** 1739–42
GIBBS A and HARLING O K 1973 *Phys. Rev.* A to be published
GIRARDEAU M and ARNOWITT R 1959 *Phys. Rev.* **113** 755–61
GOBLE D F and TRAINOR L E H 1968 *Can. J. Phys.* **46** 839–54
GOLDSTEIN L and REEKIE J 1955 *Phys. Rev.* **98** 857–70
GOLDSTONE J 1957 *Proc. R. Soc.* A **239** 267–79
GORDON W I, SHAW C H and DAUNT J G 1958 *J. Phys. Chem. Solids* **5** 117–128
GORKOV L P and PITAEVSKII L P 1958 *Sov. Phys.-JETP* **6** 486
GOULD H and WONG U K 1971 *Phys. Rev. Lett.* **27** 301–3
GREYTAK T J, WOERNER R, YAN J and BENJAMIN R 1970 *Phys. Rev. Lett.* **25** 1547–51
GREYTAK T J and YAN J 1969 *Phys. Rev. Lett.* **22** 987–90
—— 1971 *Proc. 12th Int. Conf. Low Temperature Physics* ed E Kanda (Kyoto: Academic Press) pp89–90
GRIFFIN A 1972 *Phys. Rev.* A **6** 512–3
HALLEY J W 1969 *Phys. Rev.* **181** 338–46
HALLOCK R B 1972 *Phys. Rev.* A **5** 320–30
HARLING O K 1971 *Phys. Rev.* A **3** 1073–87
HENSHAW D G 1960a *Phys. Rev.* **119** 9–13
—— 1960b *Phys. Rev.* **119** 14–21
HENSHAW D G and WOODS A D B 1961a *Phys. Rev.* **121** 1266–74
—— 1961b *Proc. 7th Int. Conf. Low Temperature Physics* eds G M Graham and A C Hollis Hallett (Toronto: University of Toronto Press) p539–42
HOHENBERG P C and MARTIN P C 1964 *Phys. Rev. Lett.* **12** 69–71
—— 1965 *Ann. Phys., NY* **34** 291–359
HOHENBERG P C and PLATZMAN P M 1966 *Phys. Rev.* **152** 198–200
HORNER H 1972 *Phys. Rev. Lett.* **29** 556–9
HUANG K and KLEIN A 1964 *Ann. Phys., NY* **30** 203–34
HUGENHOLTZ N and PINES D 1959 *Phys. Rev.* **116** 489–506
HURST D G and HENSHAW D G 1955 *Phys. Rev.* **100** 994–1002
IWAMOTO F 1970 *Prog. Theor. Phys.* **44** 1121–57

IWAMOTO F, NAGAI K and NOJIMA K 1971 *Proc. 12th Int. Conf. Low Temperature Physics* ed E Kanda (Kyoto: Academic Press) pp189–90
IYENGAR P K 1965 *Thermal Neutron Scattering* ed P A Egelstaff (London and New York: Academic Press) p98–140
JACKLE J 1972 *Z. Phys.* **257** 14–21
JACKLE J and KEHR K W 1971a *Phys. Rev. Lett.* **27** 654–7
—— 1971b *Phys. Lett.* **37A** 205–6
JACKSON H W 1969 *Phys. Rev.* **185** 186–200
—— 1971 *Phys. Rev.* A **4** 2386–98
JACKSON H W and FEENBERG E 1961 *Ann. Phys. NY* **15** 266–95
—— 1962 *Rev. Mod. Phys.* **34** 686–93
JEFFERS W A and WHITNEY W M 1965 *Phys. Rev.* **139** A1082–96
KEESOM W H and TACONIS K W 1938 *Physica* **5** 270–80
KERR W C, PATHAK K N and SINGWI K S 1970 *Phys. Rev.* A **2** 2416–26
KHALATNIKOV I M 1965 *Theory of Superfluidity* (New York: Benjamin)
KHALATNIKOV I M and CHERNIKOVA D M 1966a *Sov. Phys.-JETP* **22** 1336–46
—— 1966b *Sov. Phys.-JETP* **23** 274–86
KIM Y K and INOKUTI M 1968 *Phys. Rev.* **165** 39–43
KLEIN R and WEHNER R K 1971 *Physica* **53** 630–2
KOBE D 1968 *Ann. Phys., NY* **47** 15–39
KONDOR I and SZEPFALUSY P 1968 *Acta Phys. Hung.* **24** 81–92
LAI H W, SIM H K and WOO C W 1970 *Phys. Rev.* A **1** 1536–41
LANDAU L D 1937 *Z. Phys. Sowjetunion* **11** 26, 545
—— 1941 *J. Phys. USSR* **5** 71
—— 1947 *J. Phys. USSR* **11** 91
LANDAU L D and KHALATNIKOV I M 1949 *Zh. Eksp. Teor. Fiz.* **19** 637–50
—— 1954 *Dokl. Akad. Nauk SSSR* **11** 637
LANDAU L D and PLACZEK G 1934 *Z. Phys. Sowjetunion* **5** 172
LARSSON K E and OTNES K 1959 *Ark. Fys.* **15** 49–63
LEE D K 1967 *Phys. Rev.* **162** 134–42
—— 1969 *Physica* **43** 132–41
LUBAN M 1962 *Phys. Rev.* **128** 965–87
MA S K, GOULD H and WONG V K 1971 *Phys. Rev.* A **3** 1453–62
MCMAHON R and GUYER R 1973 to be published
MCMILLAN W L 1965 *Phys. Rev.* **138** A442–51
MCTAGUE J P and BIRNBAUM G 1968 *Phys. Rev. Lett.* **21** 661–4
MARIS H J 1972 *Phys. Rev. Lett.* **28** 277–80
MARIS H J and MASSEY W E 1970 *Phys. Rev. Lett.* **25** 220–2
MASSEY W E 1966 *Phys. Rev.* **151** 153–64
MASSEY W E and WOO C W 1967 *Phys. Rev.* **164** 256–9
MILLER A, PINES D and NOZIERES P 1962 *Phys. Rev.* **127** 1452–64
MOLINARI A and REGGE T 1971 *Phys. Rev. Lett.* **26** 1531–3
NAGAI K 1973 *Prog. Theor. Phys.* **49** 46–63
NAGAI K, NOJIMA K and HATANO A 1972 *Prog. Theor. Phys.* **47** 355–69
NAKAJIMA S 1971 *Prog. Theor. Phys.* **45** 353–69
NARAHARA Y 1968 *J. Phys. Soc. Japan* **24** 169–72
NEWELL J A and WILKS J 1956 *Phil. Mag.* **1** 588–90
OSGOOD E B, MINKIEWICZ V J, KITCHENS T A and SHIRANE G 1972 *Phys. Rev.* A **5** 1537–47
PALEVSKY H *et al* 1957 *Phys. Rev.* **108** 1346–7
PALEVSKY H, OTNES K and LARSSON K E 1958 *Phys. Rev.* **112** 11–18
PALIN C J, VINEN W F, PIKE E R and VAUGHAN J M 1971 *J. Phys.* C: *Solid State Physics.* **4** L225–8
PARRY W E and TER HAAR D 1962 *Ann. Phys.* **19** 496–539
PELLAM J R and SQUIRE C F 1947 *Phys. Rev.* **72** 1245–52
PENROSE O and ONSAGER L 1956 *Phys. Rev.* **104** 576–84
PETHICK C J and TER HAAR D 1966 *Physica* **32** 1905–20
PHILLIPS N E, WATERFIELD C G and HOFFER J K 1970 *Phys. Rev. Lett.* **25** 1260–2
PIKE E R 1972 *J. de Phys.* **33** C1 25–40

PIKE E R and VAUGHAN J M 1971 *J. Phys.* C: *Solid State Physics.* **4** L362–6
PIKE E R, VAUGHAN J M and VINEN W F 1970 *J. Phys.* C: *Solid State Phys.* **3** L40–3
PINES D 1966a *Quantum Fluids* ed D F Brewer (Amsterdam: North-Holland) pp257–8
—— 1966b *Many-body Theory* ed R Kubo (Tokyo: Syokabo; New York: Benjamin) pp36–64
PINES D and WOO C W 1970 *Phys. Rev. Lett.* **24** 1044–5
PIPPARD A B 1951 *Phil. Mag.* **42** 1209–23
PITAEVSKII L P 1959 *Sov. Phys.–JETP* **9** 830–7
—— 1970 *Zh. Eksp. Teor. Fiz. SSSR–Pis'ma Red.* **12** 118–21 (*Sov. Phys.–JETP Lett.* **12** 82–3)
PUFF R D 1965 *Phys. Rev.* **137** A406–16
PUFF R D and TENN J S 1970 *Phys. Rev.* A **1** 125–32
REATTO L and CHESTER G V 1967 *Phys. Rev.* **155** 88–100
REEKIE J 1940 *Proc. Camb. Phil. Soc.* **36** 236–41
ROACH P R, ABRAHAM B M, KETTERSON J B and KUCHNIR M 1972a *Phys. Rev. Lett.* **29** 32–5
ROACH P R, KETTERSON J B and KUCHNIR M 1970 *Phys. Rev. Lett.* **25** 1002–5
—— 1972b *Phys. Rev.* A **5** 2205–14
RUVALDS J 1971 *Phys. Rev. Lett.* **27** 1769–71
RUVALDS J and ZAWADOWSKI A 1970 *Phys. Rev. Lett.* **25** 333–7
SASLOW W M 1972 *Phys. Rev.* A **5** 1491–502
SCHIFF D and VERLET L 1967 *Phys. Rev.* **160** 208–18
SEARS V F 1969 *Phys. Rev.* **195** 200–6
—— 1970 *Phys. Rev.* A **1** 1699–704
—— 1971 *Ber. Bunsen–Ges. Phys. Chem.* **75** 376–8
SEARS V F and KHANNA F C 1972 *Phys. Rev. Lett.* **29** 549–52
SHAM L J 1967 *Phys. Rev.* **156** 494–500
SIM H K, WOO C W and BUCKLER J R 1970 *Phys. Rev.* A **2** 2024–31, 2032–37
SINGH A D 1968 *Can. J. Phys.* **46** 1801–8
SINGH K K and KUMAR S 1967 *Phys. Rev.* **162** 173–85
—— 1970 *Phys. Rev.* A **1** 497–513
SODA T, SAWADA K and NAGATA T 1970 *Prog. Theor. Phys.* **44** 860–4
SOLANA J *et al* 1972 *Phys. Rev.* A **6** 1665–75
STEPHEN M J 1969 *Phys. Rev.* **187** 279–85
SUNAKAWA S, YAMASAKI S and KEBUKAWA T 1969 *Prog. Theor. Phys.* **41** 919–40
SVENSSON E C, WOODS A D B and MARTEL P 1972 *Phys. Rev. Lett.* **29** 1148–9
SWIFT J and KADANOFF L P 1968 *Ann. Phys., NY* **50** 312–22
TAKENO S 1972 *Prog. Theor. Phys.* **48** 2107–9
TAVARD C, NICOLAS D and ROUAULT M 1967 *J. Chim. Phys.* **64** 540–4
TSERKONIKOV Y A 1965 *Sov. Phys.–Dokl.* **9** 1110–3
—— 1967 *Sov. Phys.–Dokl.* **11** 723–5
TWEET A G 1954 *Phys. Rev.* **93** 15–20
VALATIN J G and BUTLER D 1958 *Nuovo Cim.* **10** 37–54
VAN HOVE L 1954 *Phys. Rev.* **95** 249–62
VINEN W F 1971 *J. Phys.* C: *Solid State Phys.* **4** L287–9
WATERS G A, WATMOUGH D J and WILKS J 1967 *Phys. Lett.* **26A** 12–13
WEHNER R K and KLEIN R 1969a *Helv. Phys. Acta* **42** 936–8
—— 1969b *Phys. Rev. Lett.* **23** 1372–4
—— 1972 *Physica* **62** 161–97
WERTHAMER N R 1969 *Am. J. Phys.* **37** 763–82
—— 1972 *Phys. Rev. Lett.* **28** 1102–5
WERTHEIM M S 1963 *Phys. Rev. Lett.* **10** 321–23
WHITNEY W M 1956 *Phys. Rev.* **105** 38–41
WHITNEY W M and CHASE C E 1967 *Phys. Rev.* **158** 200–14
WOODS A D B 1965a *Phys. Rev. Lett.* **14** 355–6
—— 1965b *Inelastic Scattering of Neutrons* (Vienna: International Atomic Energy Agency) p191–200
WOODS A D B and COWLEY R A 1970 *Phys. Rev. Lett.* **24** 646–8

WOODS A D B, SVENSSON E C and MARTEL P 1972 *Neutron Inelastic Scattering* (Vienna: International Atomic Energy Agency) pp359–64
—— 1973 *Phys. Rev. Lett.* **43A** 223–4
WOOLF M, PLATZMAN P M and COHEN M G 1966 *Phys. Rev. Lett.* **17** 294–7
WU F Y and FEENBERG E 1962 *Phys. Rev.* **128** 943–55
YARNELL J L, ARNOLD G P, BEADT P J and KERR E C 1959 *Phys. Rev.* **113** 1379–86
YAU J and STEPHEN M J 1971 *Phys. Rev. Lett.* **27** 482–5
ZAWADOWSKI A, RUVALDS J and SOLANA J 1972 *Phys. Rev.* **5** 399–421